Doctoral Dissertation
Doctoral Program in Electrical, Electronic and Communications Engineering
(35^{th}cycle)

Multi-Band Optical Networks Capacity, Energy, and Techno-Economic Assessment

By

Rasoul Sadeghi Yamchi

******

Supervisor(s):
Professor Vittorio Curri, Supervisor
Dr. Nelson Costa, Industrial Mentor
Dr. Antonio Napoli, Industrial Mentor
Dr. João Pedro, Industrial Mentor

Doctoral Examination Committee:
Professor Nicola Sambo, Referee, university of Scuola Superiore Sant'Anna
Professor Jarosław Piotr Turkiewicz, Referee, Warsaw University of Technology

Politecnico di Torino
2023

Declaration

I hereby declare that, the contents and organization of this dissertation constitute my own original work and does not compromise in any way the rights of third parties, including those relating to the security of personal data.

<div align="right">

Rasoul Sadeghi Yamchi

2023

</div>

I would like to dedicate this thesis to my loving family and wife

Acknowledgements

Abstract

As the use of 5G/6G services, video applications on the internet, and cloud services and data centers become more popular, network traffic is constantly increasing. This means that there is a continuous need for expanding the capacity of optical networks. In the past, efforts were made to improve spectral efficiency through techniques like high-order modulation and constellation shaping. However, the Shannon limit sets a limit on spectral efficiency at a specific transmission distance, which means that there is a greater reliance on utilizing the optical spectrum from either the same optical fiber or other optical fibers. This can be achieved by extending to more wavelength bands or deploying more fibers, or through spatial division multiplexing. These methods will need to be increasingly utilized to keep up with growing network traffic. In this thesis, Multi-band optical fiber transmission is generally proposed and investigated for capacity upgrades in optical transport networks. To comprehensively assess the potential of multi-band transmission, key metrics such as the potential capacity increase, energy consumption, and the number of required interfaces must be evaluated for different transmission scenarios. Thus, first of all, it has been considered progressive spectral exploitation, starting from the C-band only and up to C+L+S+U-band transmission, for both transparent and translucent solutions that exploit optical signal regeneration. By considering accurate state-of-the-art physical layer models for each investigated multi-band configuration, a networking performance metric that enables the comparison of different solutions in terms of capacity allocation and energy consumption has been driven. For a translucent network design, different regenerator placement algorithms are compared, with the aim of minimizing energy consumption and costs. The proposed network-wide numerical analysis shows that, for spectral occupations exceeding the C+L-band, translucent solutions can significantly increase network capacity while leading to a similar energy consumption per transmitted bit as in the transparent design case, but they require the deployment of additional line interfaces.

Significantly, these results provide evidence that the transparent exploitation of an additional transmission band produces a capacity increment that is at least comparable to that of a translucent solution based on already-in-use bands. Since this is attained at the expense of fewer line interfaces, it is a key finding suggesting that extending the number of bands supported is a cost-effective approach to scaling the capacity of existing fiber infrastructures. Moreover, it has been compared and analyzed comprehensively the network capacity, along with the required number of interfaces and amplifiers for different network topologies, for both regular and extended bandwidth (super) bands which recently proposed to efficiently use already installed devices. Thus, two multi-band transmission (MBT) scenarios: first, the regular configurations, consisting of the C+L-band and C+L+S1-band – being S1 half of the standard S-band, with total bandwidths of 9.6 and 14.4 THz, respectively, and second, extended bandwidth configurations for the C- and C+L-band, with total bandwidths of 6 and 12 THz, respectively have been investigated in this thesis. Both transparent and translucent network design scenarios are applied. The numerical network assessment process assisted by an accurate physical layer model, for all MBT configurations in this part, was performed as well. It has been shown that compared to regular bands, super bands significantly increase network capacity for both uniform and nonuniform traffic distributions. Crucially, super bands require fewer line interfaces, suggesting that extending the bandwidth of already deployed bands is a cost-effective approach when up-scaling existing fiber infrastructures, in comparison to adding extra bands. Finally, To improve the network capacity signal regeneration has been done in the band(s) with a poor QoT such as the S-band; So, the performance of the optimized S-band network has been compared to that of the U-band in MBT configurations. Initially, signal regeneration was implemented in the S-band to improve its performance and achieve transmission data rates comparable to the C and L-bands in the transparent network design. Subsequently, the advantages of the S-band over the U-band in MBT configurations were evaluated. It has been shown that signal regeneration in the S-band channels results in gaining network capacity efficiently and cost-effectively.

Contents

List of Figures

List of Tables

List of Scientific Contributions

A list of the scientific contributions, with a special focus on publications, carried out during the Ph.D. are described here.

Peer Reviewed International Journals

[1] Bruno Correia, **Rasoul Sadeghi**, Emanuele Virgillito, Antonio Napoli, Nelson Costa, João Pedro, and Vittorio Curri, "Power control strategies and network performance assessment for C+L+S multiband optical transport," J. Opt. Commun. Netw. 13, 147-157 (2021).

[2] **Rasoul Sadeghi**, Bruno Correia, André Souza, Nelson Costa, João Pedro, Antonio Napoli, and Vittorio Curri, "Transparent vs Translucent Multi-Band Optical Networking: Capacity and Energy Analyses," J. Lightwave Technol. 40, 3486-3498 (2022).

Contributions to International Conferences

[1] **Rasoul Sadeghi**, Bruno Correia, Emanuele Virgillito, Nelson Costa, João Pedro, Antonio Napoli, and Vittorio Curri, "Multi Bands Network Performance Assessment for Different System Upgrades," 2020 IEEE Photonics Conference (IPC), 2020, pp. 1-2, doi: 10.1109/IPC47351.2020.9252450.

[2] Emanuele Virgillito, **Rasoul Sadeghi**, Alessio Ferrari, Giacomo Borraccini, Antonio Napoli, and Vittorio Curri, "Network Performance Assessment of C+L Upgrades vs. Fiber Doubling SDM Solutions," in Optical Fiber Communication Conference (OFC) 2020, OSA Technical Digest (Optica Publishing Group, 2020), paper M2G.4.

[3] Emanuele Virgillito, **Rasoul Sadeghi**, Alessio Ferrari, Antonio Napoli, Bruno Correia, and Vittorio Curri, "Network Performance Assessment with Uniform and Non-Uniform Nodes Distribution in C+L Upgrades vs. Fiber Doubling SDM Solutions," 2020 International Conference on Optical Network Design and Modeling (ONDM), 2020, pp. 1-6, doi: 10.23919/ONDM48393.2020.9133013.

[4] Bruno Correia, **Rasoul Sadeghi**, Emanuele Virgillito, Antonio Napoli, Nelson Costa, Joãao Pedro, and Vittorio Curri, "Networking Performance of Power Optimized C+L+S Multiband Transmission," GLOBECOM 2020 - 2020 IEEE Global Communications Conference, 2020, pp. 1-6, doi: 10.1109/GLOBE-COM42002.2020.9322068.

[5] Bruno Correia, **Rasoul Sadeghi**, Emanuele Virgillito, Antonio Napoli, Nelson Costa, João Pedro, and Vittorio Curri, "Optical Power Control Strategies for Optimized C+L+S-bands Network Performance," in Optical Fiber Communication Conference (OFC) 2021, P. Dong, J. Kani, C. Xie, R. Casellas, C. Cole, and M. Li, eds., OSA Technical Digest (Optica Publishing Group, 2021), paper W1F.8.

[6] **Rasoul Sadeghi**, Bruno Correia, Emanuele Virgillito, Antonio Napoli, Nelson Costa, João Pedro, and Vittorio Curri, "Performance Comparison of Translucent C-band and Transparent C+L-band Network," in Optical Fiber Communication Conference (OFC) 2021, P. Dong, J. Kani, C. Xie, R. Casellas, C. Cole, and M. Li, eds., OSA Technical Digest (Optica Publishing Group, 2021), paper M3E.4.

[7] **Rasoul Sadeghi**, Bruno Correia, Emanuele Virgillito, Antonio Napoli, Nelson Costa, João Pedro, and Vittorio Curri, "Comparison of Transceiver and C+L Band Upgrades: Network Traffic and Energy Assessment," 2021 International Conference on Electrical, Communication, and Computer Engineering (ICECCE), 2021, pp. 1-6, doi: 10.1109/ICECCE52056.2021.9514166.

[8] **Rasoul Sadeghi** , Bruno Correia, Emanuele Virgillito, Antonio Napoli, Nelson Costa, João Pedro, and Vittorio Curri, "Network Comparison of C+L-band Transparent versus C-band Translucent Upgrade," 2021 International Conference on Optical Network Design and Modeling (ONDM), 2021, pp. 1-6, doi: 10.23919/ONDM51796.2021.9492468.

[9] Bruno Correia,**Rasoul Sadeghi**, Emanuele Virgillito, Antonio Napoli, Nelson Costa, João Pedro, and Vittorio Curri, "Multiband Power Control Impact on the Transmission Capacity of Optical Line Systems," 2021 IEEE Photonics Society Summer Topicals Meeting Series (SUM), 2021, pp. 1-2, doi: 10.1109/SUM48717.2021.9505860.

[10] **Rasoul Sadeghi**, Bruno Correia, Emanuele Virgillito, Antonio Napoli, Nelson Costa, João Pedro, and Vittorio Curri,"C+L-band Network Upgrade: Capacity and Energy Analyses with Different Transceivers," 2021 IEEE Photonics Society Summer Topicals Meeting Series (SUM), 2021, pp. 1-2, doi: 10.1109/SUM48717.2021.9505822.

[11] **Rasoul Sadeghi**, Bruno Correia, Emanuele Virgilito, Elliot London, Nelson Costa, João Pedro, Antonio Napoli, and Vittorio Curri, "Optimized Translucent S-band Transmission in Multi-Band Optical Networks," 2021 European Conference on Optical Communication (ECOC), 2021, pp. 1-4, doi: 10.1109/ECOC52684.2021.9605809.

[12] **Rasoul Sadeghi**, Bruno Correia, Emanuele Virgillito, Antonio Napoli, Nelson Costa, João Pedro, and Vittorio Curri, "Cost-Effective Capacity Increase of Deployed Optical Networks to Support the Future Internet: the Multi-Band Approach," 2021 12th International Conference on Network of the Future (NoF), 2021, pp. 1-7, doi: 10.1109/NoF52522.2021.9609888.

[13] **Rasoul Sadeghi**, Bruno Correia, Emanuele Virgillito, Antonio Napoli, Nelson Costa, João Pedro, and Vittorio Curri, "Network Capacity and Energy Consumption: Transparent $C + L$ -band vs Translucent C-band," 2021 IEEE Photonics Conference (IPC), 2021, pp. 1-2, doi: 10.1109/IPC48725.2021.9592874.

[14] Bruno Correia, Alex Donodin, **Rasoul Sadeghi**, V. Dvoyrin, Antonio Napoli, João Pedro, Nelson Costa, Wladek Forysiak, Sergey Turitsyn, and Vittorio Curri, "QoT Evaluation of Optical Line System Transmission with Bismuth-Doped Fiber Amplifiers in the E-Band," in Asia Communications and Photonics Conference 2021, C. Chang-Hasnain, A. Willner, W. Shieh, P. Shum, Y. Su, G. Li, B. Eggleton, R. Essiambre, D. Dai, and D. Ma, eds., Technical Digest Series (Optica Publishing Group, 2021), paper M4I.5.

[15] **Rasoul Sadeghi**, Bruno Correia, Emanuele Virgillito, Antonio Napoli, Nelson Costa, João Pedro, and Vittorio Curri, "Optimal Spectral Usage and Energy Efficient S-to-U Multiband Optical Networking," in Optical Fiber Communication Conference (OFC) 2022, S. Matsuo, D. Plant, J. Shan Wey, C. Fludger, R. Ryf, and D. Simeonidou, eds., Technical Digest Series (Optica Publishing Group, 2022), paper W3F.7.

[16] André Souza, **Rasoul Sadeghi**, Bruno Correia, Nelson Costa, Antonio Napoli, Vittorio Curri, Joãoo Pedro, and João Pires, "Optimal Pay-As-You-Grow Deployment on S+C+L Multi-band Systems," in Optical Fiber Communication Conference (OFC) 2022, S. Matsuo, D. Plant, J. Shan Wey, C. Fludger, R. Ryf, and D. Simeonidou, eds., Technical Digest Series (Optica Publishing Group, 2022), paper W3F.4.

[17] **Rasoul Sadeghi** Bruno Correia, André Souza, Antonio Napoli, Nelson Costa, João Pedro, and Vittorio Curri, "Capacity and Energy Consumption Comparison in Translucent versus Transparent Multi-band Designs," 2022 International Conference on Optical Network Design and Modeling (ONDM), 2022, pp. 1-3, doi: 10.23919/ONDM54585.2022.9782854.

[18] **Rasoul Sadeghi**, Bruno Correia, Antonio Napoli, Nelson Costa, João Pedro, and Vittorio Curri, "Capacity and Energy Usage of Translucent and Multi-Band Transparent Optical Networks," in Optica Advanced Photonics Congress 2022, Technical Digest Series (Optica Publishing Group, 2022), paper NeTu3D.2.

[19] Muhammad Umar Masood, Ihtesham Khan, Lorenzo Tunesi, Bruno Correia, **Rasoul Sadeghi**, Enrico Ghillino, Paolo Bardella, Andrea Carena, and Vittorio Curri, "Networking Analysis of Photonics Integrated Multiband WSS Based ROADM Architecture," 2022 International Conference on Software, Telecommunications and Computer Networks (SoftCOM), 2022, pp. 1-6, doi: 10.23919/SoftCOM55329.2022.9911234.

[20] **Rasoul Sadeghi**, Bruno Correia, Nelson Costa, João Pedro, Antonio Napoli, Vittorio Curri, "Extending the C+ L System Bandwidth versus Exploiting Part of the S-band: Network Capacity and Interface Count Comparison," 2022 European Conference on Optical Communication (ECOC), 2022, pp. 1-4.

[21] Bruno Correia, **Rasoul Sadeghi**, Antonio Napoli, Nelson Costa, João Pedro, Vittorio Curri, "C+ L+ S-Band Optical Network Design Exploiting Amplifier

Site Upgrade Strategies," 2023 International Conference on Optical Network Design and Modeling (ONDM), 2023, pp. 1-6.

[22] **Rasoul Sadeghi**, Bruno Correia, Elliot London, Antonio Napoli, Nelson Costa, João Pedro, Vittorio Curri, "Performance Comparison of Optical Networks Exploiting Multiple and Extended Bands and Leveraging Reinforcement Learning," 2023 International Conference on Optical Network Design and Modeling (ONDM), 2023, pp. 1-6.

Chapter 1

Introduction

Traffic is growing, and escalating demands are straining over-utilized paths between source and destination within optical network routes [1, 2]. The data behind the bandwidth may differ – it could be terabyte file size data sharing between research institutions, the shift of enterprise applications, storage, and computing to the cloud, transmission of complex, high-resolution medical imaging between hospitals, evolving educational tools, or other high-bandwidth applications – but, the result is costly and complex. Moving data is highly reliant on a massive network of existing infrastructure. However, rather than expanding and overbuilding costly, inflexible network infrastructure, what if there was a way to simply integrate a solution that optimized existing fiber facilities without impacting the existing infrastructure? The bandwidth extending, exploiting other available optical bands, is a cost-effective and viable solution to improve an optical network throughput [3, 4]. So, this thesis explores the multi-band transmission (MBT) optical networks performances in terms of network throughput, energy consumption, and techno economically. Chapter 1 introduces the motivation, open and disaggregated optical networks, and Software-Defined Networking (SDN) in the optical networks. The deployed methodology and metrics from the physical layer to the network layer have been discussed in Chapter 2 with details for different scenarios in the MBT configurations. Moreover, Chapter 3 describes the statistical network performance assessment in the transparent and translucent network designs in the MBT scenarios with different upgrades. In Chapter 4 network performance for extended bandwidth bands has been compared

with regular bands in the MBT systems. Finally, in Chapter 5 we have a conclusion and discuss open challenges in this area for further work.

1.1   Motivation

Internet traffic has seen a compounded annual growth rate of 30% or higher over the last five years due to the more connected devices. According to the forecasts, a steep increase in demand for capacity in telecommunication networks will continue on a worldwide scale as a consequence of, for instance, clouds, high-definition streaming, virtual-reality applications, and 5G/6G deployment [5]. Consequently, long-term and cost-effective solutions should be found to deal with the optical transport network traffic increasing while limiting the energy consumption [6]. To deal with this rapid growth of the traffic in the optical communication systems Wavelength Division Multiplexing (WDM) has been proposed [7]. It increases bandwidth by allowing different data streams to be sent simultaneously over a single optical fiber network. In this way WDM maximizes the usefulness of fiber and helps optimize network investments by dividing the whole working frequency range to small WDM channels [8]. Most of the telecom operators use WDM bandwidth of 4.8 THz in their systems which is in the C-band of the optical fibers frequency range [9]. MBT is a natural solution to cope with the increasing request of capacity, as it requires fewer changes to existing optical fiber infrastructures. This solution implements transmission over a wider spectral range within the low-loss region of the widely deployed single-mode optical fibers, namely the ITU-T G.652.D type, exceeding a total transmission bandwidth of $\approx$ 50 THz [9, 10]. Several works have already shown the potential of MBT, considering several different combinations of spectral bands, from the O- to L-band [11–17]. Commercial availability of MBT solutions for C+L-band transmission has also been demonstrated in [18, 19]. However, The U-band (ultraviolet band) has not been extensively explored for optical communication systems, and researchers have primarily focused on the E-band (extremely high frequency), O-band (original band), and other wavelength regions for several reasons. Some of the limitations of the U-band that have discouraged widespread investigation for optical communication systems include 1) Material Constraints, 2)Signal Scattering, 3) Limited Availability of Equipment, and 4)Safety Concerns. On the other hand, the E-band and O-band have proven to be suitable for various optical communication

applications, offering a good balance between performance, signal propagation, and equipment availability. Researchers have thus prioritized exploring these bands where they can achieve higher data rates and longer communication distances. One of the key advantages of using MBT to upgrade optical networks is that by relying on the existing optical fiber infrastructure the Capital Expenditure (CAPEX) is kept low in comparison to other approaches [20, 21]. However, managing multiple bands is a challenge for the telecom industry due to the requirement to deploy more optical devices for each band which have different behaviors in different bands/frequencies. This thesis is focusing on analyzing the MBT optical transport network from the physical layer to the network layer in disaggregated optical networks in terms of capacity, energy consumption and interfaces count as a cost metric.

1.2   Software-defined optical network

Software-defined networking (SDN) is an approach to network virtualization that seeks to optimize network resources and quickly adapt networks to changing business needs, applications, and traffic [22–24]. Software-defined networking offers numerous benefits such as on-demand provisioning, automated load balancing, streamlined physical infrastructure, and the ability to scale network resources in lockstep with application and data needs [25]. SDN architecture consists of three separate planes namely Data Plane, Control Plane, and Management Plane which is depicted in Fig. 1.1.

Data Plane: The data plane in SDN architecture is divided into two sublayers: the network infrastructure and the southbound interface. The southbound interface contains the instructions for forwarding packets and defines the network protocol used to communicate between the control plane and the data plane.

- **Network Infrastructure**: In SDN architecture, the network infrastructure is made up of traditional network components such as routers and switches. However, the ability to program individual network components is removed, and flow control is handled by a central logical unit instead. This reduces the network components to simple data-forwarding elements that operate based on a set of rules. The data forwarding process uses a pipeline of flow tables, which keep track of the matched rules and the actions to be taken if those rules

are matched. For instance, OpenFlow and NETCONF [26] are responsible for maintaining these flow tables.

- **Southbound Interface**: The southbound interface in SDN architecture facilitates communication between the control plane and the data plane. SDN promotes interoperability among forwarding devices from different vendors, and OpenFlow is the most widely accepted and deployed standard for achieving this interoperability. Therefore, OpenFlow and NETCONF [26] play a crucial role in the implementation of the SDN framework.
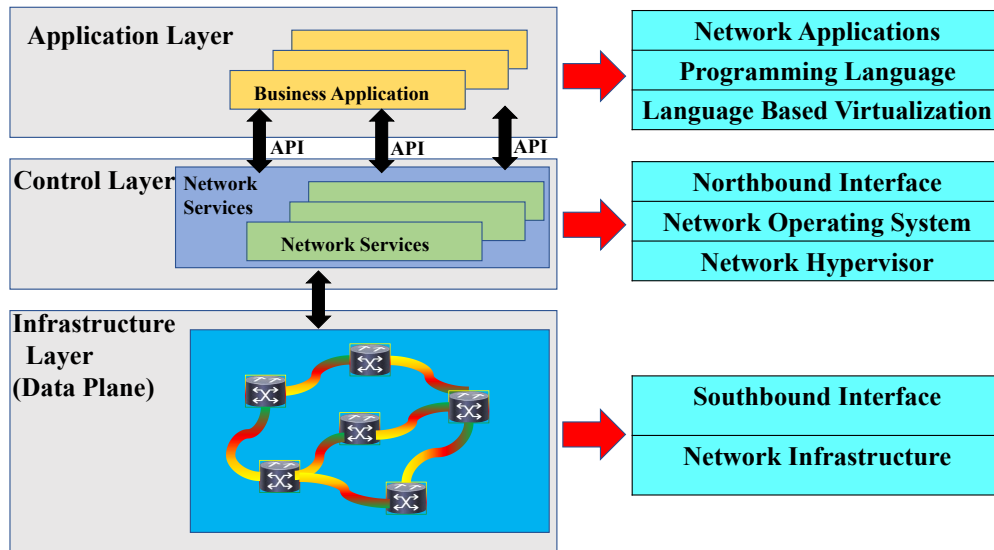
Fig. 1.1 SDN schematic diagram with some examples of the typical functions required by the application layer and performed by SDN controller.

Control Plane: The control plane in SDN architecture is dedicated to managing network traffic. It includes a centralized software component that is responsible for directing traffic within the network. It is more efficient to have centralized logical control rather than centralized physical control, as a single failure of any physical control device could cause the entire network to fail. To address this, SDN includes provision for backup controllers that can take over in the event of a failure[27]. The sublayers of the control plane are:

- **Network Hypervisor**: In SDN architecture, network hypervisors allow multiple virtual machines to access the same hardware resources over a shared

cloud infrastructure, reducing the cost of physical resources. This concept of virtualization, which was previously used in the software industry, has been implemented in networking through SDN.

- **Network Operating System**: SDN architecture uses a network operating system (NOS) to perform centralized logical control, which is a novel concept in networking. The main functions of NOS are to provide abstractions and a common development environment for network engineers.

- **Northbound Interface**: SDN architecture uses northbound APIs to communicate with applications and business requirements in the upper layers. While northbound APIs are not yet standardized, it is expected that they will be a software environment in contrast to the hardware environment supported by the southbound interface.

Last, the management layer consists of three sub-layers such as language-based virtualization, programming languages, and network applications. the language-based virtualization layer provides abstraction of network modules while preserving the protection and integrity of the network structure. The programming languages layer includes tools for defining network abstractions, with a focus on portability. These programming languages should be able to implement and install user-defined requirements during execution. The network applications layer defines the logic that is executed by the lower layers, and it specifies the business requirements that must be implemented in those layers.

1.3 Outline of the thesis

This thesis exploits transparent and translucent MBT (i.e., C-, C+L, C+L+S, C+L+S+U, super C, and super C+L, etc) network designs performance assessment in terms of throughput, energy consumption, and interfaces count as a cost metric. First, the Generalized Signal to Noise Ratio (GSNR) value as a Quality of Transmission (QoT) metric has been evaluated in each MBT configuration for each band, and under investigation network topology abstraction has been done by utilizing GNPy [28]. In the network layer, SNAP is carried out for analyzing the optical network topology. To this end, SNAP can analyze statistically an optical network topology by progressively loading the network with different traffic request sizes (100–400 Gb/s) and traffic

patterns (Uniform and nonuniform). Moreover, SNAP, developed to support different TRXs such as Multi-Source Agreement (MSA) OpenZR+ [29]. In the translucent network designs three QoT based regenerator placement algorithms are proposed. Additionally, super bands performance in terms of delivered capacity and costs has been investigated at the end of this thesis with a developed physical layer-aware network tool.

In this manner, as an opening step, in Chapter 2, the methodology and metrics in the physical layer, as well as the network layer, have been described. In this Chapter, the GSNR value calculation has been discussed with details in MBT scenarios in disaggregated optical networks, thus developed physical layer aware network tool's performance and its input requirements have been discussed and shown with flowcharts and Pseudo codes in details.

In Chapter 3, both transparent and translucent network design performances have been investigated/compared and showed that exploiting new bands in a transparent network design is more beneficial than using already deployed bands in the translucent network design in terms of capacity, etc.

Chapter 4 recently proposed extended bandwidth bands (super bands) networking benefits compared with regular bands in both transparent and translucent network designs in terms of capacity and interface count.

In Chapter 5, network performance in the optimized S-band has been compared with the U-band in the MBT configurations. First, the signal regeneration has been deployed in the S-band to gain the performance of this band and reach the transmission data rate to the C and L-band in the transparent network design. Then, the benefits of this band are compared with the U-band in the MBT configurations.

Finally, in Chapter 6, the conclusion is given, and possible future directions are reviewed.

This thesis introduces new ideas and concepts that include:

- Transparent and translucent network designs have been compared in the MBT configurations such as the C-, C+L, C+L+S, and C+L+S+U-band with developed physical layer aware network tool namely SNAP which can analyze every network topology.

- Capacity, energy consumption, and the number of demanded interfaces as a cost metric in different network designs in the MBT scenarios have been investigated.

- Three QoT based regenerator placement algorithms namely, "*General*", "*Power Optimized*", and "*Hybrid*" proposed to curb the costs and network energy consumption in the translucent network design while increasing the throughput of the network.

- Networking benefits of extended bandwidth bands compared with regular MBT scenarios and showed that the extended bandwidth bands deliver more capacity compared to the same number of deployed regular bands in a network.

- The utilization of U-band and S-band in different MBT combinations have been compared and it has been shown that due to having a good QoT of U-band it delivers slightly better performance rather than the S-band.

Chapter 2

Methodology and Metrics

Open System Interconnection (OSI) model consists of seven layers such as application, transport, network, data link, etc. In this model physical layer is the lowest layer and is concerned with optical fibers in the optical network systems. In this chapter, the physical layer modeling in MBT disaggregated optical networks with the impairments of this layer will be discussed separately, moreover, in the following of this chapter, the GSNR value as a QoT metric evaluated which is a crucial parameter in optical networks to establish a Lightpath (LP) between source and destination. Moving to the upper layer, the network layer, after calculation of GSNR value for each channel in the physical layer domain, we will abstract the optical network topology as a weighted graph that the weight of each link considered as a QoT of that link in each channel. In other words, the network abstraction will be done after QoT calculation. Afterward, the physical layer aware network tool developed during the Ph.D. thesis has been described along with its input requirements in the following sections.

Definitions

In this section, the frequency/wavelength ranges for different considered bands and the characteristics of different equipment have been provided here before moving to the following sections namely methodology and metrics, and physical layer parts. The optical bands, also known as the O- to U- bands (in this thesis the bands

Table 2.1 Investigated band parameters in the MBT scenarios.

Band	Wavelength[nm]	Frequency[THz]	BW[THz]	Avg. NF[dB]	Amp. P[W]	N_{ch}	Att. α[dB/km]
C	1530.38-1568.14	191.31-196.03	4.8	4.3	20 [30]	64	0.191
Super C	1525.79-1573.15	190.70-196.62	6	4.3	20 [30]	80	0.191
L	1572.24-1612.38	186.06-190.81	4.8	4.7	30 [31]	64	0.2
Super L	1577.29-1628.05	184.27-190.20	6	4.7	30 [31]	90	0.2
S1	1490.61-1526.48	196.53-201.26	4.8	6.5	30 [32]	64	0.22
S2	1490.60-1455.90	206.06-201.34	4.8	6.5	30 [32]	64	0.22
U	1668.80-1626.00	179.78-184.50	4.8	6	30	64	0.26

from the U- to S-band have been investigated), refer to specific wavelength ranges used in various applications involving optics and light-based technologies. Each band is associated with different frequency and wavelength ranges. In Table 2.1 the definitions and corresponding frequency and wavelength ranges along with the bandwidth of each band and average NF value of amplifiers and their power consumption for the U- to S-band are depicted. Moreover, regarding the fiber parameters, in this thesis, the investigated fiber is the SSMF that the attenuation value for all investigated bands has been mentioned in Table 2.1. The number of channels for each band has been considered with a symbol rate of 64 GBaud in the 75 GHz WDM grid.

2.1 Physical Layer Modeling

In the context of WDM optical networks, the physical layer refers to the transmission of data over optical fibers using different wavelengths of light. The physical layer in WDM networks includes the optical transceivers, amplifiers, and other hardware components that are used to transmit and receive the optical signals in various bands, frequency ranges, namely the C-, L-, S-band, etc. Modeling the physical layer in WDM networks involves understanding and predicting the performance of the hardware components and the transmission characteristics of the optical fibers in a single band or MBT scenarios which degrades the QoT through an LP. This can include linear and nonlinear (NLI) noises. When the degradation caused by an optical element does not depend on the power of the signals transported through the optical element, the impairment is said to be linear and can be assessed independently for the different channels (wavelengths) transiting the element. Contrarily, NLI impairments depend on the power of the signals transported, and therefore, the level of degradation on each wavelength strongly depends on the intensity of the
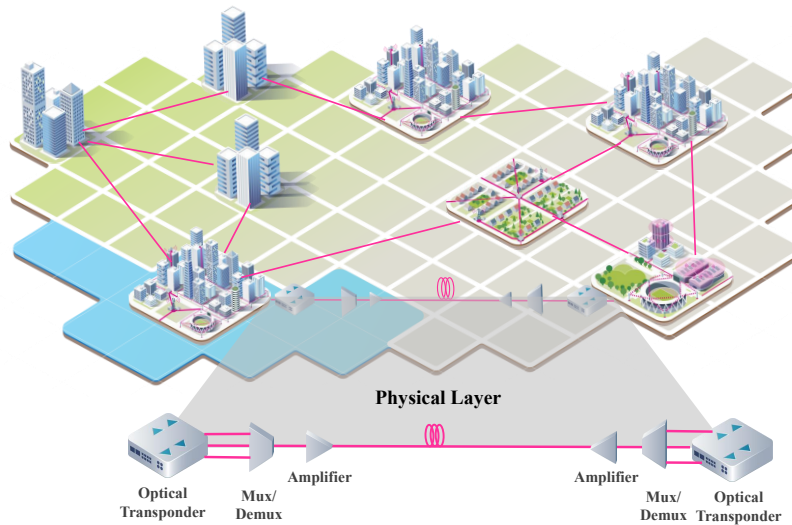
Fig. 2.1 Both network and physical layers in a WDM optical network.

optical signals carried by other wavelengths transiting an optical element [33, 34]. Consequently, physical layer modeling is important in the design and optimization of WDM networks, as it allows network designers to understand the capabilities and limitations of the hardware and the optical fibers, and to predict the performance of the network under various conditions, especially in the MBT configurations that each element has a specific characteristic in different bands. It can also be used to evaluate the trade-offs between different hardware options and to determine the optimal configuration for a given set of requirements. To this end, Fig. 2.1 has been depicted which shows the both physical and network layer in a Point to Point (P2P) WDM optical network. In the following sections of this chapter, the OLS configuration and physical layer impairments in MBT scenarios have been discussed separately with details.

2.1.1 Lightpath Configuration in MBT Scenario

Growing traffic demand in optical networks leads to the use of low-loss frequency ranges of deployed optical fibers in recent years. To this end, operators extended the capacity of the fiber many times [35] in the WDM systems. Nowadays, although WDM systems mostly use the C-band, telecom operators deployed the L-band and investigate the S-band to extend the network capacities which requires different
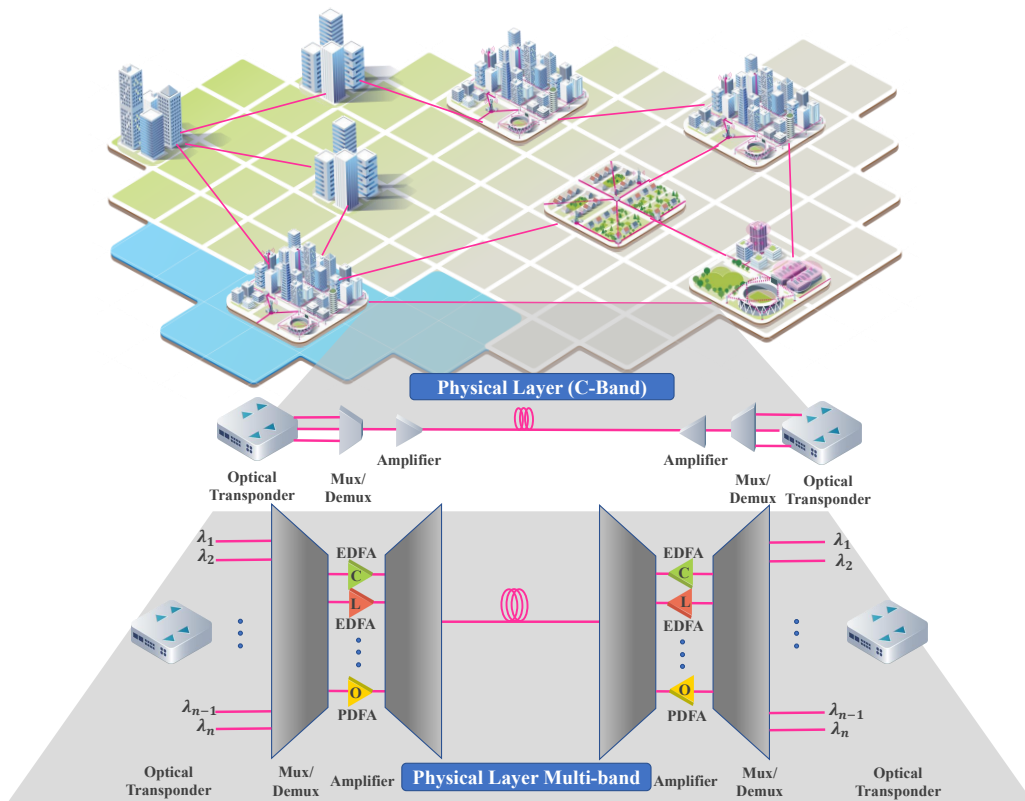
Fig. 2.2 An LP configuration in the single band and MBT configuration.

types of amplifiers for that band. In MBT scenarios, and as illustrated in Fig. 2.2, several optical amplifiers are needed at each amplification site (at least one for each transmission band). This approach is implemented to cope with the limited amplification bandwidth and maximum output power of existing optical amplifiers. Fig. 2.2 shows the LP configuration for the single C-band as well as MBT scenario. According to this figure, the utilized optical amplifiers in the C- and L-band are EDFA (the most common type of the C and L-band optical amplifiers used in optical communication systems) with average NF values of 4.3 and 4.7 dB, respectively, which operates in 1530–1565 nm and 1565–1625 nm wavelength ranges, respectively. In the S-band, however, TDFA type optical amplifier utilizes which has an average NF value of 6.5 dB in the frequency range of 1460–1530 nm. Although optical amplifiers gain the traversed signal power after a single span (usually 75/80 km), they introduce ASE noise, known as a linear noise, that degrades the signal's QoT after several spans. Due to having frequency dependent NF values for each type of amplifier, the introduced ASE noise varies in each band and frequency. In the MBT scenarios, along with ASE noise, which introduces by optical amplifiers, optical

signals inside the fiber face other effects such as NLI and SRS effect result in NLI noise which causes to degradation on the optical channels' QoT and consequently limits the optical networks throughput. In the following sections the propagation impairments (linear and nonlinear) as well as the GSNR value as a QoT metric will be discussed in detail.

2.1.2 Propagation Impairments in Optical Fibers

Optical communication systems rely on the transmission of light through optical fibers as a means of conveying information over long distances. However, during the propagation of light through the fiber, various impairments can occur, which can degrade the signal quality and limit the transmission distance. These impairments can be classified into linear and nonlinear effects. In this subsection, the main propagation impairments namely ASE, SRS, and NLI arising in the propagation of modulated data signals in an optical fiber has been discussed.

2.1.2.1 Attenuation and Losses

Telecommunications transmission systems have adopted optical fiber as the primary transmission medium for long-haul systems in order to achieve a high capacity times length product. This is due to the low attenuation of optical fiber, which is approximately <0.2 dB/km at 1550 nm. The attenuation is primarily caused by absorption, Rayleigh scattering, and loss due to geometric effects. Intrinsic Infra Red (IR) and Ultra Vilot (UV) absorption are natural properties of the glass itself and contribute to the absorption of very short and very long wavelengths [36–38]. Impurities, on the other hand, are a significant source of loss resulting from manufacturing procedures in fibers. In this thesis the standard single mode fiber (SSMF) has been considered because of its vast utilization in the optical networks infrastructures. Fig. 2.3 shows the attenuation and dispersion profile for a SSMF in different bands from the U to the S-band [39]. According to this Fig., the attenuation profile is almost less than 0.22 dB/km in the L, C, and S-band (left side *y-axis* which is blue). Moreover, the dispersion profile drops from about 25 ps/nm/km in the U-band to less than 12.5 ps/nm/km in the S-band in the frequency range of 180–205 THz (right side *y-axis* which is red). It is worth mentioning that attenuation and dispersion values are interpolated for the U-band.
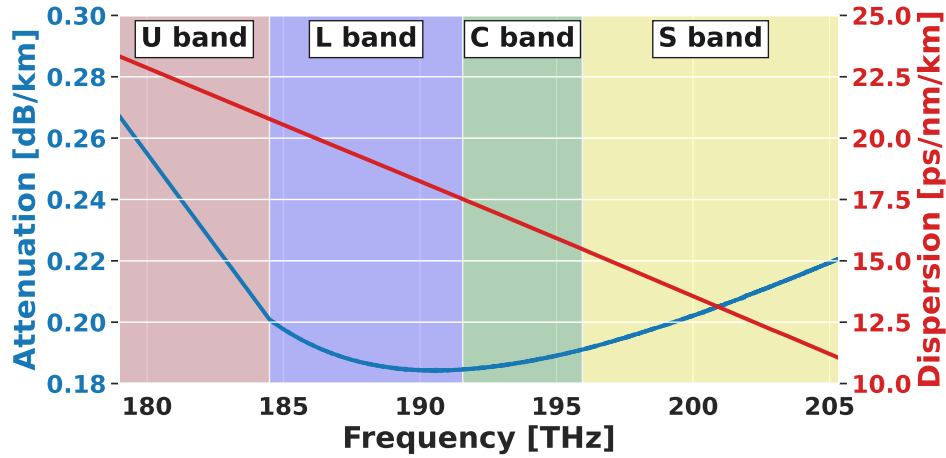
Fig. 2.3 Attenuation and chromatic dispersion profiles versus frequency for SSMF.

2.1.2.2 Amplified Spontaneous Emission (ASE)

Amplified Spontaneous Emission (ASE) noise is a type of noise that can affect the performance of WDM optical networks. ASE noise is a result of the spontaneous emission of photons from an optical amplifier, which is amplified along with the intended signal. In WDM optical networks, multiple signals at different wavelengths are combined and transmitted through a single optical fiber. Each signal is amplified by an optical amplifier, which is typically an EDFA in the C and L-band and TDFA in the S-band amplifier. When an optical amplifier is used to amplify multiple signals in a WDM network, ASE noise is generated, which can be modeled as an Additive White Gaussian Noise (AWGN) with a power spectral density (PSD) G_{ASE}, due to the spontaneous emission of photons from the amplifier.

$$G_{ASE} = hf_0F(G-1) \tag{2.1}$$

where h, f_0, F, and G are the Planck constant, the central frequency of the amplified channel, amplifier noise figure, and amplifier gain in linear units, respectively. It is worth mentioning that Eq. 2.1 is valid only for the EDFA amplifiers type and for other types of amplifiers such as hybrid Raman-EDFA amplification it has been demonstrated in [40–42]. Moreover, the NF profile for a commercial amplifier has been depicted in Fig. 2.4. In this thesis, the U-band NF value has been assumed about 6 dB, due to the lack of commercial availability of the U-band amplifier. However, for other bands the NF value in the C, L, and S-band the average NF values are about 4.3,
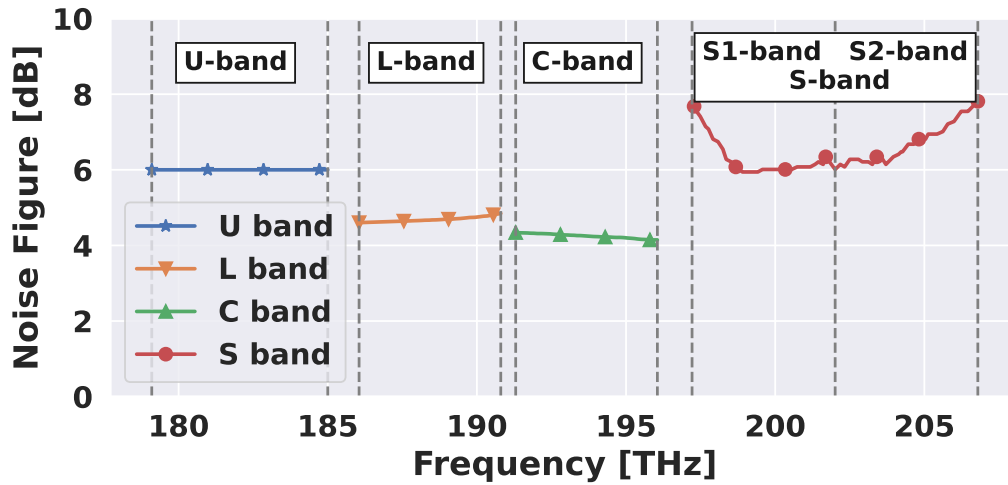
Fig. 2.4 NF for the U-, L-, C-, and S-band optical amplifiers.

4.7, and 6.5 dB in the C, L, and S-band, respectively. This noise is amplified along with the intended signals, which can cause interference and degrade the performance of the network. The amount of ASE noise depends on several factors, including the type of amplifier used, the number of channels in the network, and the optical power levels. To minimize the impact of ASE noise in WDM networks, several techniques can be used. For example, an optical band-pass filter can be used to remove unwanted noise from the amplifier output. Additionally, the optical power levels can be optimized to reduce the amount of ASE noise generated in the first place.

2.1.2.3   Stimulated Raman Scattering (SRS)

Stimulated Raman Scattering (SRS) [40, 43] is caused by the interaction of light with molecular vibrations. Light incident on the molecules creates scattered light at a longer wavelength than that of the incident light. A portion of the light traveling at each frequency in a Wan-active fiber is downshifted across a region of lower frequencies. The light generated at the lower frequencies is called the Stokes wave. The range of frequencies occupied by the Stokes wave is determined by the *Raman gain spectrum* [1] which covers a range of around 40 THz below the frequency of the

---

[1] the Raman gain spectrum typically describes the measured Raman gain coefficient for silica fibers as a function of the frequency shift at a pump wavelength of 1.0 pm.
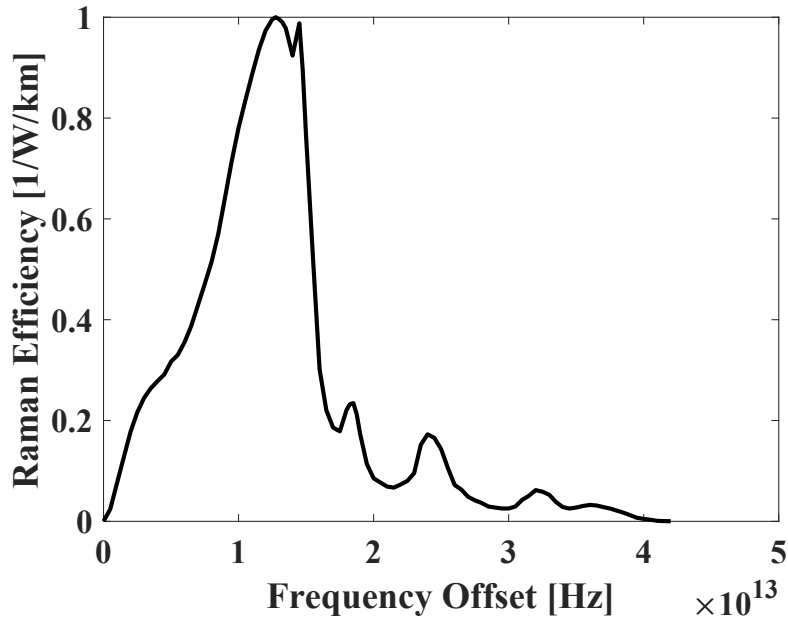
Fig. 2.5 The normalized Raman efficiency vs the frequency distance for a typical optical fiber.

input light. In Fig. 2.5 the Raman gain spectrum has been depicted for a SSMF. In silica fiber, the Stokes wave has a maximum gain at a frequency of around 13.2 THz less than the input signal. The fraction of power transferred to the Stokes wave grows rapidly as the power of the input signal is increased. Under very high input power, SRS will cause almost all of the power in the input signal to be transferred to the Stokes wave. In MBT systems which is our main focus in this thesis, the shorter-wavelength channels will lose some power to each of the higher-wavelength channels within the Raman gain spectrum. To reduce the amount of loss, the power on each channel needs to be below a certain level [44, 45].

2.1.2.4   Kerr Effect

The Kerr effect [40, 46] is a non-linear optical phenomenon where the refractive index of material changes with the intensity of light passing through it. In the context of WDM optical communications systems especially in the MBT configurations due to having different signal powers in each band, the Kerr effect can have significant impacts on the QoT of the transmitted signal. The nonlinear coefficient *gamma* of the

optical fiber, which is commonly reported in units of *mathrm*$1/W/km$, is a common approach for quantifying the Kerr effect in a systematic manner. This coefficient can be used to calculate the Kerr effect's impact on optical signal transmission through fiber, and the greater the value of *gamma*, the more pronounced the Kerr effect. The *Manakov* equation is useful for gaining full knowledge of the distortions generated by the Kerr effect in an WDM transmission configuration. This equation governs the behavior of WDM signals in optical fibers when the polarization dependence of the propagation constant (also known as birefringence) can be disregarded. Examining the *Manakov* equation can provide valuable insights into the impact of the Kerr effect on the transmission of WDM signals through optical fibers.

$$\frac{\partial E(z,t)}{\partial z} = -\alpha E(z,t) - j\frac{\beta_2}{2}\frac{\partial^2 E(z,t)}{\partial t^2} - j\gamma\frac{8}{9}E^\dagger(z,t)E(z,t)E(z,t) \qquad (2.2)$$

Here, β_0 and β_1 coefficients have been neglected since they carry a constant phase shift and a propagation delay. The dispersion slope term β_3 has been neglected for simplicity. The first and second terms describe the field loss and the chromatic dispersion in Eq. 2.2, respectively, which depend on the utilized optical fiber in a networking system. On the other hand, the third component is the Kerr effect term depending on the WDM signal power. $E(z,t) = [E_x(z,t), E_y(z,t)]^T$ is the WDM field Jones vector of the WDM signal and $E^\dagger(z,t)E(z,t) = |E(z,t)|^2$ its power, where $\dagger$ stands for the Jones vector conjugate transpose. The WDM signal $E(z,t)$ can be thus conveniently expressed as the sum of the optical fields complex envelopes of its N_{ch} tributary channels $E_k = [E_{k,x}(z,t), E_{k,y}(z,t)]^T$, each modulated at its central angular frequency $\omega_k = 2\pi f_k$. Since the Kerr effect is a nonlinear phenomenon that occurs when the refractive index of a material varies with the intensity of the light passing through it. This effect can cause pulse broadening and distortion due to self-phase modulation (SPM) and cross-phase modulation (XPM). SPM is a nonlinear effect that causes the pulse to broaden due to the self-phase shift induced by the Kerr effect. XPM, on the other hand, is a nonlinear effect that causes a phase shift in one signal due to the intensity of a different signal passing through the same fiber. Four-wave mixing (FWM) is another nonlinear phenomenon that occurs when two or more optical signals interact with each other to produce new signals. FWM can cause spectral broadening and crosstalk between channels in wavelength-division multiplexing (WDM) systems.

SPM

SPM is caused by the interaction of the optical signal with the fiber material. The Kerr effect causes the refractive index of the fiber to vary with the intensity of the light passing through it. When a high-intensity optical signal passes through the fiber, the Kerr effect causes the refractive index to increase, which results in a reduction in the group velocity of the signal. As a result, the optical pulse experiences a frequency shift that leads to phase modulation, which is known as self-phase modulation. SPM can cause pulse broadening and distortion. When a high-intensity optical pulse passes through the fiber, the Kerr effect causes the refractive index of the fiber to change, which results in a change in the phase of the pulse. This change in phase leads to a change in the group velocity of the pulse, causing it to broaden in time. As a result, the optical pulse becomes longer, which can reduce the data rate and limit the transmission distance. SPM can also cause spectral broadening, which can result in crosstalk between channels in WDM systems. When an optical signal passes through the fiber, the Kerr effect causes the refractive index to change, resulting in a frequency shift. This frequency shift can cause the signal to overlap with neighboring channels, resulting in crosstalk.

XPM

XPM is caused by the Kerr effect, which is a nonlinear effect where the refractive index of the fiber varies with the intensity of the light passing through it. When two or more optical signals pass through the fiber simultaneously, the Kerr effect causes the refractive index to vary, resulting in a phase shift between the signals. The phase shift can be either positive or negative, depending on the intensity and wavelength of the signals. XPM can cause spectral broadening and crosstalk between channels in WDM systems. When two or more optical signals pass through the fiber simultaneously, the Kerr effect causes the refractive index of the fiber to vary, resulting in a frequency shift. This frequency shift can cause the signals to overlap with neighboring channels, resulting in crosstalk. XPM can also cause signal distortion and degradation. When two or more optical signals pass through the fiber simultaneously, the Kerr effect can cause the signals to interfere with each other, resulting in signal distortion. This distortion can result in errors in the transmitted data and reduce the signal quality.

FWM

FWM is caused by the Kerr effect, which is a nonlinear effect where the refractive index of the fiber varies with the intensity of the light passing through it. When two or more optical signals pass through the fiber simultaneously, the Kerr effect causes the refractive index to vary, resulting in a phase shift between the signals. This phase shift can cause energy to transfer from one signal to another, resulting in FWM. FWM can cause crosstalk and signal degradation in optical communication systems. When multiple optical signals pass through the fiber simultaneously, FWM can cause energy to transfer from one signal to another. This energy transfer can cause crosstalk between channels and degrade the signal quality, resulting in errors in the transmitted data. FWM can also cause spectral broadening, which can reduce the channel spacing in WDM systems. This reduction in channel spacing can limit the number of channels that can be transmitted over the fiber and reduce the system's capacity.

2.1.3   GSNR as a metric of QoT

The accurate modeling of signal propagation along an optical fiber, especially in MBT scenarios, requires that the frequency dependence of the fiber parameters (mainly fiber attenuation and chromatic dispersion) is taken into account. As an example, both attenuation and chromatic dispersion dependence on frequency for a SSMF are depicted in subsec. 2.1.2.1 Fig. 2.3 (in this subsection it has been abbreviated in Fig. 2.6). In the C- and L-band, the attenuation coefficient of an SSMF is usually <0.2 dB/km whereas it may reach ~0.22 dB/km in the S-band and further increases up to 0.27 dB/km in the U-band (refer to Fig. 2.3). Additionally, the SRS that described in subsec. 2.1.2.3, a nonlinear effect that causes power transfer from higher to lower frequency signals [47] and that can be mostly neglected in C-band only systems, must be taken into account in MBT systems due to the much broader transmission spectrum. The optical power transfer due to SRS will add on top of the higher fiber loss in the S-band causing this band to have lower QoT than the C- and L-band. Contrarily, despite having a higher fiber loss than the other spectral bands, the U-band benefits from the effect of SRS, receiving optical power from the data channels transmitted in the higher frequency bands. In this thesis, the QoT at the end
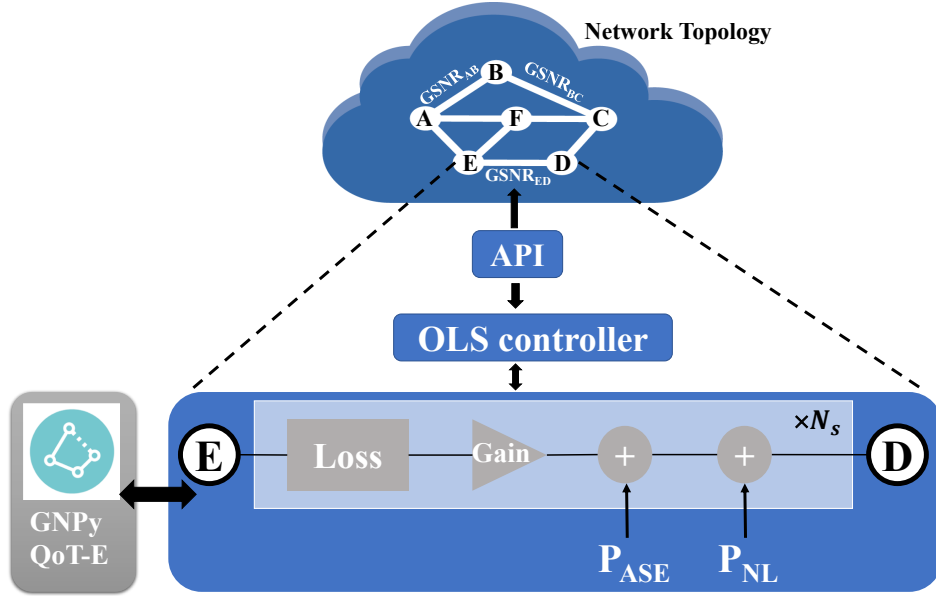
Fig. 2.6 Optical line system abstraction in a disaggregated approach.

of each fiber span for the i-th channel is computed using the GSNR [48]:

$$\text{GSNR}_i = \frac{P_{S,i}}{P_{\text{ASE},i} + P_{\text{NLI},i}} = \left(\text{OSNR}_i^{-1} + \text{SNR}_{\text{NL},i}^{-1}\right)^{-1}, \qquad (2.3)$$

where $P_{S,i}$ is the span input power, and OSNR_i and $\text{SNR}_{\text{NL},i}$ are the optical signal-to-noise ratio and nonlinear signal-to-noise ratio, respectively. In this case, we are assuming that the LPs optical performance degradation results from two main contributors: the ASE noise and the nonlinear interference (NLI) noise introduced by optical amplifiers and fiber propagation, respectively. Both effects can be approximated as Gaussian disturbances for most of the relevant transmission scenarios. The ASE noise power ($P_{\text{ASE},i}$) is given by eq. 2.1. The NLI power ($P_{\text{NLI},i}$) contribution is computed using the Generalized Gaussian Noise (GGN) model [49], which takes into account the effects of spectral and spatial variations of fiber loss and the SRS-induced inter-channel power cross-talk. Finally, following a disaggregated abstraction of the physical layer [50, 51], the total QoT of an LP l is computed by:

$$\text{GSNR}_{i,l} = \frac{1}{\sum_{s \in l}(\text{GSNR}_{i,s})^{-1}}, \qquad (2.4)$$

which depends on the GSNR of each fiber span *s* traversed by the LP under test. The open-source GNPy library [52] implements the described QoT estimation methodology. Given the extensive use of this library, it is now a robust implementation of the methodology and, therefore, it is used in this thesis.

In MBT scenarios, and as illustrated in Fig. 2.2, several optical amplifiers are needed at each amplification site (at least one for each transmission band). This approach is implemented to cope with the limited amplification bandwidth and maximum output power of existing optical amplifiers. For the same reason, we assume also the split of the S-band into two identical sub-bands: here named S1- and S2-band, to lessen the requirements on the S-band amplifier. By following this approach, two optical amplifiers are used in the S-band, one for each sub-band, whose required amplification bandwidth and output power should be similar to the ones of the C- and L-band optical amplifiers. EDFA provide enough amplification in C- and L-band. However, their performance degrades significantly when used in other transmission bands, and, therefore, different doping materials are required in these cases [9]. Thus, we consider lumped EDFA amplification for the C- and L-band, and the use of a benchtop TDFA for the S-band, characterized as reported in [53]. Average NFs of 4.3 dB, 4.7 dB, and 6.5 dB are assumed for the C-, L-, and S-band optical amplifiers, respectively. The TDFA shows a higher NF mainly because of the not yet fully mature technology. Similarly, optical amplifiers for the U-band are still in an early stage of development and, therefore, reliable characterization data is still hard to obtain. In this thesis, we assume that the U-band optical amplifiers can be approximated by a flat NF of 6.0 dB. The resulting noise figure as a function of frequency is illustrated in Fig. 2.4. As also highlighted in Fig. 2.2, the transmission bands in a MBT system need to be separated/combined before/after optical amplification. In this thesis, Consequently, MBT leads to increased insertion losses when compared to single-band transmission, resulting from the multiplexing and demultiplexing of the different bands (which are assumed to be of 1 dB for each operation [54, 55]). Additionally, a guard band of 0.5 THz is also set between each band. Fig. 2.7 depicts the GSNR profile after transmission of 64 channels with a symbol rate of 64 GBaud in the 75 GHz WDM grid along a single 75 km ITU-T G.652D optical fiber span (whose attenuation and chromatic dispersion are modeled as shown in Fig. 2.3 and with a nonlinear fiber coefficient of 1.27 W^{-1}/km, for all four MBT scenarios considered in this thesis. Please note that MBT should be seen as a future-looking solution to tackle traffic growth; consequently, the use of at least

current state-of-the-art TRXs should also be assumed in combination with MBT. Thus, this assumption corresponds to using 64 Gbaud TRXs and the corresponding channel spacing of, at least, 75 GHz. In the following subsections the GSNR value for each investigated MBT scenario has been discussed and the GSNR values for each case have been depicted.

2.1.3.1   QoT in MBT scenario

In this subsection the GSNR value has been evaluated for the regular bands in the MBT scenarios namely: (i) C-band only; (ii) C+L-band; (iii) L+C+S1+S2-band; and (iv) U+L+C+S1+S2-band. The launch power is optimized for each MBT scenario separately, targeting the QoT maximization in all bands. The local-optimization, global-optimization (LOGO) [56] approach is used to compute the starting point of the launch power per channel in each band. In this case, a per-channel launch power of 0.6, 1, and 2.9 dBm is estimated for the C-, L- and U-bands, respectively, whereas 1.4 and 1.7 dBm are estimated for S1 and S2 within the S-band, respectively. Starting from these initial estimates, and as described in [57], we then run a multi-evolutionary algorithm to find the optimum average launch power and tilt that maximizes the average GSNR in each band while still maintaining an acceptable GSNR flatness. Comparing the reference case (C-band only transmission) with C+L-band transmission, Fig. 2.7 shows that the latter presented a GSNR decrease of about 1 dB in the C-band. This degradation of optical performance results from the SRS effect, which transfers power from the C-band into the L-band. Consequently, higher ASE noise is added to the C-band by optical amplifiers when recovering the signal power. Regarding the L-band, the best GSNR is attained for the C+L+S1+S2-band transmission scenario, as a consequence of receiving power from all other bands. In this case, smaller ASE noise is added by optical amplifiers when compensating for the link loss. Similarly, Fig. 2.7 show also that in the C+L+S1+S2+U-band transmission scenario, the performance of C-band can be significantly impacted, presenting a GSNR penalty of about 2 dB, mainly due to the power transfer from the C-band to the U-band. The average GSNR value in each band for each considered MBT scenario is presented in Table 2.2. The average is computed among all channels within the band, also for a single span of 75 km. As expected, the best QoT is achieved in the C- and L-band. Moreover, the S-band is the one showing the worse QoT, mainly as a consequence of power depletion caused by the SRS effect. Indeed, the GSNR attains
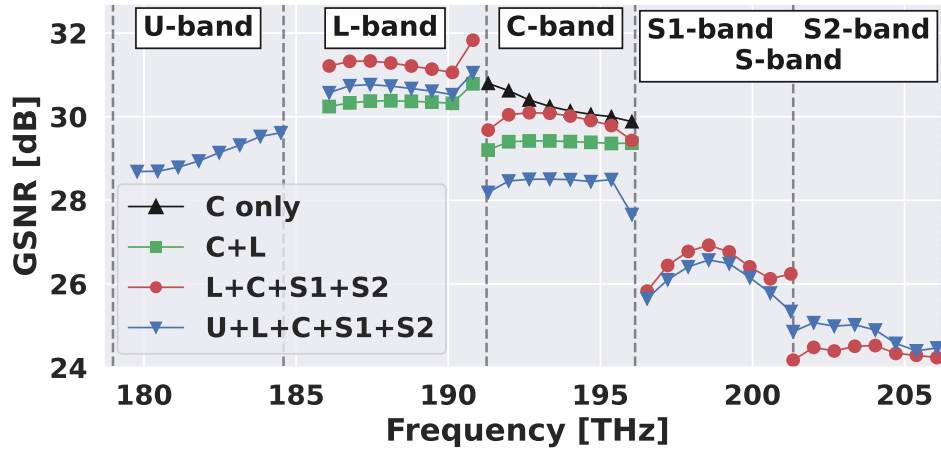
Fig. 2.7 GSNR value for a single span of 75 km in the MBT scenarios.

Table 2.2 Average GSNR [dB] for different MBT scenarios.

Scenario	N_{ch}	U	L	C	S1	S2
C only	64	–	–	30.25	–	–
C+L	128	–	30.37	29.38	–	–
L+C+S1+S2	256	–	31.28	29.94	26.48	24.38
U+L+C+S1+S2	320	29.08	30.69	28.42	26.13	24.79

almost 31 dB in the best performing LP in the C-band only transmission scenario, whereas it decreases to about only 25 dB in the best performing LP in the S2-band. The dependence of the QoT, in each band, on the actual MBT scenario is also clear from this set of results, where it is shown that the optical performance of each band may increase or decrease depending on the activation status of the neighbor bands. Interestingly, only a small variation of the QoT within each band is usually obtained independently of the considered MBT scenario, which might potentially reduce the complexity of routing and spectrum assignment algorithms. After the QoT of the LP is computed, the SDN controller (depicted in Fig. 2.11) can determine the most spectrally efficient modulation format that can be used based on the obtained GSNR. In order to gain the network throughput by utilizing the maximum efficiency of the already deployed devices, super bands have been proposed compared to the regular bands which have a higher bandwidth in comparison to the regular bands. In the next subsection, the GSNR value is computed for the super bands and compared with the regular bands GSNR value, and in the next chapters the network capacity of these scenarios have been compared together.
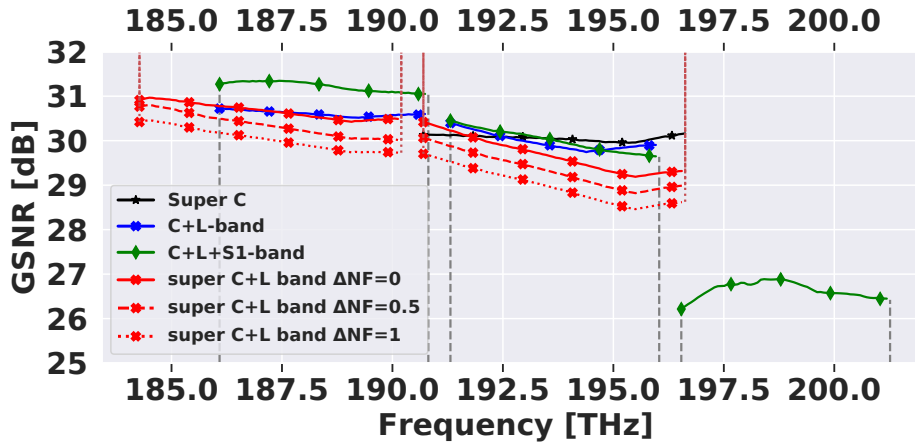
Fig. 2.8 GSNR value for a single span of 75 km in the MBT scenarios for regular and super bands.

2.1.3.2   QoT in the super bands

In this subsection the GSNR value as a QoT metric has been evaluated for the regular and MBT scenarios. Here as well, We make use of EDFA for all super and regular C- and L-bands, with one device for each band, and a TDFA is used for the S1-band [9] with the same average NF values in the subsec. 2.1.3.1. For any NF values lying outside the experimental data, especially for the super bands, an interpolation was performed to generate any required additional values. Moreover, in this subsection's MBT scenarios, we include an insertion loss penalty due to multiplexing and demultiplexing of the signals equal to 1 dB [54, 55]. The MBT scenarios investigated are: (1) super C-band only, (2) regular C+L-band, (3) super C+L-band, with three different NF values, and (4) regular C+L+S1-band. The three super C+L-band NF values, denoted with ΔNF, are equal to, 0.5 dB higher, and 1 dB higher than the regular C+L-band NF; these values were considered to investigate the impact of amplifying a wider bandwidth by the same device. Fig. 2.8 shows the GSNR profile after transmission for these scenarios; with 64 channels for the regular bands and 80 channels for the super bands, over a single span of ITU-T G.652D fiber with a length of 75 km. ITU-T G.652D fiber type has been considered for all investigated scenarios with loss values always below 0.21 dB/km and chromatic dispersion ranging from 13 to 21 ps/nm/km. Concerning launch power optimization, an approach was implemented that achieves a trade-off between flatness and maximum average GSNR for transmission in the MBT scenarios. As a

Table 2.3 Parameters used for each scenario under investigation, along with average GSNR.

Scenario	Nch	L			C			S1		
		Tilt [dB/THz]	AVG. Pow. [dBm]	GSNR [dB]	Tilt [dB/THz]	AVG. Pow. [dBm]	GSNR [dB]	Titlt [dB/THz]	AVG. Pow. [dBm]	GSNR [dB]
Super C	80	–	–	–	0.3	-1.4	30.0	–	–	–
C+L	128	0.5	-0.7	30.6	0.3	0.6	29.9	–	–	–
C+L+S1	192	0.6	-2.4	31.2	0.6	-0.8	30.0	0.2	1.9	26.6
Super C+L ΔNF=0	160	0.3	-1.0	30.6	0.3	0.4	29.6	–	–	–
Super C+L ΔNF=0.5	160	0.2	-1.0	30.5	0.4	0.6	29.3	–	–	–
Super C+L ΔNF=1	160	0.2	-0.8	30.0	0.4	0.8	28.9	–	–	–

starting point, the local-optimization, global-optimization (LOGO) [56] approach has been used to compute the average launch power per channel for each band separately, without considering additional propagation effects. This approach calculates the optimally flat power per band by considering the average amplifier gain and NF values, using these to find the optimal working point of the system under investigation. We then used a multi-evolutionary algorithm [58] to improve these values and apply an optimal tilt. Table 2.3 presents the tilt, average power per channel, and average GSNR values for each configuration, whereas Fig. 2.8 depicts the GSNR as a function of frequency. Comparing the super C band scenario to that of the regular C+L-band scenario, it is visible that SRS effects cause a GSNR decrease in the C-band of the latter, reducing the overall QoT. However, in the C+L+S1-band system, the average GSNR in the C- and L-bands has increased as a result of power transfer from the S1-band. Additionally, both Fig. 2.8 and Tab. 2.3 show that, as expected, increasing the NF penalty lowers the average GSNR, which is visible when comparing the three super C+L-band cases.

2.2   Network Layer

After evaluation of the GSNR value as a QoT metric in the physical layer by using GNPy [28, 59], in this section, in the network layer, we will be able to abstract the network topology as a weighted graph that the weight of each link is the QoT of that link. Thus, the abstracted network topology will be fed to the developed physical layer-aware network tool (the flowchart has been provided and described in the following sections) which can analyze any provided network's performance in terms of capacity and energy consumption, etc.

2.2.1   The Abstraction of Optical Network

The availability of DSP-based coherent transmission and the potential for an all-optical network [60, 61], at least within the same network domains, as a result of the development of optical amplifiers and ROADMs and have significantly altered the operational scenario enabling elastic and transparent optical networking [62, 60]. Due to the availability of hybrid modulation format and flexible rate transceivers [63], optical channels may be dynamically built and changed in this circumstance so that they can adapt to the time-varying traffic pattern in a timely manner [61] [46]. Knowing the limitations of the physical layer has become essential to creating a LP between two network nodes since the WDM transport layer now mostly functions in the optical domain. Due to the availability of hybrid modulation format and flexible rate transceivers [63], optical channels may be dynamically built and changed in this circumstance so that they can adapt to the time-varying traffic pattern in a timely manner [61].

The abstracted network is the one of main input parameters of the developed physical layer aware network tool (SNAP). After getting the GSNR value (refer to Sec.2.1.3) for each wavelength in the single band/MBT scenarios for each band the network topology abstracts as a weighted graph that the weight of each link is equal to the GSNR value of each link in the corresponding wavelength(s). Optical network abstraction is a modeling technique used to simplify the complex nature of optical networks topologies. In this abstraction, the optical network is modeled as a collection of light paths, with each path having a specific GSNR value. The GSNR value of a light path is a measure of the quality of the optical signal transmitted over that path. A higher GSNR value indicates a stronger signal and lower levels of noise, which translates to better transmission quality and higher data rates. Moreover, one approach to RWA is the use of waveplanes, which are virtual layers that represent the wavelengths available for transmission in the network. By creating waveplanes, network engineers can visualize the available wavelengths and their potential routes, allowing them to choose the optimal route for each light path. The use of waveplanes in RWA provides a powerful tool for optimizing optical network performance. By visualizing the available wavelengths and routes, network engineers can choose the most efficient paths for each light path, which can result in lower latency, higher throughput, and improved network reliability. Overall, the optical network abstraction with GSNR value of each light path and waveplanes for RWA

provides a powerful approach to designing, analyzing, and optimizing high-speed optical networks.
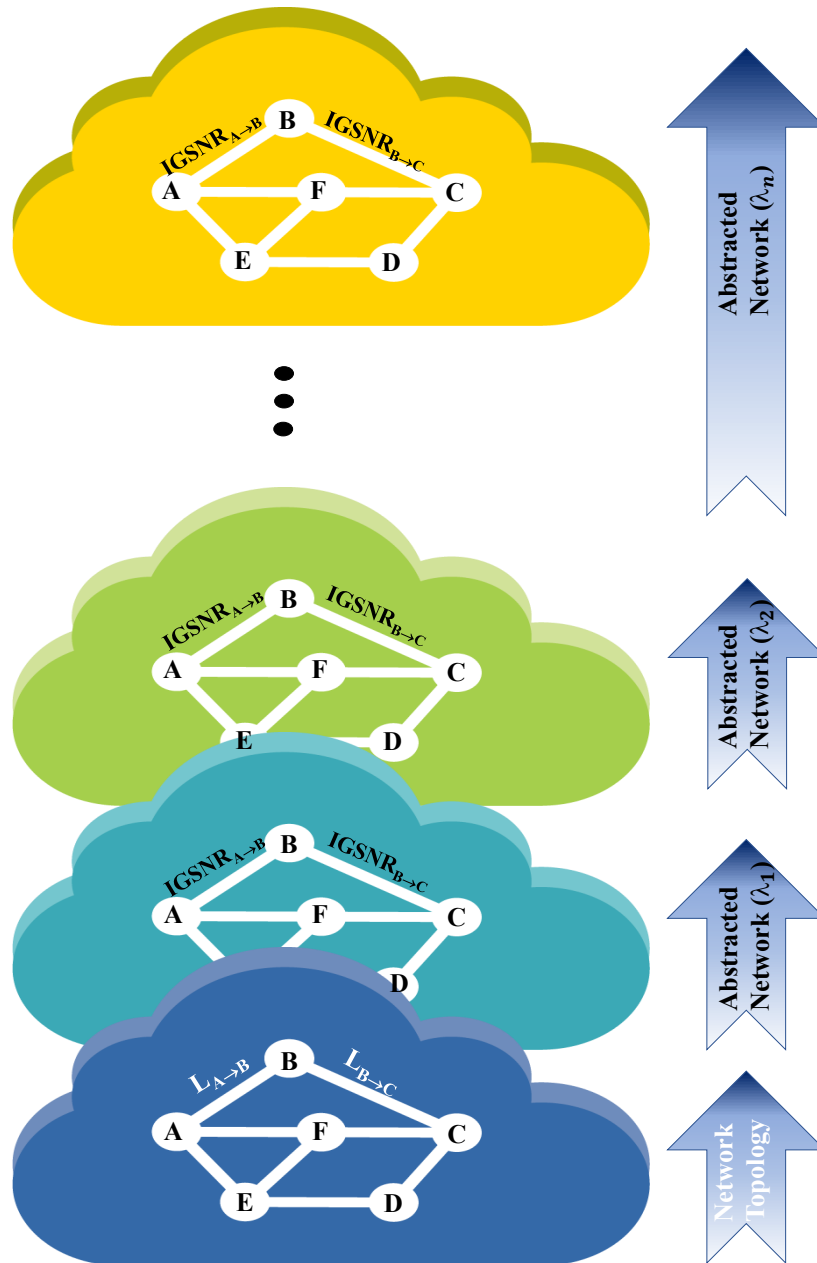
Fig. 2.9 The model of a network topology and abstracted network with IGSNR of each link for each WDM wavelength.

Fig. 2.9 shows an example of optical network topology abstraction and creating waveplanes for all available wavelengths in a scenario under investigation. To

be more clear, assume that the optical network topology under investigation is in the blue cloud, and the length of each edge (OLS) in the graph is equal to the $L_{\text{source node} \rightarrow \text{destination node}}$ (i.e $L_{A \rightarrow B}$ [km]). Thus, in order to create the waveplanes, after evaluation of GSNR of each channel (described in the previous sections) the GSNR of all LPs between all source and destination nodes can be evaluated for the corresponding channel. Fig. 2.9 illustrate the created waveplanes for each wavelength/channel (λ_1 to λ_n) in a simple optical network topology.

2.2.2 Statistical Network Assessment Process (SNAP)

In this section, the flowchart of the developed physical layer-aware network tool has been described. Figure 2.10 presents the SNAP flowchart that has been used to statistically test the network, which is a Monte Carlo (MC) based procedure comprising two main parts. The first part, shown in Fig. 2.10, is the high-level workflow view containing the input variables, such as the traffic pattern, network abstraction, interface parameters (TRX parameters), and routing space. SNAP works with progressive traffic loading [61]. In this case, different traffic patterns can be selected by changing the joint probability density function (JPDF) of the nodes. For example, uniform or population-based (nonuniform) JPDF can be chosen [64]. As shown in Fig. 2.10, the network abstraction is performed using GNPy, which provides a weighted graph corresponding to the QoT per channel. The k-shortest path algorithm is then used to find the first k shortest paths among all source and destination node pairs. The user can set the k_{max} base on its work. In this thesis k_{max} value considered equal to 5 ($k_{max} = 5$). The MC simulation starts after defining all input variables. This simulation approach relies on repeated random sampling to obtain numerical results. In order to compute networking metrics with high confidence, a total of ≥ 1000 MC iterations can be considered. For network analysis, the SNAP can load the network with different traffic request sizes such as 100 and 400 Gb/s. As a consequence, the capacity of some LPs may not be immediately fully exploited when setting up a new traffic demand, i.e., when the available QoT allows creating a LP with a capacity higher than the one requested by the new demand, especially for the small traffic request sizes such as 100 Gb/s. Hence, as shown in Fig. 2.10, SNAP verifies if there is any existing LP with the same source and destination nodes with enough spare capacity to support the new request before creating a new LP. If spare capacity is found, the new traffic demand will use the
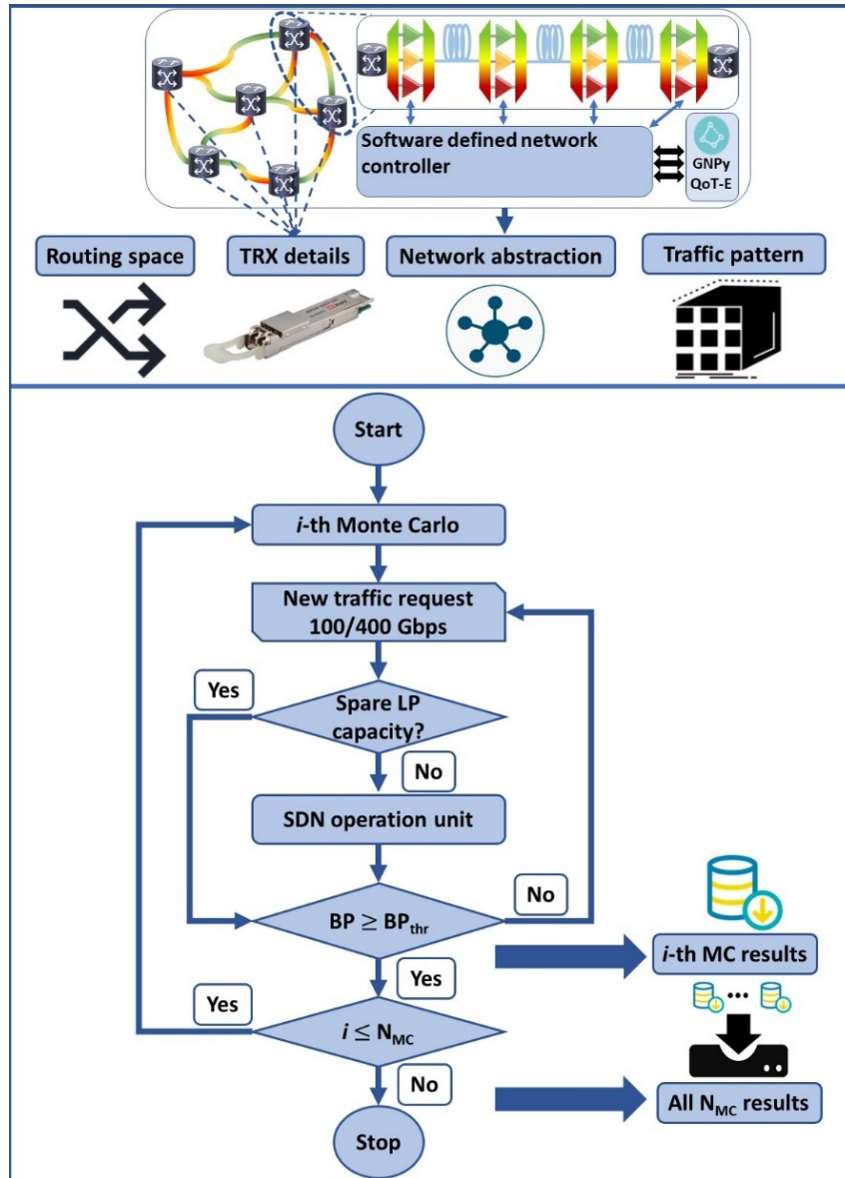
Fig. 2.10 The SNAP framework flowchart with its input requirement parameters.
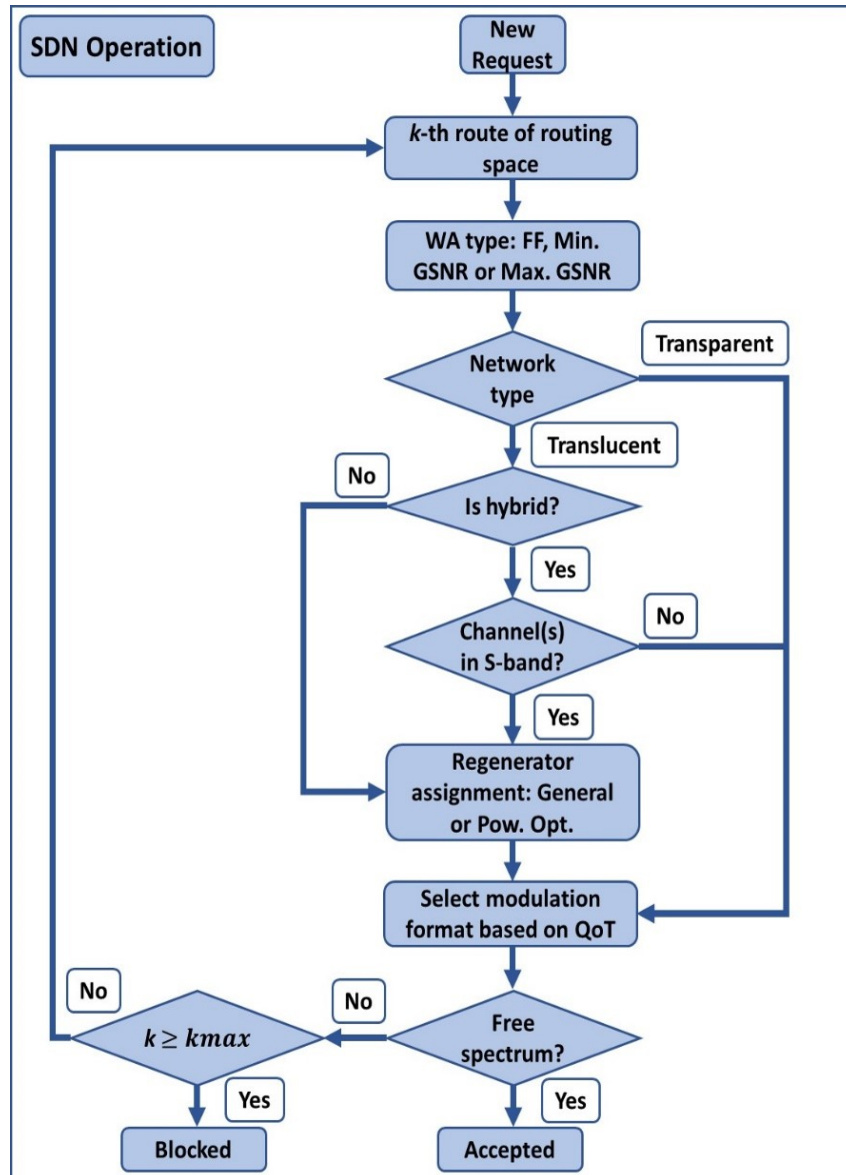
Fig. 2.11 The flowchart of SDN operation unit of SNAP.

already deployed LP, avoiding the increase in cost and power consumption associated with creating new LP(s). Otherwise, the SDN operation unit (Fig. 2.11) will try to establish a new LP based on the network design strategy and the routing, and wavelength assignment (RWA) policies. In case a new LP needs to be established, the SDN operation unit starts to do the wavelength assignment from the first shortest path, according to the wavelength assignment policy chosen. The policies tested in our framework are described in Section 2.3.1. Then, the SDN unit selects the best (highest capacity) available modulation format based on the QoT. Afterward, it assesses if there are resources available to serve the traffic request with the selected modulation format. Please note that the SDN unit is also responsible for selecting the nodes where LP regeneration takes place in a translucent network design. Different algorithms can be used in this case. The ones considered in this work are described in Section 2.3.2. Particularly, a hybrid network design, where regeneration is only considered for the channels within a spectral band with low QoT (S-band in our case), is also considered in this thesis. The network blocking probability (BP) is evaluated after routing each traffic demand. If it exceeds a given threshold ($\mathrm{BP}_{thr} = 20\%$ in our case), the current MC iteration is concluded. In that case, the network simulation data is stored and a new MC iteration begins, continuing until the total number of iterations is performed.

2.2.3 Traffic Distribution

According to Fig. 2.10, it is observable that the SNAP supports two different types of traffic distributions such as *uniform* and *nonuniform* ones which can load the network progressively. In the uniform traffic distribution, the JPDF of all nodes are equal. However, in the nonuniform case, the JPDF of nodes depends on the population of that node/city in the network topology. To be more precise the probabilities, $P(s,d)$, of a source-destination node pair to be chosen in the uniform and nonuniform JPDFs, respectively, are given by

$$P(s,d) = \frac{1}{N(N-1)} \tag{2.5}$$

$$P(s,d) = \frac{pop_s \cdot pop_d}{\sum_{(i,j)\in A} pop_i \cdot pop_j} \tag{2.6}$$
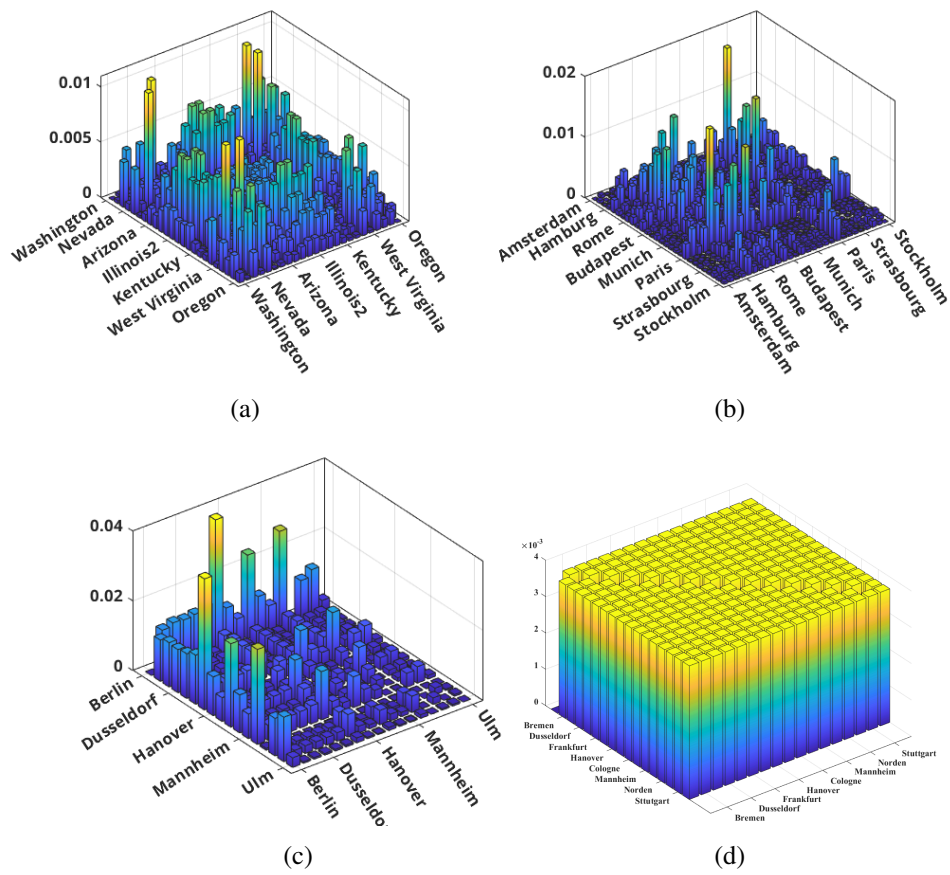
Fig. 2.12 a) US-NET and b) European Cost c) DT network topologies Nonuniform, and d) DT network topology's uniform JPDF.

where N is the total number of nodes in the considered network topology, pop_x is the population of the city geographically located in node x, and $(i, j) \in A$ represents all possible source-destination nodes pairs (i, j) in the network topology A. Fig. 2.12d represents the uniform traffic's JPDF in the DT network topology, and Figs. 2.12a, 2.12b, and 2.12c represents the nonuniform JPDF profile for all US-NET, European COST, and DT network topologies.

2.2.4   Routing and Wavelength Assignment (RWA)

As already explained in Chapter 1, One technology that has helped in meeting the traffic demand is the WDM technology. WDM technology allows for the transmission of multiple wavelengths of light over a single optical fiber. The use of WDM technology has helped in increasing the bandwidth of optical fiber from 4.8 THz in the C-band to the $\approx$10 THz in the C+L-band, which is vital in meeting the increasing demand for bandwidth. One critical aspect of WDM technology is the routing and wavelength assignment (RWA) algorithm, which plays a crucial role in managing the traffic on the network. This section will explore the RWA algorithm in WDM optical networks, focusing on the LP, wavelength continuity, and constant wavelength.

Lightpath (LP)

A LP is a connection established between two ROADMs/nodes in an optical network. It is the optical equivalent of a circuit in an electronic network. LPs are essential in optical networks as they provide a dedicated connection between nodes, and this ensures that there is no contention for bandwidth. LPs are established using a wavelength, and the RWA algorithm is responsible for determining which wavelength to use. When a connection is requested between two nodes, the probabilities of node pairs defines by the JPDF which are already described in the previous section, the RWA algorithm searches for a free wavelength that can be used to establish the connection. If no free wavelength is available, the RWA algorithm must select a wavelength that is already in use, which means using the vacant capacity of already established LPs with the same source and destination (supported by developed SNAP, refer to the Sec. 2.2.2), but the selection must not cause interference with other connections that are already established.
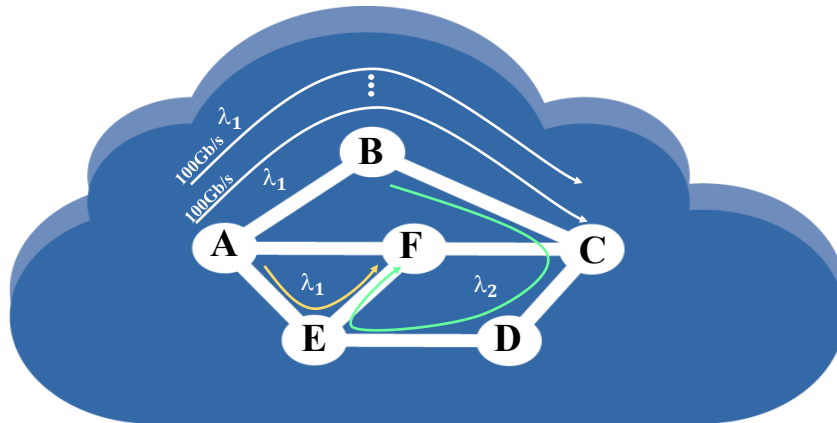
Fig. 2.13 RWA example with traffic grooming which is utilized in this thesis in an optical network.

Wavelength Continuity

Wavelength continuity is the property of the RWA algorithm that ensures that a connection between two nodes is established on the same wavelength throughout the entire path. This property is essential as it helps in minimizing the number of wavelengths used in the network. The use of the same wavelength throughout the path also helps in reducing the complexity of the network and simplifies the management of the network. The RWA algorithm achieves wavelength continuity by searching for a free wavelength in the same wavelength range as the one used for the previous hop. If no free wavelength is available, the RWA algorithm must search for a wavelength that is already in use in the same wavelength range, but it must not cause interference with other connections. The use of wavelength continuity helps in reducing the number of wavelengths used in the network, and this results in efficient utilization of the available bandwidth.

Constant Wavelength

Constant wavelength is another property of the RWA algorithm that ensures that the same wavelength is used for a connection for the entire duration of the connection. This property is important as it helps in reducing the complexity of the network and simplifies the management of the network. The use of the same wavelength for the entire connection also helps in reducing the number of wavelengths used

in the network, and this results in efficient utilization of the available bandwidth. The RWA algorithm achieves constant wavelength by reserving the wavelength for the entire duration of the connection. When a connection is requested, the RWA algorithm reserves a wavelength for the entire duration of the connection, and this ensures that the wavelength is not used by any other connection for the duration of the connection. The use of constant wavelength helps in reducing the complexity of the network, simplifying the management of the network, and reducing the number of wavelengths used in the network.

Traffic Grooming

Traffic grooming in the optical network refers to the process of efficiently utilizing the available bandwidth by aggregating low-rate traffic streams into high-rate wavelengths. This is done to reduce the number of wavelengths required to carry traffic, which in turn reduces the cost of network infrastructure. In the context of RWA, traffic grooming involves selecting an appropriate route and wavelength for a given traffic stream. The goal is to minimize the number of wavelengths required while ensuring that all traffic demands are satisfied [65].

Consider an optical core network that carries several independent traffic streams. Each traffic stream represents a load that can be quantified in terms of a proportion of a wavelength bandwidth (λ). A stream may thus demand 0.25λ, 0.5λ, 0.75λ, or 1λ worth of bandwidth to be transported (in this thesis). However, if the network is based on Optical Circuit Switching (OCS) [66] without any traffic grooming capability, each traffic stream will have to be assigned a single/more wavelength for transport. Hence, part of the link capacity will have to be unused. According to Fig. 2.13 Let each traffic stream present a load that requires n wavelengths for a given buffer size and packet loss probability (PLP), where $n = 1, 2, 3, ..., x$. Hence, a total of $4n$ wavelength channels would be required to transport all streams from node A to node C. Figure 2.2 shows a simplified schematic of this case of traffic grooming in this thesis. Now, if traffic grooming capability is introduced, traffic can be groomed in such a way as to achieve significant savings in bandwidth [67]. With grooming capability, the node can consolidate the same total magnitude of traffic into one set of channels.

According to the developed SNAP SDN part, there is the option of doing traffic grooming or ignoring traffic grooming in the RWA time. Fig. 2.13 shows the RWA in the simple network topology for a connection request with and without traffic grooming. According to this figure, once a request arrives the SDN part of the SNAP finds the first available free channel between source and destination. For instance, the first channel is the free channel to establishing a LP between the source (node A) and destination (node C) and between (node B) and (node F) nodes (white and yellow LP, respectively). However, due to being occupied by the first channel in the primary requests, the second channel has been utilized in the later requests between Node-A and Node-F (yellow LP). After finding the first available channel to allocate the serving traffic, 100 Gb/s in this thesis, if the QoT of the established LP supports efficient modulation formats such as 16QAM or 8QAM, the most part of LP's capacity would be used by future traffic requests between the same source and destination nodes which is node A to node C in this example.

2.2.5   Transceiver

Global optical networks continue to evolve, necessitating new and innovative solutions to meet the requirements of network operators to maximize optical fiber utilization and reduce the cost of data transport. Coherent optical transmission has been the key technology supporting both requirements over the last decade and this will continue for the next stages of network evolution [68–73]. In 2021, coherent pluggable supporting data rates from 100G to 400G optimized for low power and small space requirements for high-density modular systems have been started to be deployed in optical networks. This latest generation of products extends the economic benefits of coherent innovation into new application areas [74–79]. *400ZR* [80] is an example of one of the first 400G solutions in this new class of pluggable coherent products to hit the market and will initially be used by hyperscale data center operators for single-span connectivity between data centers, Fig. 2.14. Implemented predominantly in QSFP-DD form factors, 400ZR will serve the specific requirement for large-scale switch fabric extension by plugging directly into router face plates for massively parallel data center interconnect of 400GbE for distances of ≤120km. Pluggable innovation is not stopping there though. Beyond 400ZR, referred to as *ZR+* [29], is a range of coherent pluggable solutions with line capacities up to 400 Gb/s and reaches well beyond the 120 km specification for 400ZR that
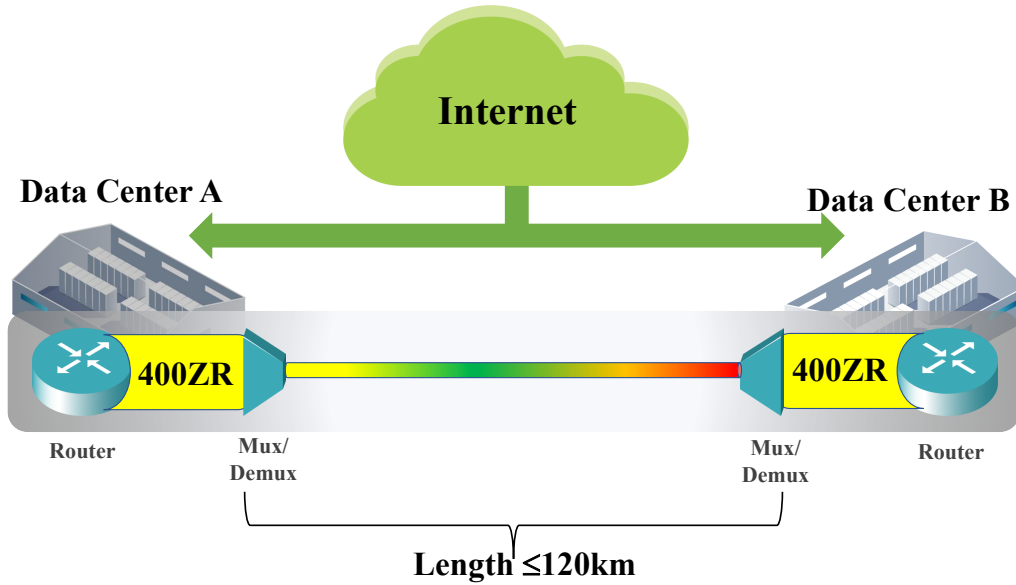
Fig. 2.14 DCI with ZR TRXs.

will support a number of application requirements. The recent OpenZR+ multi-source agreement (MSA), extends the usage of this type of coherent interface to longer transmission systems by slightly increasing its complexity while keeping the target form factor. The support of an improved forward error correction (FEC), ≈ 60 *GBaud*, code and the ability to use also lower order modulation formats (8QAM, QPSK) allows supporting a wider variety of applications than 400ZR [81]. In this thesis, MSA OpenZR+ TRX has been used for the investigated scenarios. In Tab. 2.4 the supporting modulation formats, data rates, power consumption of each modulation formats, and RGSNR for each modulation format has been provided [82, 29].

Table 2.4 TRX modeling assumption.

Modulation Format	Data Rate [Gb/s]	Power [W]	RGSNR [dB]
16QAM	400	20	21
8QAM	300	18	18
QPSK	200	16	14

According to this table, this TRX supports three different modulation formats namely 16QAM, 8QAM, and QPSK with the data rates of 400, 300, and 200 Gb/s, respectively. The consumed power for the 16QAM is equal to 20 Watts, although

this value for the other two modulation formats is 18 and 16 Watts for the 8QAM
and QPSK, respectively. To use each modulation format the QoT of the LP should
satisfy the minimum RGSNR. For the most efficient modulation format which is
16QAM the QoT of the LP should be higher than 21 dB. However, this value for the
other less efficient modulation formats such as 8QAM and QPSK is 18 and 14 dB,
respectively. It is worth mentioning that this TRX technical specifications have been
feed to the developed network tool (SNAP), and in this thesis, this TRX has been
utilized for all investigated scenarios.

2.3   Network Design

In this section two different network designs namely *transparent* and *translucent*
have been discussed. Moreover, three different QoT based algorithms for the 3R re-
generator assignment algorithms have been proposed and discussed in the translucent
network design.

2.3.1   Transparent Network Design

According to Figs. 2.10 and 2.11, SNAP supports three different wavelength
assignment (WA) policies, namely first-fit (FF), minimum GSNR margin (min.
GSNR), and maximum GSNR margin (max. GSNR). The FF spectrum allocation
policy used in this thesis prioritizes the channels with lower frequencies over the
higher-frequency channels. The main goal of this well-known WA policy is to pack
as many as possible LPs on one part of the spectrum (or spectrum band), keeping
the other part free to establish future LPs when the network is more loaded. In the
remaining WA policies (min. GSNR and max. GSNR) SNAP has to evaluate the
difference (margin) between the GSNR of every channel and the RGSNR of the
possible modulation formats. Firstly, the highest-order modulation format feasible
over the LP is determined. This consists of the modulation format with the highest
capacity for which at least one available channel has a GSNR equal to or higher
than the RGSNR. All available channels that also support this modulation format
are identified and then ordered based on the GSNR margin, from higher to lower for
the max. GSNR method and from lower to higher for the min. GSNR policy. The
min. and max. GSNR margin WA policies seemed promising to increase network

capacity since they explore better the existing QoT. However, in all investigated scenarios, it has been seen that FF performed better than or similar to these WA policies. This is because, in the long-term and as the network becomes more loaded, FF is more effective in keeping the diminishing number of free channels available in the same spectrum slots over consecutive links (i.e., verifying the spectrum continuity constraint). Consequently, the results shown in this thesis always assume FF as the WA method.

2.3.2   Translucent Network Design

A translucent network design consists in enabling the regeneration of the optical signal in intermediate nodes. The use of colorless, directionless, and contention-less (CDC) features of reconfigurable optical add-drop multiplexers (ROADMs) can facilitate rapid end-to-end service provisioning and restoration. The contention less ROADMs can handle the same wavelength at the same add/drop structure, avoiding the use of optoelectronic regenerators for wavelength conversions. To prevent signal deterioration caused by noise sources, optical regenerators that enable signal re-amplification, re-shaping, and re-timing (3R) are used to create a translucent optical network [83–85]. Deploying ROADMs with regenerators at selected locations reduces the time to provision a new communication request and enables recovery from network failures. Prior deployment of regenerators at a few ROADM sites optimizes the system effectively to reduce the overall CAPEX and OPEX. In the upcoming EONs, the bandwidth availability on a fiber link and the selected modulation level determines the data transfer capacity. The regenerator placement problem becomes even more relevant in EONs since we need to deal with connections having variable optical reach [84, 86–88]. Although optical signal regenerators are one of the factors that increase cost and energy consumption [89–93]. Therefore, this is a resource that must be managed efficiently. In this case, we assume the use of 3R regenerators, where OEO operation is performed. Although possible, the potential benefit enabled by 3R regenerators of also performing wavelength conversion is not explored in this thesis. In this thesis, three different 3R regenerator placement algorithms are considered. Two of them can be used to assign 3R regenerators in any band whereas the last one focuses only on placing 3R regenerators in the S-band only, since this band presents the lowest QoT in comparison to the other bands (refer to Subsec. 2.1.3.1). in the following subsections and chapters the algorithms and efficiency of the three
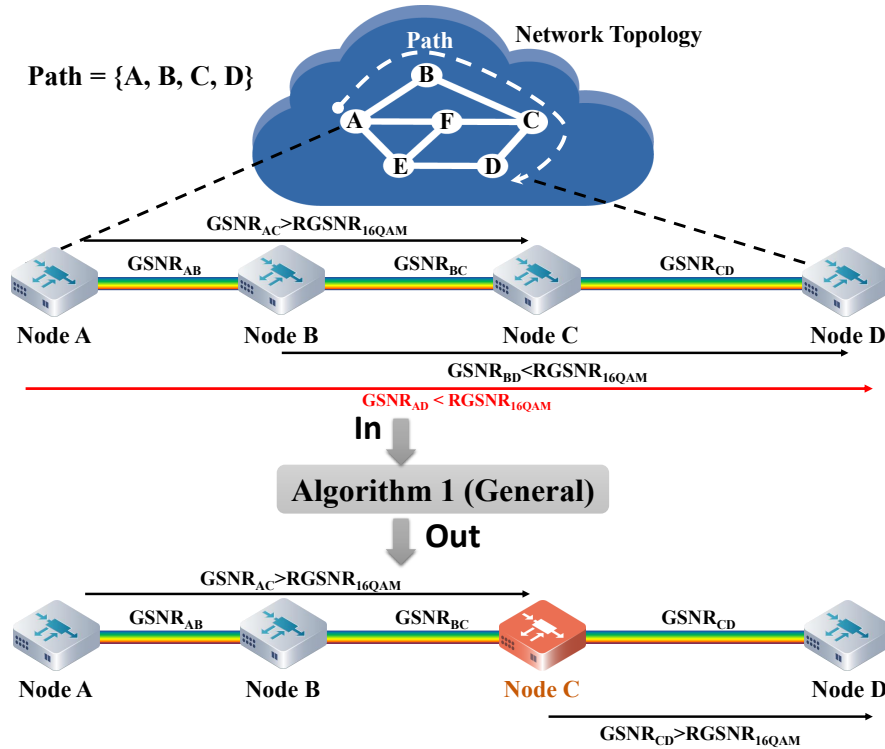
Fig. 2.15 An Example of 3R regenerator assignment with *General* algorithm (Alg. 1).

different algorithms are described and compared in terms of total allocated traffic, consumed energy per Terabit, interface count as a cost, and allocated LPs. In this thesis, each 3R regenerator receives and transmits signals in the optical domain at an intermediate node, and therefore, each device counts as two interfaces.

2.3.3 Regenerator Assignment Algorithms

2.3.3.1 General Algorithm

Algorithm 1 describes the general method for 3R regenerator placement based on the QoT of the LP. This method creates an LP using the most efficient modulation format possible, while simultaneously implementing the highest possible spectral efficiency (SE) that avoids using unnecessary interfaces. The algorithm inputs are channel (ch), source and destination route path ($path_{tot}$) and a list of RGSNR for all possible modulation formats supported by the TRXs (RGSNR$_{list}$); the output of this algorithm is a LP with the indication of the regeneration nodes ($path_{reg}$), if any.

After the initialization (lines 1 and 2), the algorithm starts by trying the most efficient modulation format and saves it in an auxiliary list, $RGSNR_{aux}$ (lines 3-5). Then, it iterates over the path links (l) and saves the current link in the temporary path list ($path_{temp}$ (lines 6 and 7). Afterward, it checks the range of the modulation format and determines which intermediate nodes are reachable. When an unreachable node is found (line 10), a regenerator is assigned to the last reachable node defined in $path_{pre}$ (lines 12 and 13). If $path_{temp}$ containing the last link l has enough QoT to reach the last node, it is added to $path_{reg}$ (lines 16 and 17) and the algorithm is finished. However, if there are any links that are unable to support this modulation format, the loop terminates and a new attempt is carried out using a modulation format that requires a lower RGSNR (e.g., 8QAM and QPSK) (line 15). Please note that the worst-case complexity of this algorithm is $O(G \cdot l)$, where l and G are the numbers of links in the LP and the number of available modulation format, respectively. A workflow example of Alg. 1 regarding regenerator placement has been depicted in Fig. 2.15. According to this figure, the GSNR of the LP between A to D (path={A, B, C, D}) is less than RGSNR of 16QAM which means this LP does not support 16QAM modulation format for the establishment and SDN will try less efficient modulation formats. Moreover, the GSNR of sub-paths, A to C and B to D are higher and lower than RGSNR of most efficient modulation format supporting by MSA ZR+, respectively. The algorithm finds the best place for the regenerator(s) (minimum number of regenerator deployments) to achieve the highest capacity for candidate LP; in this case, the best place is node C. The sub-paths before and after node C have a higher GSNR than $RGSNR_{16QAM}$

2.3.3.2   Power Optimized Algorithm

Algorithm 2 describes the Power Optimized (Pow. Opt.) method/policy for 3R regenerator placement at intermediate nodes. Similarly to the General algorithm, it is based on the QoT of the LPs. However, it also factors in power consumption. Firstly, this algorithm finds all possible regeneration combinations for the LP (C in line 2). Then, it considers each combination (c) and, for all transparent segments (s) of the LP, it computes the bit rate and estimates the power consumption (lines 4-8) and saves it in the R_b and P_{temp} lists. At the end of the iteration, the combination leading to the lowest power consumption and equal bit rate for all transparent segments r_b is selected (line 9-11). Although this algorithm causes a small decrease in the
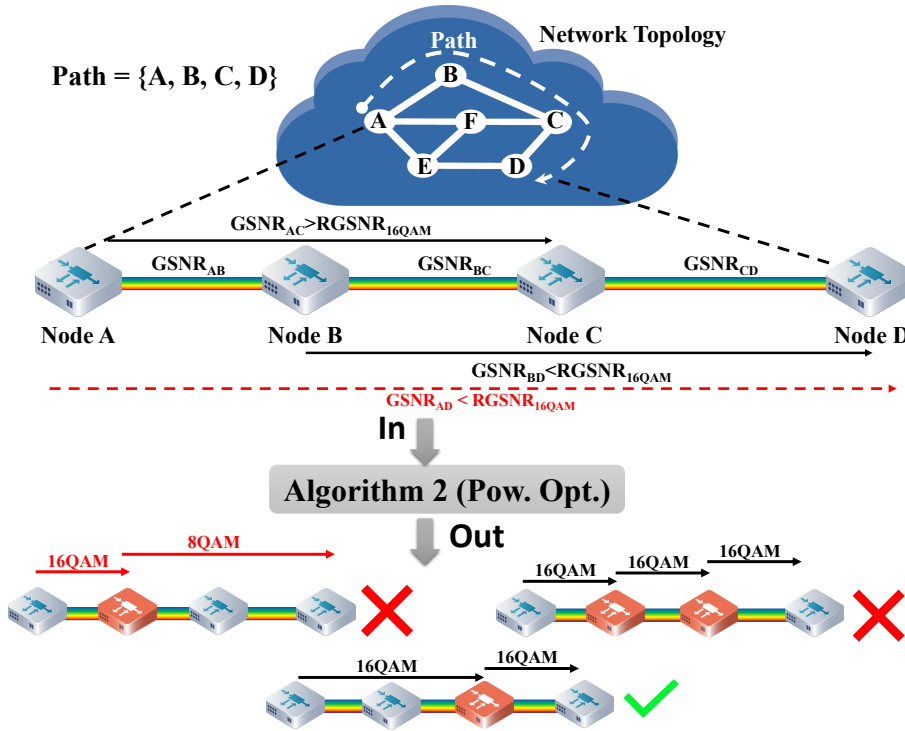
Fig. 2.16 An Example of 3R regenerator assignment with *General* algorithm (Alg. 1).

total allocated traffic in comparison to the General algorithm, it has the ability to reduce the energy consumption per Terabit by selectively decreasing the number of 3R regenerators installed. Moreover, the worst-time complexity of this algorithm is $O(n \cdot 2^n)$, where n is the number of nodes in the LP.

2.3.3.3 Hybrid Algorithm

From the GSNR profiles presented for a single span in the Subsec. 2.1.3.1, along with their average values for different bands as given in Table 2.2, it is observable that the S-band QoT is worse than the other bands namely the C-, L-, and even U-bands. For this reason, employing signal regeneration devices on wavelengths within this lower QoT spectral band can lead to capacity increases comparable to the better-performing C- and L-bands. In the following, this approach is designated as *Hybrid* multi-band [94]. The Hybrid approach can provide a more evenly distributed LP capacity within the network, as it becomes possible to transmit similar data rates across the different bands. This is an important benefit from an operational

perspective, by allowing higher layers to assume a single channel capacity figure for a given pair of end nodes, i.e., independently from the band the optical channel will be allocated to. Moreover, it can also lead to reductions in energy consumption and costs when compared to the General algorithm approach. Note that the Hybrid approach enforces the use of the General Algorithm (Alg. 1) for the regenerator placement in the S-band (see Fig. 2.11).

In the next chapter, the network performance of the three proposed regenerator assignment algorithms will be compared together and the transparent and translucent network designs' performances in terms of delivered capacity, energy consumption, and costs in the MBT scenarios will be discussed.

Chapter 3

Transparent Versus Translucent MBT Network Design

3.1 Network Performance results

In this section, the statistical network assessment results for several MBT scenarios have been presented and discussed for the transparent and translucent network designs, with the latter using either the *General* or *Pow. Opt.* algorithms for 3R regenerators deployment. As already discussed in the previous chapter, SNAP developed to support different traffic request sizes such as 100 and 400 Gb/s; thus, first the statistical network performance in these two traffic requests is investigated, and then in the following sections the proposed 3R regenerator assignment algorithms effect on the network performance in terms of network throughput and energy consumption have been investigated and discussed. Afterward, for a wide set of MBT scenarios, the statistical network performance in the transparent and translucent network designs have been provided and discussed.

3.2 Topology and Traffic Requests (100/400 Gb/s)

The potential of MBT for capacity upgrade is assessed in the US-NET reference topology which has been provided in Appendix 6 Fig. 3. As illustrated in Fig. 3, this
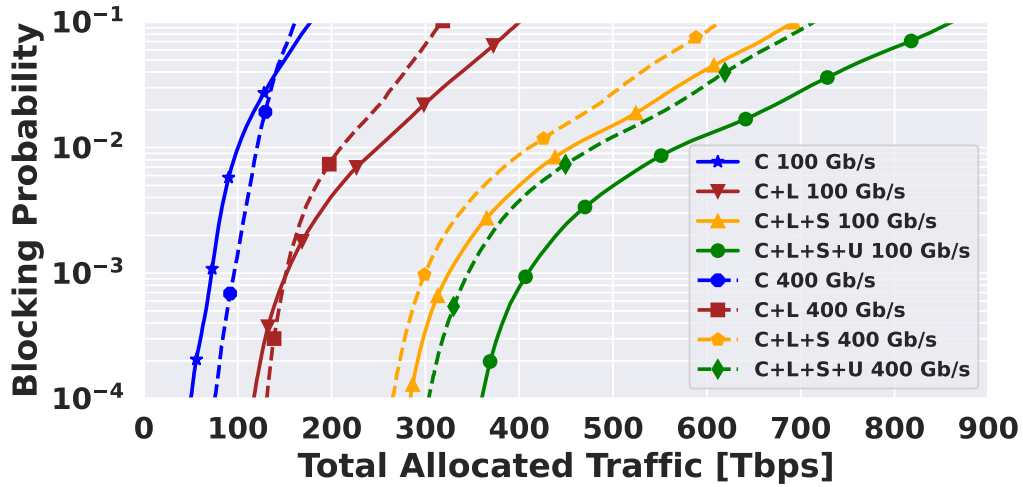
(a)
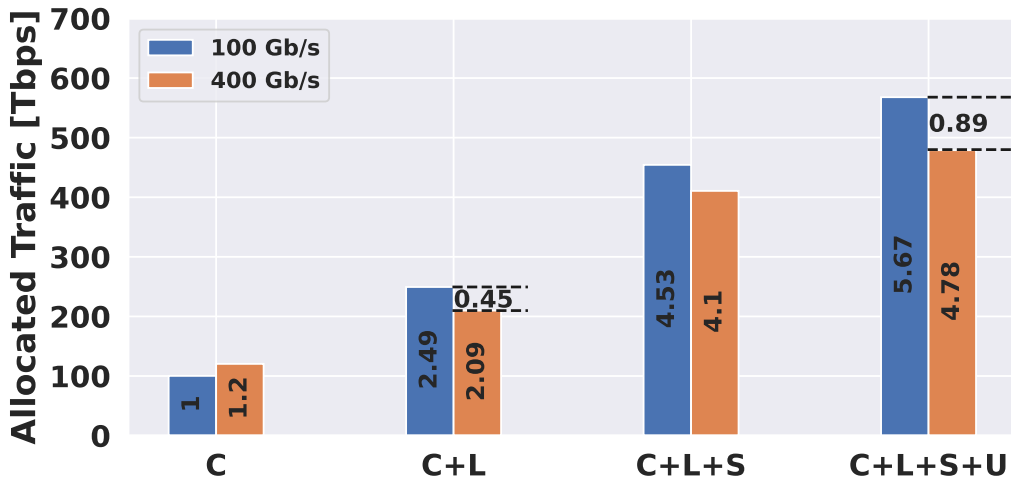
(b)

Fig. 3.1 a) Total allocated traffic in the US-NET topology with serving 100 Gb/s and 400 Gb/s traffic requests for different BPs and b) the MF of allocated traffic at the BP of 1%.

network topology consists of 24 optical nodes and 43 edges, with an average nodal degree of 3.6 and an average link length of 700 km [53].

We start by evaluating the impact of loading the network with 100 or 400 Gb/s traffic requests only. In case the QoT of the selected LP required to directly carry a 400 Gb/s traffic request is insufficient, this traffic request is divided into two or lower capacity requests. In the extreme case, four 100 Gb/s LPs may be set to carry a single 400 Gb/s traffic request. Fig. 3.1a shows the total allocated traffic versus BP using a

transparent network design for both request types. In the C-band only transmission scenario, more traffic is supported for a BP of 1% when loading the network with 400 Gb/s connection requests than with 100 Gb/s ones. The higher network capacity in the case of serving 400 Gb/s connection requests is a consequence of having a limited number of wavelengths/channels only. Indeed, in the case of C-band only transmission and when serving 100 Gb/s connections, we may reach a quick network saturation without fully using the existing LP total capacity. However, by exploiting MBT, the advantage of serving 100 Gb/s traffic requests becomes clear due to the more efficient use of the available QoT and management of the existing LPs. Fig. 3.1a clearly illustrates this behavior. In the C-band only transmission scenario, having 100 Gb/s connection requests leads to smaller allocated traffic for the same blocking probability when compared to 400 Gb/s connection requests for the most relevant BPs. Only for heavily loaded networks, leading to (BP $> 10^{-2}$), having 100 Gb/s connection requests may be beneficial. However, for the C+L-band transmission scenario, having 100 Gb/s connection requests may already be beneficial for BP as low as 10^{-3}. When using even more transmission bands, having 100 Gb/s connection requests always leads to higher allocated traffic than 400 Gb/s connection requests for all relevant BPs. Fig. 3.1b depicts the allocated traffic multiplicative factor (MF) for all scenarios at the BP of 1%. The network capacity using C-band only transmission with serving 100 Gb/s traffic requests is used as a reference (solid blue curve in Fig. 3.1a). According to Fig. 3.1b, the total allocated network traffic in the case of C-band serving 400 Gb/s traffic requests is about 1.2 times higher than the one supporting 100 Gb/s traffic requests. However, by doubling the number of available channels (exploiting the L-band), the allocated traffic increases by about 2.49 and 2.09 times in the cases of serving 100 Gb/s and 400 Gbs traffic requests, respectively. This result highlights that the total allocated traffic serving 400 Gb/s traffic requests in a network leads to a drop of 18% in the MF. Moreover, in the C+L+S+U-band MBT scenario (green curves in Fig. 3.1a), this difference is 16% (5.67 and 4.78 with serving 100 Gb/s and 400 Gb/s traffic requests, respectively). This preliminary analysis shows that optical networks operating with 100 Gb/s connection requests may benefit more from the MBT upgrade in terms of total allocated traffic. In the remainder of this work, we focus our analysis solely on supporting 100 Gb/s traffic requests.
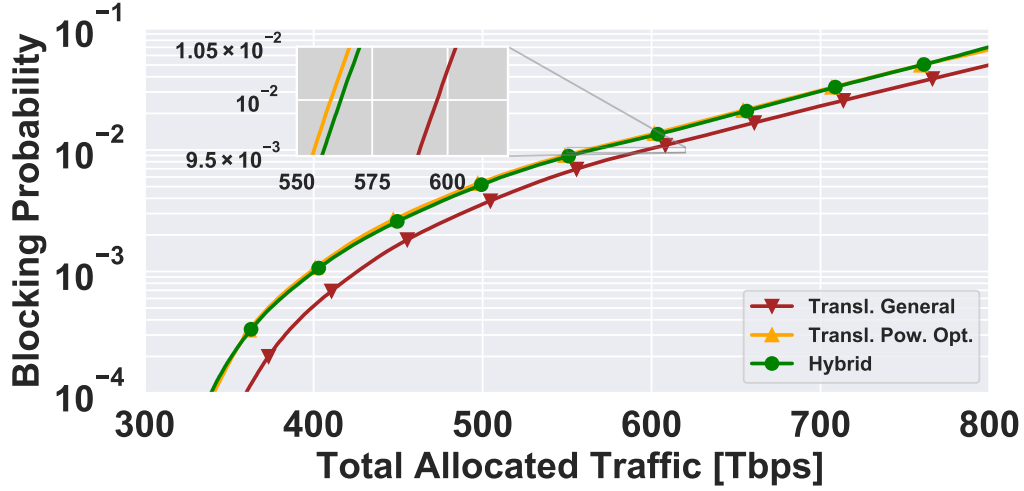
Fig. 3.2 Network performance in the translucent MBT scenario (C+L+S-band) using the Hybrid, General, and Pow. Opt. algorithms for different BPs. The C- and L-bands contain the same number of wavelengths, $N_{ch} = 64$. The S-band contains 128 channels, $N_{ch} = 128$.

3.3   3R Assignment Algorithm Comparison

The evaluation of network performance for the different translucent network designs considered in this work (General, Pow. Opt., and Hybrid) is presented in this subsection. Fig. 3.2 shows the progressive total allocated traffic versus BP for a translucent C+L+S-band network, using the General, Pow. Opt., and Hybrid algorithms, with 256 channels in total (C- and L-band containing 64 channels each and the S-band containing 128 channels). The General algorithm provides the highest delivered capacity for the entire range of BP values shown, as this approach prioritizes the most efficient modulation formats and, consequently, optimizes the capacity of each LP. Conversely, the Pow. Opt. algorithm provides smaller capacity for all BP values, as it focuses on power consumption minimization by reducing/limiting the number of assigned 3R regenerators. In the hybrid case, where signal regeneration occurs in the S-band only, the network performance in terms of total allocated traffic is similar to the translucent network with Pow. Opt. algorithm. According to Fig. 3.2, the total allocated traffic in a translucent network design with the Pow. Opt., Hybrid and General algorithms is 561, 564 and 596 Tbps at a BP = 1%, respectively.

We now analyze the total energy consumption for each translucent algorithm using the interface power consumption provided in Table 2.4 in the previous section.
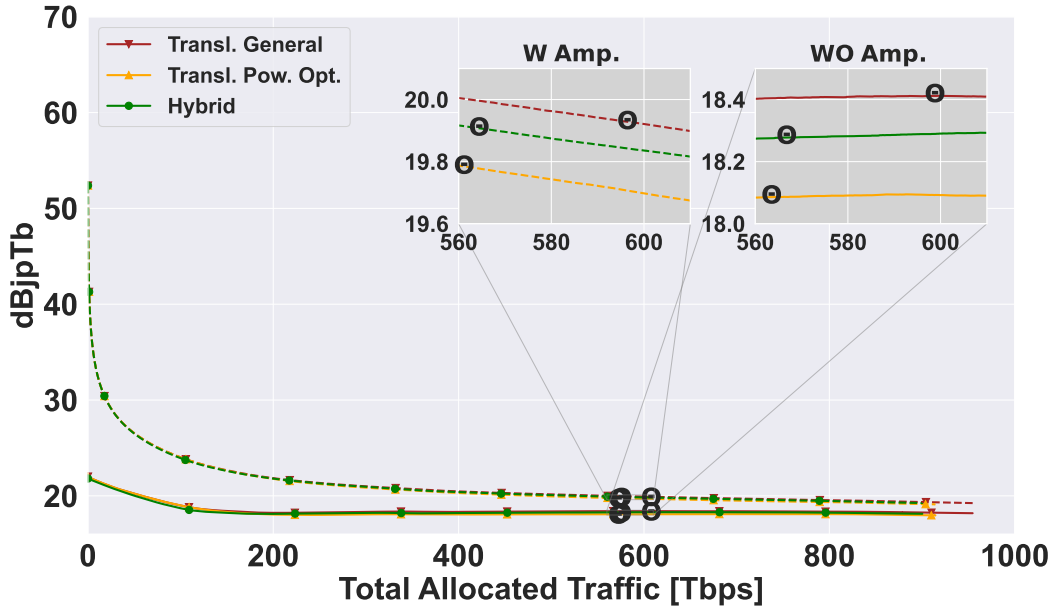
Fig. 3.3 Energy consumption in a translucent C+L+S MBT design using the Hybrid, General and Pow. Opt. algorithms for different allocated traffics with (dashed curves) and without (solid curves) considering the amplifiers' power consumption. The BP value of 1% is indicated in the figure by θ.

Besides the interfaces, the optical amplifiers' power consumption is also taken into account. The consumed power of a single amplifier is assumed to be 20 Watts for the C-band [30] and 30 Watts for the L- [31], S- [32], and U-bands. Given the lack of commercially available amplifiers for the U-band, we assumed the highest value among the used options. Using equal spans of 75 km, a total of 173 amplifiers, for each band, are deployed in the US-NET topology. Both energy analyses, with (W Amp.) and without (WO Amp.) considering the amplifiers' power consumption, are shown in Fig. 3.3 (dashed and solid line curves, respectively).

Table 3.1 Capacity, energy consumption, interface count and number of allocated LPs and 3Rs in a C+L+S MBT design using the General, Pow. Opt. and Hybrid algorithms at the BP = 1%, with traffic request size of 100 Gb/s.

BP=10^{-2}	Capacity [Tbps]	Energy consumption [dBjpTb]	No. interfaces	No. allocated LP's	No. regenerators		
					L	C	S
General	596.52	WO Amp = 18.41 W Amp. = 19.92	5450	2725	30	117	703
Pow. Opt.	561.27	WO Amp = 18.08 W Amp. = 19.78	4658	2329	30	114	417
Hybrid	564.52	WO Amp = 18.27 W Amp. = 19.90	4896	2448	-	-	638

The energy consumption is shown in dB Joule per Terabit (dBjpTb) versus the progressively allocated traffic, i.e., the average consumed energy per Terabit is evaluated by dividing the total consumed power by the amount of allocated traffic. The θ symbol in Fig. 3.3 highlights the result for BP = 1%. For this BP value, considering the amplifiers power consumption increase the energy consumption by about 1.5 dB. As expected, the consumed energy in a translucent network design with Pow. Opt. algorithm presented a lower value when compared with the other algorithms. For instance, when neglecting the amplifiers' power consumption and at a BP of 1% (shown in the right zoom plot), using the Pow. Opt. algorithm leads to energy consumption of about 18.1 dBjpTb, while this value exceeds 18.3 dBjpTb when using the other algorithms. When taking into account the amplifiers' power consumption, the difference in energy consumption when using the different algorithms decreases. For instance, at a BP = 1%, while using the General algorithm leads to an energy consumption of about 19.9 dBjpTb, using the Pow. Opt. and Hybrid algorithms lead to an energy consumption of about 19.8 and 19.9 dBjpTb, respectively. According to Fig. 3.3, the energy consumption of the translucent network design using the General algorithm is higher than when using the other two algorithms for the same BP value. This higher energy consumption can be attributed to the fact that the main focus of this algorithm is to increase the network capacity regardless of the resulting power consumption.

Cost is obviously one of the main considerations when comparing different network upgrade solutions. Usually, in regional and long-haul networks, the interfaces are responsible for a large share of capital expenditures. Fig. 3.4 depicts the number of required interfaces when using the three different translucent network design algorithms versus the network total allocated traffic, along with the number of used interfaces at a BP of 1% (marked with θ). According to Fig. 3.4, the number of required interfaces in the translucent network design when using the Pow. Opt. algorithm is smaller than when using the General and Hybrid algorithms for the same total allocated traffic, which highlights the potential of this algorithm. As an example, for a traffic load leading to a BP=1%, the Pow. Opt. algorithm provides almost the same capacity as the Hybrid algorithm but requires 6% (238 interfaces) fewer interfaces.

The main results of this subsection are summarized in Table 3.1, which shows the allocated traffic, the energy consumption per Terabit, and the number of interfaces, allocated LPs, and 3R regenerators in each band. These values are obtained for a
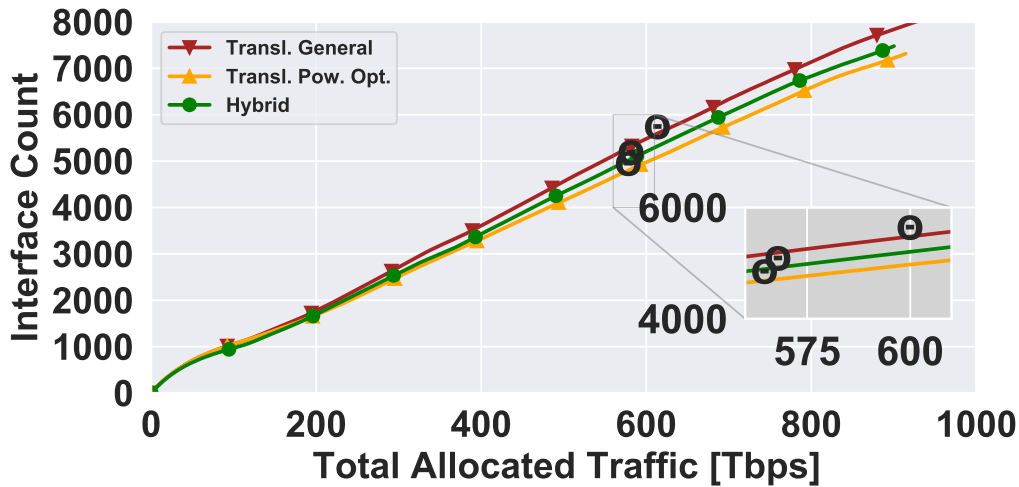
Fig. 3.4 The number of used interfaces in a translucent C+L+S MBT design using the Hybrid, General and Pow. Opt. algorithms versus total allocated traffic. The BP value of 1% is indicated in the figure by θ.

$BP = 1\%$. From the allocated traffic viewpoint, the translucent network design using the General algorithm enables >30 Tbps additional traffic when compared to the other translucent algorithms. In terms of the number of interfaces, and consequently allocated LPs, the Pow. Opt. algorithm was the one leading to the best result, requiring 4658 and 2329, respectively. Moreover, as expected, the algorithm leading to higher cost was the General one, requiring 5450 interfaces and 2725 allocated LPs to carry all traffic load. Additionally, the S-band, given its lower QoT, used the vast majority of 3R signal regenerators. Conversely, the L-band required the least amount of regenerators, in view of its higher QoT. Particularly, the number of 3R regenerators in the L-band was kept constant (30), independently of using the General or Pow. Opt. algorithm. On the contrary, for the S-band, this value is considerably reduced to about 400 when using the Pow. Opt. algorithm instead of the General one (which required using about 700 3R regenerators). These results highlight once more the potential of the Pow. Opt. algorithm to decreases power consumption in a network by limiting the deployment of 3R regenerator at intermediate nodes. In the Hybrid network design, 638 3R regenerators are required to improve the capacity of LPs in the S-band to attain similar capacity as the one of those in the L- and C-bands. We remark that the total number of 3R regenerators required by Pow. Opt. algorithm is much smaller than the one of the Hybrid algorithm, even though similar network capacity is achieved in both cases. Consequently, in the following subsections, only

the transparent and translucent with General and Pow. Opt. algorithms MBT designs are compared.

3.4 Capacity

Fig. 3.5a shows the network allocated traffic for a BP ranging from 10^{-4} to 10^{-1}. The performance of a transparent network with C-band only transmission with ideal Shannon interfaces is also presented for benchmarking purposes (ideal C, depicted with a purple dashed-dot line with ✖ markers). This figure shows that exploiting more transmission bands increases the network capacity due to the higher number of available wavelengths. It is also noticeable that, for the same number of bands being exploited, the higher LP capacities obtained by deploying 3R regenerators reduce the BP with respect to the transparent network design. For example, the transparent network design with the C+L-band system has 40 Tbps less capacity than the C+L-band translucent case at a BP of 1% for any regenerator placement algorithm; this capacity difference increases with adding more transmission bands to the system. The difference between the transparent and translucent network designs increases from 8 Tbps in the C-band to approximately 200 Tbps in the C+L+S+U-band system. This increase is related to the higher probability of finding vacant capacity in already deployed LPs with the same source and destination when using more transmission bands. Moreover, the difference in allocated traffic between the *General* and *Pow.Opt.* translucent scenarios also become more significant for a higher number of transmission bands. In the C- and C+L-band systems, both algorithms have almost the same behavior, whereas in the MBT C+L+S- and C+L+S+U-band scenarios their difference becomes more distinct; the translucent network designed using the General algorithm provides higher capacity. Additionally, exploiting the U-band leads to approximately the same capacity increase achieved by deploying 3R regenerators in the transparent C+L+S-band scenario. Moreover, using ideal Shannon interfaces in a transparent network design with C-band only transmission provides a better performance than using C+L-band in a transparent or translucent network. For BPs smaller than 10^{-3}, the allocated traffic of the ideal C-band scenario is comparable to the C+L+S-band system in a transparent network. This provides evidence that adopting high-end interfaces is also key to better exploiting the existing fiber infrastructure [95].
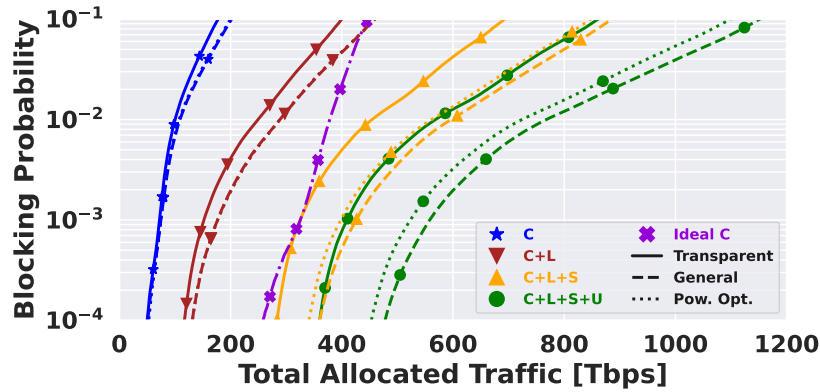
(a)
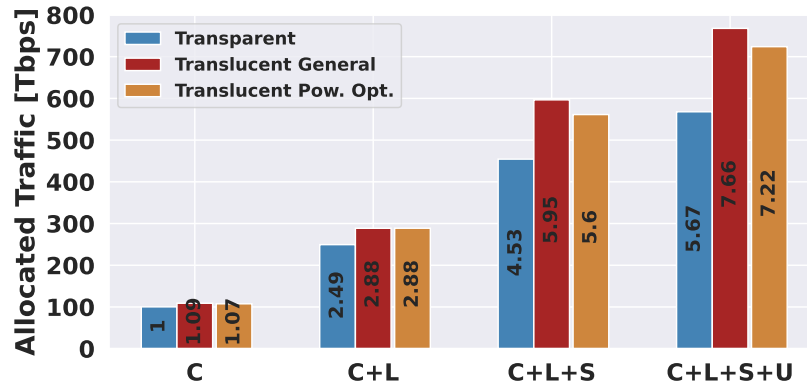
(b)

Fig. 3.5 Network capacity for transparent and translucent network design for the C-, C+L-, C+L+S-, and C+L+S+U-band with 100 Gb/s traffic request size a) in different BPs, and b) their capacities MFs at the BP = 1%.

To better visualize the difference between the scenarios for a given BP, Fig. 3.5b shows the total allocated traffic for all scenarios and their MF at a BP of 1%, considering the transparent network design with the C-band only transmission as a reference. It can be observed that increasing the network capacity by exploiting more bands is more effective than deploying 3R regenerators in the C-band only scenario. Indeed, enabling the L-band in a transparent network design leads to more than twice the capacity, but performing signal regeneration only increases the network capacity by ×1.09 and ×1.07 times with the General and Pow. Opt. algorithms, respectively. In the other scenarios, a transparent network exploiting more transmission bands has almost the same or greater capacity than the translucent network. For example, the C+L+S-band translucent network has an MF value of 5.6

and 5.95, whereas the C+L+S+U-band transparent network that factor is 5.67. As the number of channels (N_{ch}) in the S-band is twice as much as those in the C- and L-band, the number of available wavelengths has quadrupled and the MF has increased from ×2.5, ×2.88, and ×2.88 in the C+L-band scenario to ×4.53, ×5.95, ×5.6 times in the C+L+S-band, for the transparent, translucent General and translucent Pow. Opt. cases, respectively. Overall, these results support that exploiting more bands while keeping a transparent network design approach is an effective upgrade strategy. The translucent network design can also be used to augment capacity but is likely not the most cost-effective approach to accomplish this goal.

3.5   Energy Consumption

Fig. 3.6a shows the energy consumption per transmitted bit as a function of the total allocated traffic for all the scenarios, considering the interfaces' and the optical amplifiers' power consumption. The figure indicates that the consumed energy per Terabit is very high at the beginning of the network loading phase. This behavior is due to the fact that many of the LPs established have spare capacity but are already consuming the same amount of power as if they were being fully used. As new LPs are established, and some requests use the free capacity of already-deployed LPs, the energy consumption is reduced from approximately 55 dBjpTb down to around 20 dBjpTb.

Although exploiting more bands and deploying 3R regenerators increases power consumption, it also leads to higher network capacities. Fig. 3.6b shows the energy consumption per Terabit and the MF of all scenarios for a BP of 1%. This figure indicates that the energy consumption per Terabit is very similar for all scenarios. This behavior is related to the higher probability of new requests exploiting the free capacity in already deployed LPs with a higher number of available wavelengths. Consequently, for a given BP, the capacity increases more than or is equal to the energy consumption for all upgrade scenarios (even with the worse QoT of additional bands). We observed similar MF values for all the scenarios as we considered a fixed BP of 1%. However, the energy consumption would change if we considered the same network capacity. For instance, at a network capacity of 200 Tbps, the consumed energy is about 19 dBjpTb in the transparent and translucent network types with the C-band. However, this value increases to 23 dBjpTb in the C+L+S+U
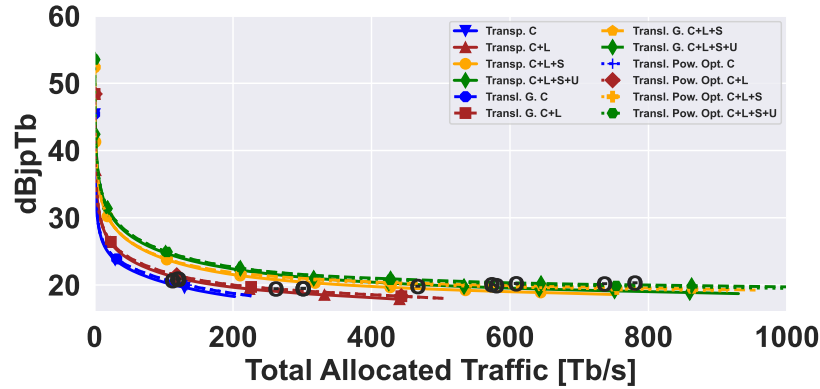
(a)
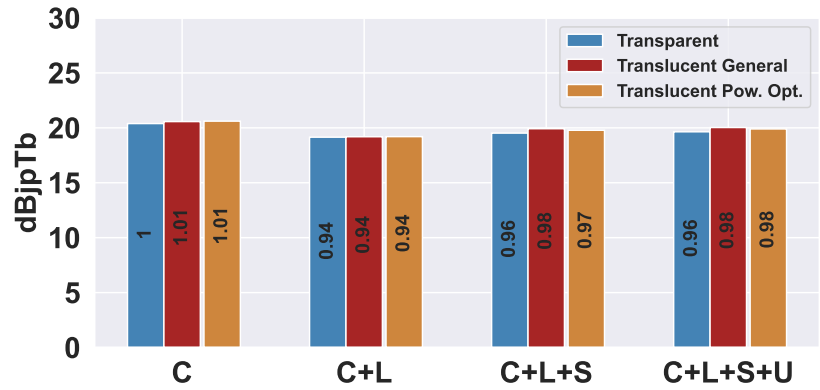
(b)

Fig. 3.6 Network energy consumption per Terabit for transparent and translucent solution from C-, C+L-, C+L+S-, C+L+S+U-band with 100 Gb/s traffic request a) at different BPs, and b) their energy consumption MF at a BP = 1%. Optical amplifier power consumption is considered and the BP value of 1% is indicated in the figure by θ.

transparent scenario due to the additional amplifiers power consumption, which leads to a change in MF value from $\times 0.96$ to $\times 1.21$ times. These results highlight the importance of using a pay-as-you-grow approach, i.e., only deploying additional bands when the links congestion increases and the target threshold BP is reached, in order to maintain high levels of energy efficiency.
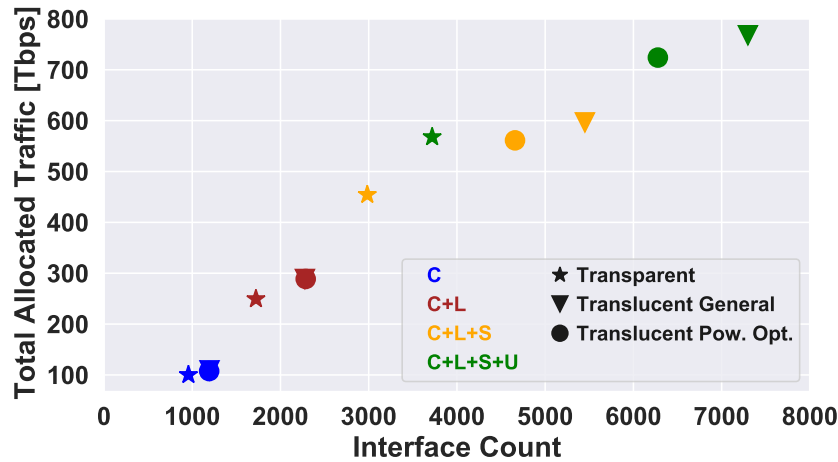
Fig. 3.7 The number of used point-to-point interface numbers versus total allocated traffic with 100 Gb/s traffic request size at the BP of 1% for transparent and translucent network design from the C-band only to the C+L+S+U-band.

3.6   Costs and Links Congestion

In this section, we show the results in terms of the number of interfaces, as a cost indicator, and the number of allocated LPs. Fig. 3.7 shows the interface count versus total allocated traffic at a BP of 1% for different scenarios in the transparent and translucent network designs, whereas Fig. 3.8 shows the total allocated LP values and MF of each scenario at a BP of 1%. The transparent network design with C-band only transmission was considered as a reference. From Fig. 3.7, the difference in the number of interfaces between the transparent and translucent network designs is small in the C-band scenario. However, by exploiting more bands, this difference becomes greater, and the advantages of transparent network design outweigh those of the translucent types. For instance, a transparent network in the C+L+S+U-band scenario uses about 3719 interfaces to give a capacity of 570 Tbps; however, a translucent network design with one band less (C+L+S) needs about 5450 interfaces to reach the same capacity at the BP of 1%. Overall, by exploiting more bands progressively the allocated traffic increases in both the transparent and translucent network designs. On the contrary, the number of interfaces in the transparent network increases slightly in comparison to the translucent network type, which has a significant increase. For instance, with respect to the reference C-band only transparent network design, which demands 956 interfaces, the number of interfaces increases less than ×4 times by exploiting all C-, L-, S-, and U-band and reaches
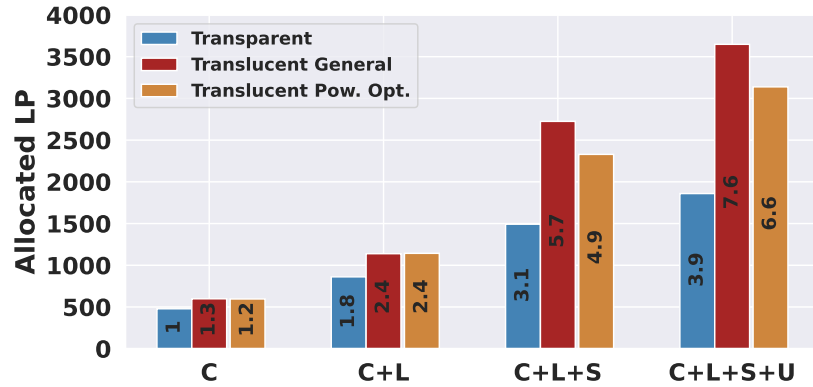
Fig. 3.8 MF at the BP of 1% for the allocated LPs with 100 Gb/s traffic request size for transparent and translucent network design from the C-band only to the C+L+S+U-band.

3720 when keeping the transparent network design strategy. On the contrary, this value surges to more than $\times 7.6$ times (for a total of 7298 interfaces) in the translucent network type with the General algorithm.

As expected, the number of allocated LPs have an almost identical behavior as the number of interfaces (Fig. 3.8). For these results, an LP with one 3R regenerator was considered to be two distinct LPs. We observed that the number of allocated LPs sharply grows in the translucent network when adding the S-band, in contrast to the transparent case. As a result, the number of allocated LPs for the transparent network design in the C+L+S+U-band scenario increased about $\times 4$, but increased by $\times 7.6$ and $\times 6.6$ in the translucent network design with the General and Pow. Opt. algorithms, respectively. Moreover, from Fig. 3.5a, although the transparent network design in the C+L+S+U-band scenario has an almost equal capacity to the translucent network design in the C+L+S-band scenario, in Figs. 3.8 and 3.7 we see that the number of interfaces and allocated LPs is approximately more than $\times 2$ times fewer in the transparent design.

3.6.0.1   Link congestion

Not only do transparent and translucent network designs provide different capacities, but employing signal regeneration leads to differences in link congestion. Fig. 3.9 shows the link congestion for the transparent and translucent network designs in the network topology investigated. Fig. 3.9a and Fig. 3.9b show the link con-

gestion in the transparent (C+L+S+U) and translucent (C+L+S) cases at a BP=1%. These two scenarios have almost equivalent capacities of ≈580 Tbps. In the former, four links are almost saturated, but the congestion of some links is less than 50%. For example, the *Tucson-Salt Lake City*, *Chicago-Ithaca*, *San Diego-Las Vegas*, and *Raleigh-Knoxville* links are almost completely saturated, whereas in the translucent case, the congestion of these links decreased. On the other hand, the *Boulder-Chicago* and *Portland-Seattle* links experienced an increase in congestion for the translucent case. We finally remark that the link congestion distribution for the transparent (C+L+S) with ≈450 Tbps capacity (shown in Fig. 3.9c) is approximately the same as for the transparent (C+L+S+U) scenario (shown in Fig. 3.9a). A more detailed analysis of the link congestion shows that the average link congestion in the transparent cases (C+L+S+U and C+L+S-band transmission) is about 38%. However, signal regeneration in the translucent network design leads to an average link congestion increase of about 5%, exceeding 43% on average. Moreover, among all links between transparent network design in the CL+S+U-band and translucent network design in the C+L+S-band, the link that has changed the most due to signal generation is the *Chicago-Ithaca* and its congestion increased more than 15% because of signal regeneration in the translucent network design. On the contrary, the link of *El Paso-San Antonio* is the one that did not face any charges in its congestion.
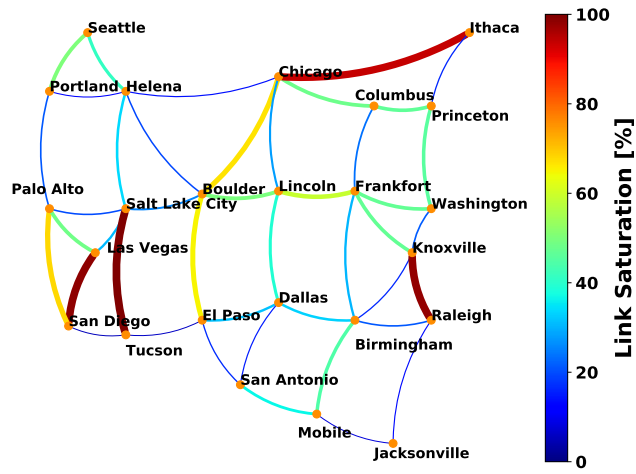
(a)
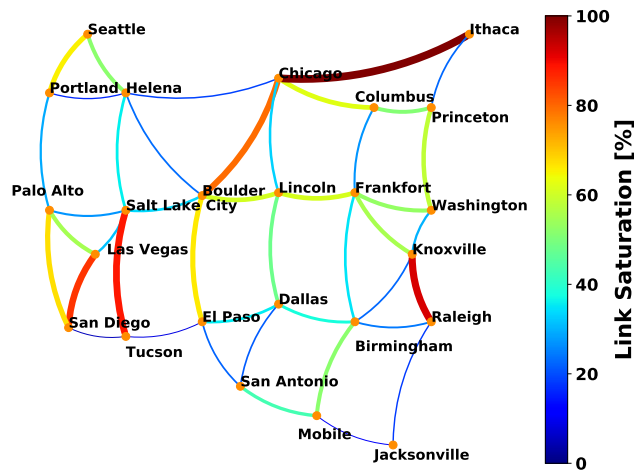
(b)
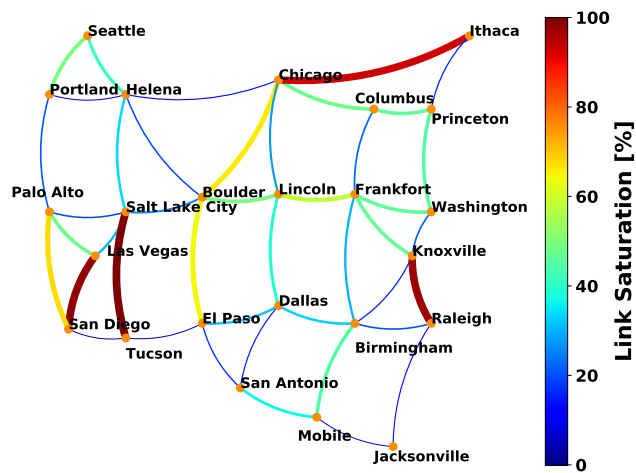
(c)

Fig. 3.9 Link congestion at a BP of 1% for a) transparent (C+L+S+U), b) translucent (C+L+S), and c) transparent (C+L+S) network design.

Chapter 4

Extended Bandwidth Bands versus Regular Bands

4.1 Extended Bandwidth C and L-band

In this section, the specification of extended bandwidth/super bands and regular bands is presented. Fig. 4.1 shows the spectra of the MBT scenarios considered, in both frequency and wavelength domains. Note that the S1-band used in our analysis (in green) represents only half of the bandwidth of the entire S-band as a result of amplification and maximum output power limitations of current S-band amplifiers. The details of each band, such as frequency range, bandwidth, and the number of channels supported are summarized separately in Tab. 4.1. Particularly, this table shows the difference in bandwidth between the regular and super bands of 4.8 THz and 6 THz, respectively, and the corresponding increase in the number of channels from 64 to 80, when considering the 75 GHz WDM grid spacing and 64 GBaud symbol rate values that are assumed in all scenarios reported in this work. Additionally, a 500 GHz guard band is set between adjacent bands. In MBT scenarios, to achieve an optimally high and flat GSNR value, it is necessary to optimize the launch power [53]. This technique, along with other details about the system under investigation, is described in the following section.
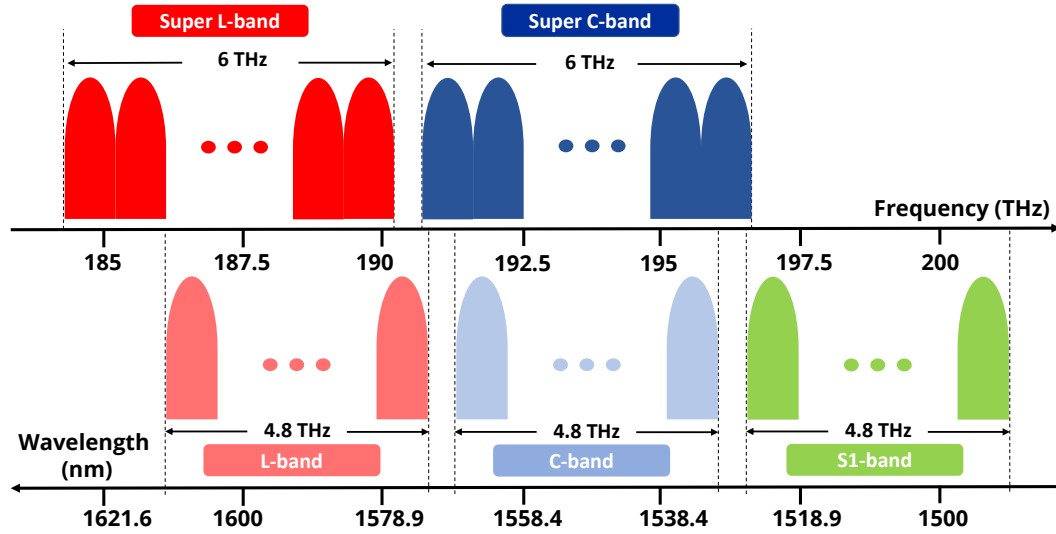
Fig. 4.1 Super bands versus regular bands in both frequency and wavelength domain.

Table 4.1 Spectral occupation of the bands under investigation.

Band	Wavelength [nm]	Frequency [THz]	BW [THz]	Channels
C	1530.38-1568.14	191.31-196.03	4.8	64
Super C	1525.79-1573.15	190.70-196.62	6	80
L	1572.24-1612.38	186.06-190.81	4.8	64
Super L	1577.29-1628.05	184.27-190.20	6	80
S1	1490.61-1526.48	196.53-201.26	4.8	64

4.2 Network Assessment Results

Following, the physical layer investigation of the single span, next we report a network analysis using a Monte-Carlo (MC) Statistical Network Assessment Process (SNAP) framework based on [96]. The SNAP requires different input parameters such as route space, TRX details, network topology abstraction, and traffic pattern to analyze a network topology. The routing space is the k shortest path among all pair of nodes in the network topology, with $k_{max} = 5$. The TRX details include all technical characteristics of the TRX, such as supported modulation formats, power consumption, supported fiber lengths, and minimum required GSNR (RGSNR) for each modulation format. The RGSNR for specific modulation formats with different symbol rates has been investigated in [82]. In this work, an OpenZR+ [29] TRX is considered, with all relevant TRX details given in Tab. 2 of [96]. Particularly, three different modulation formats are supported by the TRX – 16QAM, 8QAM,

and QPSK – resulting in a channel capacity of 400, 300, and 200 Gb/s, respectively. The network topology is abstracted using GNPy before being fed into the SNAP – specifically, the length of each edge changes with the QoT of the corresponding edge for all supported channels. Both the US-NET and the European COST [53] network topologies have been investigated as a test bed. The US-NET topology consists of 24 nodes and 43 links, with average nodal degrees and link lengths of 3.58, and 971 km, respectively. The European COST topology consists of 28 nodes and 41 links with average nodal degrees and link lengths of 2.93, and 636 km, respectively. The SNAP also supports different traffic patterns, such as uniform and nonuniform. In the uniform traffic distribution, the joint probability density function (JPDF) of all nodes is equal, whereas in the nonuniform case, this value depends on the population assumed to be served by each node [53]. Additionally, the SNAP supports two network designs: transparent and translucent. In the transparent network design, the LP for each connection request considers a single transparent segment. Channel capacity is evaluated on the basis of the QoT of the corresponding LP and the highest order feasible modulation format. In the translucent network design, the LP for each connection request can be divided into multiple transparent segments, in order to increase the LP capacity by limiting QoT degradation. The *General algorithm* (Alg. 1 in ref. [96]) has been used as the 3R regenerator placement algorithm for translucent network design. This algorithm uses the minimum number of regenerators to create an LP that supports the most efficient available modulation format. Each simulation runs for a number of MC iterations, N_{MC}=1000, as ensuring accurate results, and the SNAP progressively loads the network [61] in each MC iteration up to reaching the threshold saturation blocking probability ($B_{th} = 20\%$ considered in this work) for each scenario under investigation. A 100 Gb/s traffic request size is considered with a first-fit (FF) wavelength assignment policy for all scenarios.

4.3   NF Penalty

The effect of the EDFA NF penalty on the QoT of a single span that exploits the super C + L band has been shown in Sec. 2.1.3. In this subsection, its effect on the network capacity is evaluated. Fig. 4.2 shows the Blocking Probability (BP) as a function of the total traffic load for different NF penalties (ΔNF=0, 0.5, and 1 dB) and considering both transparent and translucent network designs in the US-NET
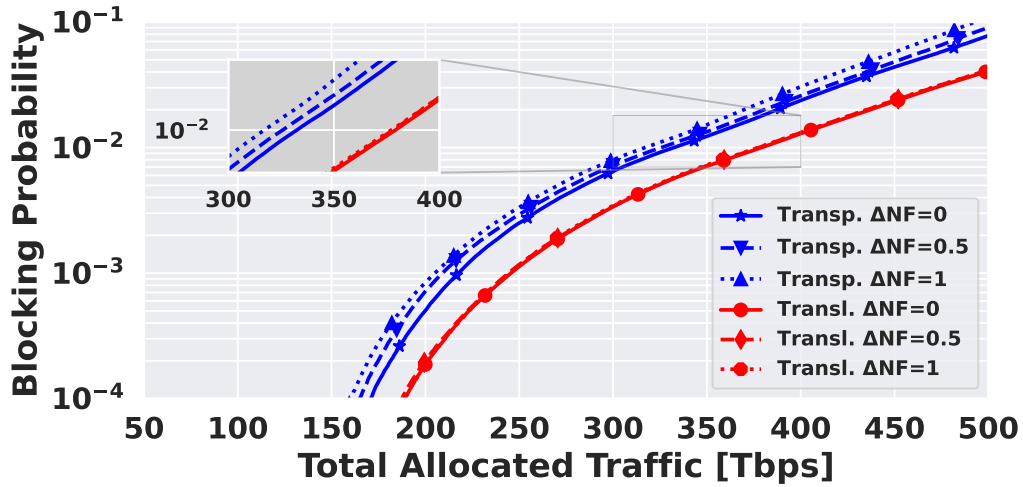
Fig. 4.2 The effect of the super C+L-band NF penalty on network capacity in the transparent and translucent network designs.

topology. According to these results, network capacity drops by 15 Tb/s by increasing the NF penalty from 0 to 1 dB in the transparent network design (blue curves). More precisely, the total allocated traffic at a reference BP of 1% is about 332 Tb/s in the transparent super C+L-band without NF penalty (ΔNF=0). Increasing the NF penalty by 0.5 and 1 dB causes a decrease in this total traffic value to 325 and 317 Tb/s, respectively. This reduction is due to the lower QoT resulting from the higher amplifiers' NF, which results in the need to use lower-order modulation formats in some of the routing paths. Interestingly, the utilization of signal regeneration in the translucent network design not only increases the network capacity but is also more robust to the variation of the amplifiers' NF values. It can be observed that the total allocated traffic decreases only $\cong$3 Tb/s when increasing the NF by 1 dB NF in the translucent network design (red curves). In this case, the total allocated traffic at the BP of 1% is equal to 379, 378, and 377 Tb/s for ΔNF values of 0, 0.5, and 1 dB, respectively. The reason behind these very minor capacity penalties when increasing by up to 1 dB the amplifiers' NF, is that originally (i.e. with ΔNF=0), the majority of provisioned LPs with the translucent network design approach are relatively short and with high GSNR. Hence, they can accommodate a decrease in GSNR without having to switch to a lower-order modulation format. In view of the observations above, which suggest that even if the amplifiers' NF is slightly degraded due to the need to amplify a 6 THz band instead of 4.8 THz, the total allocated traffic is only reduced by up to 4.5% (0.8%) when enforcing a transparent (translucent)

network design, in the remaining of the paper it is assumed that ΔNF=0 for the super C+L-band MBT scenario.

4.4   Capacity

In this subsection, the throughput of the US-NET and European COST networks in transparent and translucent MBT designs is presented. Fig. 4.3 shows the total traffic allocated versus BP for the US-NET topology with uniform (4.3a) and nonuniform (4.3b) traffic distributions. Note that all total allocated traffic values presented in this subsection are obtained for a BP of 1%. From Fig. 4.3a, the total allocated traffic in the super C-band (solid blue curve) is approximately 130 Tb/s in the transparent network design, increasing to 150 Tb/s in the translucent network design (dashed blue curve). This demonstrates that selective signal regeneration in the intermediate nodes can increase the network capacity by approximately 20 Tb/s (15%) in the super C-band. In the C+L-band (solid and dashed red curves) with 128 channels, the total allocated traffic is 254 and 287 Tb/s in the transparent and translucent network designs, respectively. This corresponds to a difference of 33 Tb/s (13%). However, exploiting super bands such as the super C+L-band (solid and dashed yellow curves) leads to a higher network capacity in comparison to the C+L-band. For instance, the network capacity increases to 332 and 379 Tb/s (47 Tb/s difference) in the transparent and translucent network designs, respectively, by exploiting the super C+L-band. Importantly, the network capacity of 379 Tb/s in the translucent super C+L-band offers almost the same capacity as the C+L+S1-band (192 channels) in the transparent network scenario, which has a capacity of 369 Tb/s. Naturally, given the extended bandwidth exploited by the C+L+S1-band, the delivered network capacity in this scenario when employing translucent network design is approximately 458 Tb/s.

In Fig. 4.3b the total allocated traffic for different BPs in the US-NET topology is shown for the nonuniform traffic distribution in the transparent and translucent network designs. Compared to Fig. 4.3a, the trends observed in Fig. 4.3b are similar, although there is an increase of BP for the same traffic load. For example, the network capacity in the super C-band decreased to about 102 and 120 Tb/s in the transparent and translucent network designs, respectively. In the C+L-band, the network capacity in the transparent and translucent network designs are 183 and

(a)

(b)

(c)
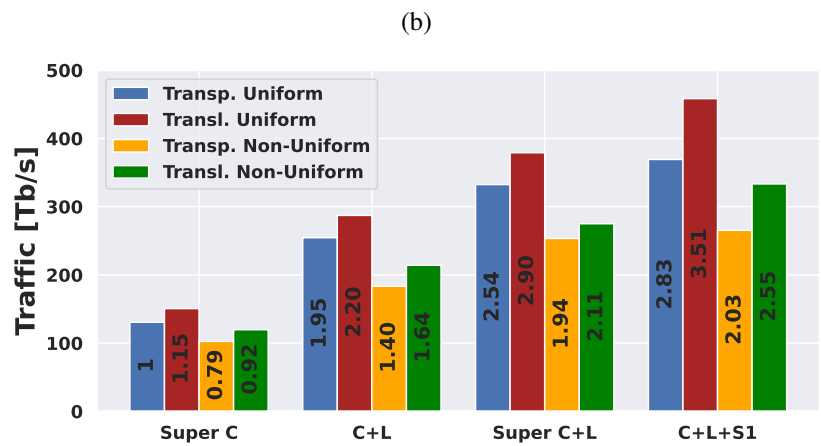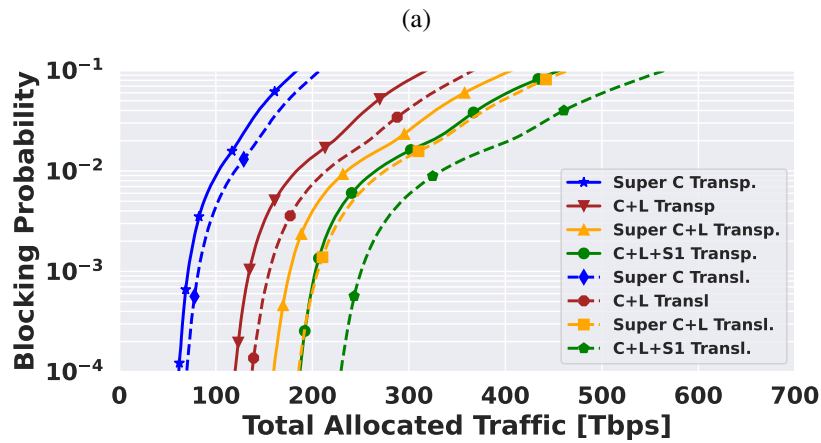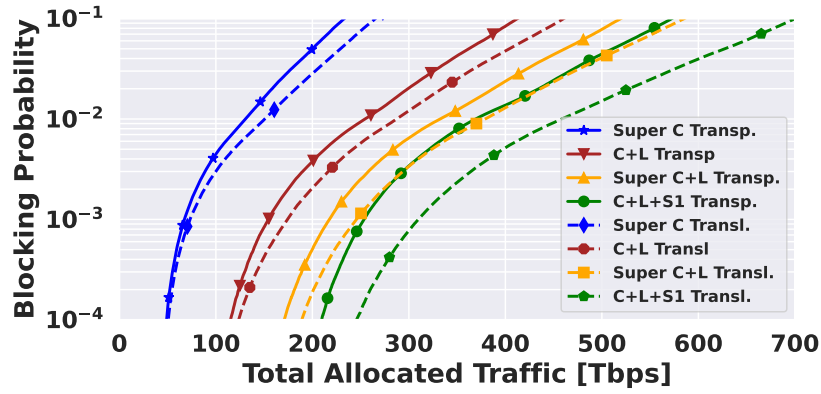
Fig. 4.3 Total allocated traffic versus BP for: a) uniform, b) nonuniform traffic distribution, and c) MF at the BP=1% for the US-NET topology.
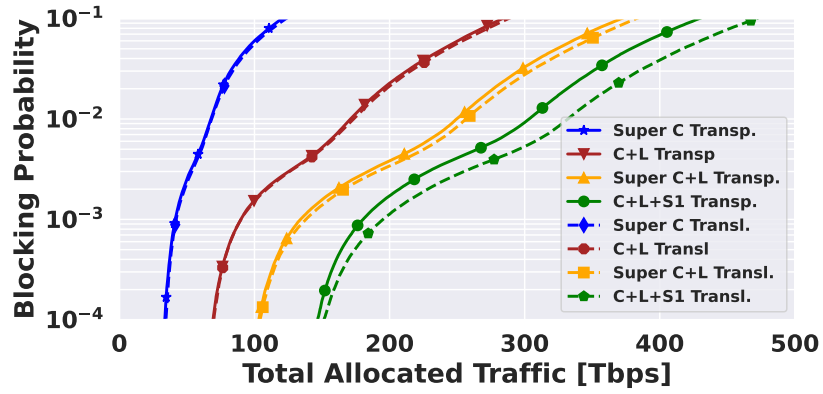
(a)

(b)
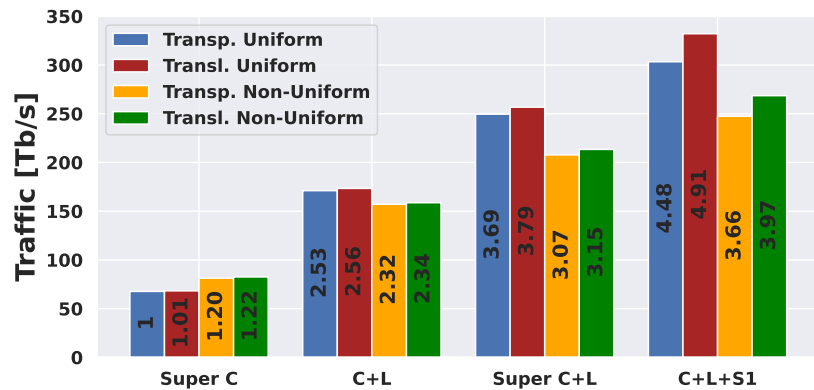
(c)

Fig. 4.4 Total allocated traffic versus BP for a) uniform, b) nonuniform traffic distribution, and c) MF at the BP=1% for the European COST topology..

214 Tb/s, respectively. The super C+L-band allows to increase these figures to 235 Tb/s and 275 Tb/s. Moreover, it should be noted that in the translucent case, this value is almost 10 Tb/s higher than that of when exploiting the C+L+S1-band in the transparent case (265 Tb/s). Finally, the translucent C+L+S1-band leads to the highest capacity with a value of 333 Tb/s.

The multiplicative factor (MF) of the total allocated traffic for all spectral configurations, with all different network designs and traffic distributions at a BP=1% level is summarized in Fig. 4.3c. The value obtained with the transparent super C-band with uniform traffic distribution is utilized as the reference. Fig. 4.3c shows that the network capacity is lower for the nonuniform traffic distribution, in both the transparent and translucent cases, with an equal amount of bands. For instance, the delivered capacities in the transparent C+L-band scenarios are $\times 1.40$ and $\times 1.95$ in the nonuniform and uniform traffic distributions, respectively. Although signal regeneration in the C+L-band nonuniform traffic distribution increased the network capacity by $\times 1.64$, this value is still less than that of the transparent and translucent C+L-band cases with uniform traffic distributions. The maximum achievable capacity in the nonuniform traffic distribution (the translucent C+L+S1-band) is $\times 2.55$ higher than the transparent super C-band with uniform traffic distribution. However, it is less than that with the translucent super C+L-band with a uniform traffic distribution, which increases the network capacity by $\times 2.90$. Furthermore, not only is the network capacity in the translucent super C+L-band with the uniform traffic distribution higher than all other nonuniform traffic distribution scenarios, but it also delivers a higher network capacity compared to the transparent C+L+S1-band with a uniform traffic distribution, even bearing in mind the latter has 32 more channels. The translucent C+L+S1 scenario with a uniform traffic distribution increased the network capacity by more than $\times 3.5$.

Fig. 4.4 shows the same set of results for the European COST topology, with Fig. 4.4a depicting the total allocated traffic in the BP range of 10^{-4} to 10^{-1} for the uniform traffic distribution. In the super C-band, the total allocated traffic at a BP of 1% is 67 Tb/s in the transparent case, with selective signal regeneration leading to a network capacity increase of only 1 Tb/s to 68 Tb/s. The total allocated traffic values in the transparent and translucent C+L-band MBT scenarios are 171 and 173 Tb/s at a BP of 1%, respectively. Extending the bandwidth to a super C+L-band scenario leads to an increase in total allocated traffic to 249 and 256 Tb/s in the transparent and translucent super C+L-band cases, respectively. This greater GSNR

degradation in MBT scenarios makes the effects of signal regeneration more evident, the C+L+S1 scenarios in the European COST topology being clear examples of this. The total allocated traffic is 303 Tb/s in the transparent network design for the C+L+S1-band MBT system. In this scenario, signal regeneration in the translucent network produces a network capacity growth of 29 Tb/s due to the deployment of more regenerators in the intermediate nodes between the source and destination pair. This difference in the translucent C+L+S1-band is mainly due to the lower QoT of the S1-band (refer to Fig. 2.8). Consequently, signal regeneration maintains the QoT of LPs with a higher QoT value, and consequently utilizes/supports the most efficient modulation formats offered by the deployed TRX.

Fig. 4.4b shows the total allocated traffic in the European COST topology for transparent and translucent network designs with nonuniform traffic distribution. Similar trends as those observed for uniform traffic can be identified in this plot. The network capacity in the transparent MBT scenarios is 81, 157, 207, and 247 Tb/s for the Super C, C+L, super C+L, and C+L+S1-band, respectively. In the translucent network design, the total allocated traffic increases to 82, 158, 213, and 268 Tb/s in the super C, C+L, super C+L, and C+L+S1-band systems, respectively.

The MF of total allocated traffic for all MBT systems at a BP of 1% is depicted in Fig. 4.4c, again considering the transparent super C-band with uniform traffic pattern as the reference. Fig. 4.4c shows that the capacity delivered with the non-uniform traffic distribution is less than for the uniform cases, except for the super C-band. In the case of super C-band only transmission with uniform traffic distribution, we may reach a quick network saturation without fully using the existing LPs total capacity. However, this advantage becomes clear due to the more efficient use of the available QoT and management of the existing LPs by exploiting MBT configurations such as C+L, super C+L, and C+L+S1-band. This behavior is clear in the network performance in Fig. 4.4. We observe that the maximum achievable capacity in the C+L-band scenario increases by $\times 2.56$ compared to the super C-band. This value is further extended to $\times 3.79$ with the super C+L-band. Although the maximum increase in traffic in this network topology with nonuniform traffic is $\times 3.97$ (translucent C+L+S1-band), this value increases to $\times 4.91$ with uniform traffic distribution. Figs. 4.3c and 4.4c present three key findings: (i) the use of super bands gives more capacity when considering the same number of bands (i.e., super C+L-band versus C+L-band), (ii) uniform traffic distribution delivers the highest network capacity in both investigated network topologies, and (iii) exploiting more bands

and consequently increasing the number of channels results in a greater difference between the transparent and translucent network designs.

4.5   Interface Count

In this subsection the number of used interfaces (i.e., TRXs) versus allocated traffic for all investigated scenarios in section 4.4 is presented. Fig. 4.5 shows the number of interfaces versus total allocated traffic for BPs≤1% in all investigated MBT systems with uniform and nonuniform traffic distributions, for the US-NET topology with both transparent and translucent network designs. Figs. 4.5a and 4.5b show that there is only a small difference in the number of utilized interfaces in the transparent network design case, for all investigated MBT systems. However, this difference is more pronounced when considering the translucent case.

This higher interface utilization in the translucent super C-band case is due to both the allocation of the first channels by the first-fit wavelength assignment (FF-WA) policy and due to the super C-band having a poor QoT in its first allocated channels compared to the other three MBT scenarios because of SRS effect. For example, the GSNR values in the first channels of the super C-band (30 dB) only case are lower than first channels of the L-band (30.6, 30.6, and 31.2 dB) in the C+L, super C+L, and C+L+S1-band cases (refer to Tab. 2.3). Consequently, the 3R regenerator is used less because it supports the most efficient modulation formats for the primary requested services of the C+L-, super C+L-, and C+L+S1-band cases. Furthermore, for high allocated traffic values, high-frequency channels have a poorer QoT, so require a larger number of interfaces, for example in Fig. 4.5a for allocated traffic greater than 150 Tb/s. This effect is clearly observable in the C+L+S1-band scenario; extra interfaces are implemented to support the most efficient modulation formats, as the average GSNR of the S1-band is comparatively lower. Additionally, the channels with higher frequency in the super C+L-band case whose have a poor QoT cause to grow in the number of demanded interfaces in this MBT scenario compared to the regular C+L-band. The number of interfaces used for transparent and transparent cases in the European COST topology is shown in Fig. 4.6, showing that uniform and nonuniform traffic distributions are almost equal. This is because LPs in this network topology have the most efficient modulation formats and a small number of regenerator assignments, which results in no significant changes to
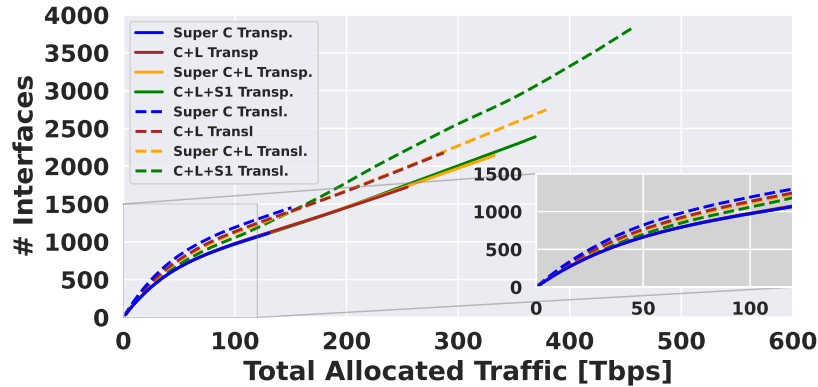
(a)
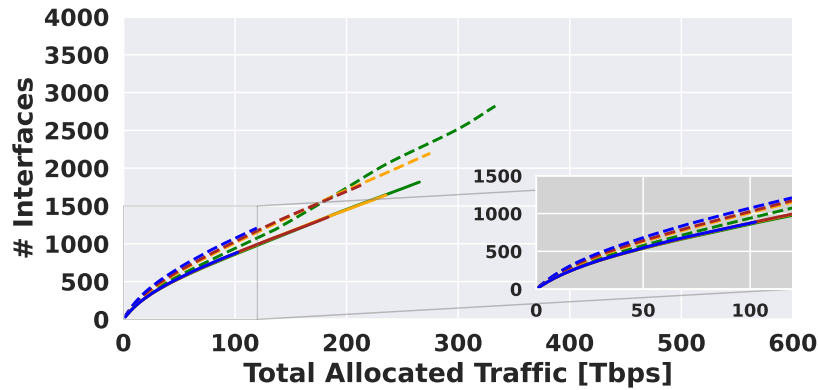
(b)

Fig. 4.5 Total allocated traffic versus utilized interfaces for a) uniform, b) nonuniform traffic distribution for the US-NET topology.

the total allocated traffic and interface count. However, the GSNR degradation in the higher frequencies due to the SRS and NF affects the assignment of the more regenerator and causes it to increase the number of demanded interfaces. For instance, the C+L+S1 and super C+L-band is a clear example of this point. According to Figs. 4.6a and 4.6b, the number of demanded interfaces grows especially in the C+L+S1-band scenario due to the assignment of more regenerators to support the most efficient modulation formats of TRX (solid and dashed green curves). This effect is negligible in the super C+L-band configuration because of having better QoT compared to the C+L+S1-band (solid and dashed yellow curves). According to these Figs, although the super C+L-band requires almost the same amount of interfaces compared to the regular C+L-band scenario, it offers higher throughput in comparison to the regular C+L-band configuration.
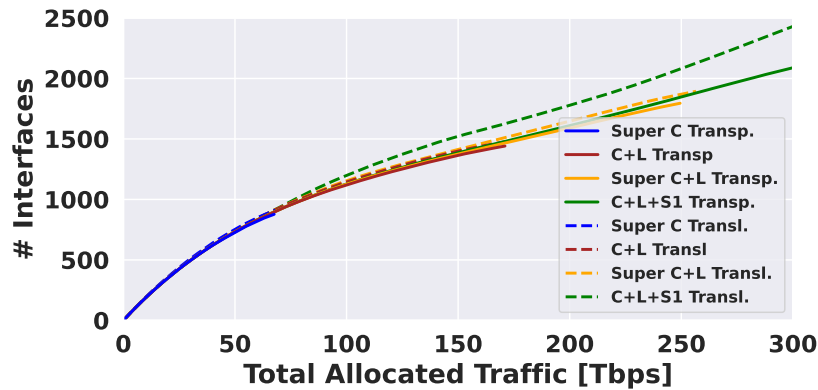
(a)
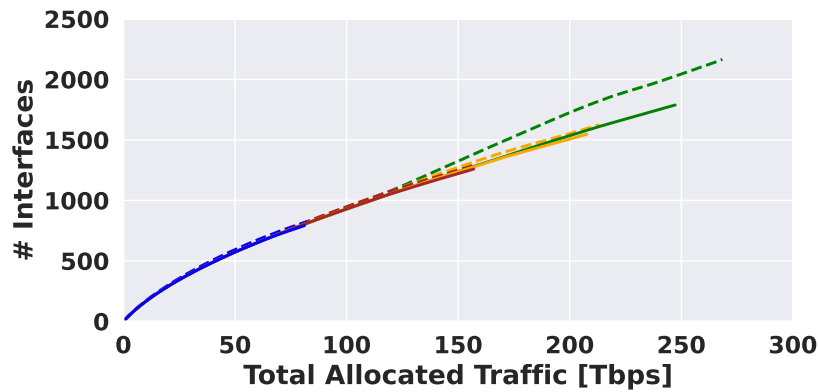
(b)

Fig. 4.6 Total allocated traffic versus utilized interfaces for a) uniform, b) nonuniform traffic distribution for the European COST topology..

To be more precise about the advantages and disadvantages of each investigated configuration in terms of costs, Tabs. 4.3 and 4.2 are provided for the US-NET and European COST topology, respectively, for an allocated traffic of 250 Tb/s. We note that the BP value for a delivered capacity of 250 Tb/s in the super C-band scenario is very high, and as such represents an unrealistic network configuration – as a result, this specific scenario is excluded from these tables. From Tabs. 4.3 and 4.2 we see not only that increasing the number of wavelengths increases the number of interfaces used, but also that this effect is larger for the translucent network design.

Considering the US-NET topology, these results show that the super C+L-band scenario provided a capacity increase of more than 59% (Fig. 4.3c) compared to the regular C+L-band scenario, for a transparent network design with uniform traffic

distribution. However, the number of interfaces required remained almost equal, despite the super C+L-band scenario having 25% more channels than the regular C+L-band scenario. Moreover, not only does the transparent super C+L-band allows to support more traffic load than the translucent regular C+L-band (Fig. 4.3a), but it also demands fewer interfaces than the latter, which requires 1960 interfaces to deliver a 250 Tb/s capacity. Please note that the number of amplifiers used for both the C+L and super C+L-band configurations is equal to 1122. Based on Fig. 4.3a and Tab. 4.3, the translucent super C+L-band design delivers an approximately equal capacity to the transparent C+L+S1-band, although it demands 238 more interfaces to deliver a 250 Tb/s capacity. However, the number of amplifiers required in the C + L + S1-band configuration is higher than that in the super C+L-band, i.e., 1683 versus 1122 (a difference of 561) amplifiers. In general, the average bit rate per interface tends to decrease as a larger transmission bandwidth is exploited.

Table 4.2 Interface count, bit rate per interface, and number of deployed optical amplifiers at a delivered traffic of 250 Tb/s in the European COST topology.

	Uniform		Non-Uniform		
	#Interf.	Bit rate/Interf. [Gbs^{-1}/interf.]	#Interf.	Bit rate/Interf. [Gbs^{-1}/interf.]	#Amps.
Transp. C+L	1679	149	1677	149	696
Transp. Super C+L	1796	139	1755	142	696
Transp. C+L+S1	1846	135	1803	138	1044
Transl. C+L	1711	146	1711	146	696
Transl. Super C+L	1869	134	1814	137	696
Transl. C+L+S1	2081	120	2044	122	1044

Tab. 4.2 shows the number of demanded interfaces, bit-rate per interface, and the number of amplifiers for each investigated scenario in the European COST topology. In this topology, the deployment of a super C+L-band increases the network capacity (refer to Fig. 4.4a), but at the expense of a higher interface count than that with the regular C+L-band. For instance, to deliver a 250 Tb/s capacity in a transparent network design, with a uniform traffic distribution, the number of used interfaces is 1679 and 1796 for the C+L-band and super C+L-band, respectively. This is due to the fact that regular C+L-band network design uses mostly already allocated LP capacities to deliver a capacity of 250 Tb/s which is in a higher BP range; however, super C+L-band configuration establishes new LPs which is in a

Table 4.3 Interface count, bit rate per interface, and number of deployed optical amplifiers at a delivered traffic of 250 Tb/s in the US-NET topology.

	Uniform		Non-Uniform		
	#Interf.	Bit rate/Interf. [Gbs^{-1}/interf.]	#Interf.	Bit rate/Interf. [Gbs^{-1}/interf.]	#Amps.
Transp. C+L	1702	147	1698	147	1122
Transp. Super C+L	1714	146	1724	145	1122
Transp. C+L+S1	1732	144	1730	144	1683
Transl. C+L	1960	127	2011	124	1122
Transl. Super C+L	1970	127	2031	123	1122
Transl. C+L+S1	2185	114	2161	115	1683

lower BP range. This behavior is observable in the ramp of curves in figs. 4.3 and 4.4. These values increase to 1711 and 1869 in the translucent network design with uniform traffic distribution. We note that both C+L+S1-band designs require the highest amount of interfaces and optical amplifiers. Furthermore, this increase in interfaces corresponds to a decrease in the amount of traffic per interface, also visible in Tabs. 4.3 and 4.2. Overall, the number of demanded interfaces and amplifiers is valid for both types of traffic distribution.

4.6 Impact of QoT margins on Network Capacity and Demanded Interfaces

To show the benefits of different MBT configurations such as super bands versus regular bands, in this section, the network capacity and the number of demanded interfaces in specific delivered traffic have been investigated for both network topologies with uniform traffic distribution with different QoT margins that can be caused by various effects namely fiber aging, filtering penalties, etc. In this section, we have considered up to 4 dB QoT penalty in each scenario which may have different sources. Fig. 4.7 represents the both total allocated traffic at the BP of 1% and the number of demanded interfaces at the delivered traffic of 250 Tb/s for the US-NET network topology. According to Fig. 4.7a, increasing the QoT margin from 0 to 4 dB cases decreases the network throughput in the transparent network design; This is due to deploying the TRX's less efficient modulation formats; however, signal regeneration in the translucent network design resists to capacity decreasing because
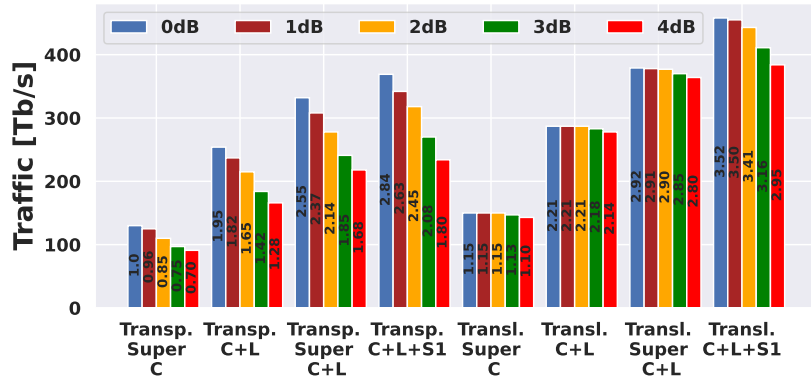
(a)
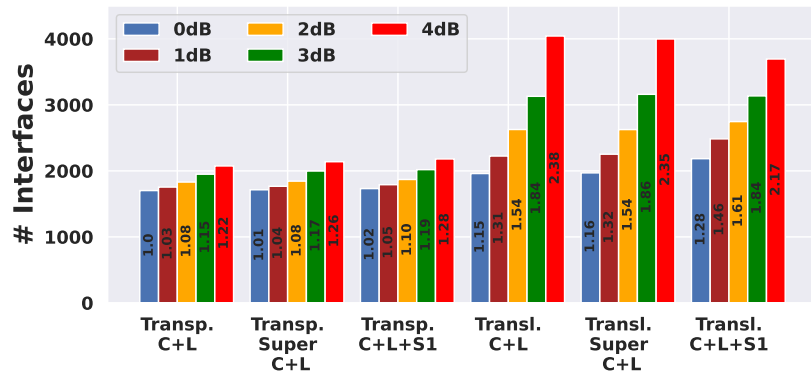
(b)

Fig. 4.7 a) Total allocated traffic at the BP of 1% and b) the number of demanded interfaces to allocated 250 Tb/s traffic for different MBT scenarios with the QoT margin of 0 to 4 dB in the US-NET topology.

of dividing LPs to sub transparent segments results in supporting higher efficient modulation formats of TRX. To be more precise, in the transparent super C-band scenario the network capacity drops 30% by considering a 4 dB QoT margin compared to the without considering any margin. On the contrary, the network throughput decreases less than 5% in the translucent network design with a maximum QoT margin which is 4 dB. It is worth mentioning that in this scenario, super C-band, the network's delivered capacity is still higher than the transparent one for all applied QoT margins.

In the transparent C+L, super C+L, and C+L+S1-band the network throughput decreases less than 37% in each scenario. In the C+L and super C+L-band translucent
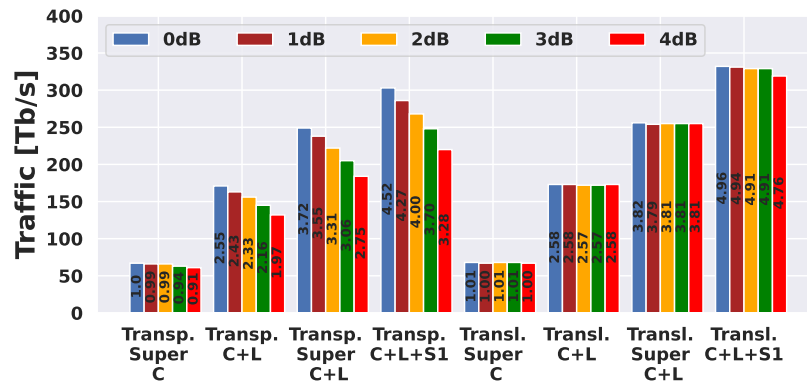
(a)
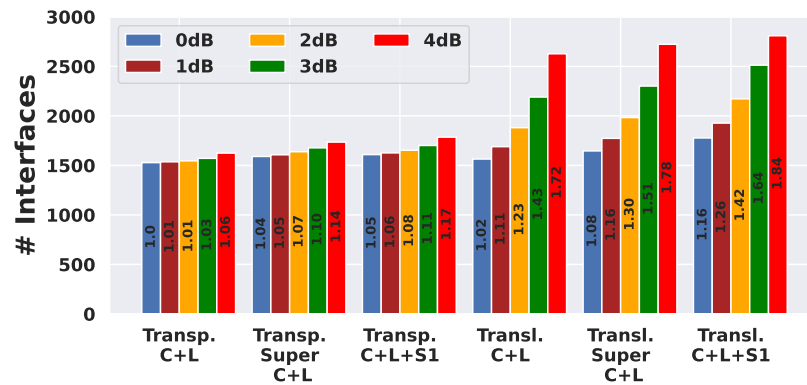
(b)

Fig. 4.8 a) Total allocated traffic at the BP of 1% and b) the number of demanded interfaces to allocated 200 Tb/s traffic for different MBT scenarios with the QoT margin of 0 to 4 dB in the European COST topology.

network design, the network capacity decreases by less than 4%. However, increasing the QoT margin in turn reduces the capacity in the translucent C+L+S1-band scenario by about 16%. This is due to the poor performance within the S1-band preventing deployment of efficient modulation formats within links inside the LP. Regarding the number of demanded interfaces considering QoT margins, Fig. 4.7b has been depicted in the specific delivered traffic of 250 Tb/s. It is observable that the number of demanded interfaces in both transparent and translucent network designs increases by growing the QoT margin.

On the one hand, the number of required interfaces to allocate the traffic of 250 Tb/s in the transparent C+L, super C+L, and C+L+S1-band configurations

grows by 25%. On the other hand, although signal regeneration resisted significant capacity decrease in the translucent network design, the required number of interfaces increased more than 100% in the translucent C+L and super c+L-band and about 69% in the translucent C+L+S1-band scenario to deliver the capacity of 250 Tb/s. Overall, the translucent super C+L-band configuration in the worst QoT penalty, 4 dB, has a better performance compared to the transparent C+L+S1-band, exploiting one band more, configuration with delivered traffic of 365 Tb/s at the BP of 1% (Fig. 4.7a). Moreover, although translucent super C+L-band requires more interfaces to deliver 250 Tb/s traffic compared to the transparent C+L+S1-band case, it exploits 30% less amount of amplifiers due to exploiting one band less. Fig. 4.8 shows the QoT margin effect on the total allocated traffic at the BP of 1% and the number of required interfaces to allocate the traffic of 200 Tb/s for four MBT upgrades with transparent and translucent network designs in the European COST network topology. According to Fig. 4.8a, increasing the QoT margin causes to decrease in the network throughput in the transparent network designs in all MBT upgrades. For instance, at the BP of 1%, the network throughput decreases about 9, 22, 26,27% in the transparent super C+L, C+L, super C+L, and C+L+S1-band cases, respectively. However, gaining the margin results in deploying more regenerators and consequently efficient modulation formats to be utilized in the translucent; thus, network throughput does not changes in the translucent super C, C+L, super C+L, and C+L+S1-band scenarios significantly. Regarding the number of demanded interfaces to allocated 200 Tb/s traffic, Fig. 4.8b has been depicted. According to this figure, the number of demanded interfaces increases by less than 10% to deliver a capacity of 200 Tb/s

Table 4.4 The percentage of capacity loss at the BP of 1% and interface demands in the delivered traffics of 250 Tb/s and 200 Tb/s for different network designs and upgrades in the US-NET and European COST network topologies with different QoT margins.

	US-NET		European COST	
	Capacity [%]	Interface [%]	Capacity [%]	Interface [%]
Transp. Super C	30.0	–	8.9	–
Transp. C+L	34.6	21.9	22.8	6.2
Transp. Super C+L	34.3	24.7	26.1	9.1
Transp. C+L+S1	36.5	25.9	27.3	10.9
Transl. Super C	4.6	–	1.4	–
Transl. C+L	3.1	106.2	0.0	69.9
Transl. Super C+L	3.9	102.9	0.3	65.4
Transl. C+L+S1	16.1	69.1	3.9	58.0

in the transparent configurations. However, the QoT margin causes deploying more regenerators/interfaces, on average 64%, to deliver this amount of capacity in the translucent cases.

As a key finding of this section, i) super C+L-band in the translucent network design has a better/equal performance compared to the transparent C+L+S1-band configuration in terms of delivered capacity and the number of demanded interfaces in the presence of considerable QoT margins. ii) translucent network design saves the network delivered capacity at a higher level compared to the transparent design by deploying more regenerators, especially in the super C+L-band which is comparable with all transparent cases. iii) Although the super C+L-band – with 30% fewer amplifiers compared to the C+L+S1-band configuration – in the translucent scenario performs better compared to the transparent C+L+S1-band, the required number of interfaces/amplifiers is higher/less than transparent C+L+S1-band configuration's requirements. Tab. 4.4 has been provided to have a general view of the networking performance of each scenario with different QoT margins for both investigated network topologies. This table shows the percentage of capacity loss and percentage of increased demand of interfaces for each scenario with respect to the delivered capacity without any QoT margin in the corresponding scenario.

Chapter 5

Optimized S-band versus U-band

In this chapter, for multi-band optical networks that encompass the C-, L-, and S-bands, the latter provides the poorest Quality of Transmission (QoT). We have evaluated the optimization of the S-band in a multi- band optical network scenario, demonstrating the possibility of increasing overall network capacity in a cost-effective manner. Then, we will investigate using the U-band instead of the complete S-band and show that it is a more effective solution for increasing capacity while still reducing energy consumption and cost in transparent and translucent network designs.

5.1   Optimized Translucent S-band Transmission

In this section, we focus on the optimization of a translucent approach in the S-band targeting: a) attaining similar capacity in S-band as in the C-band, which we refer to as S-band with limitations and b) achieving the maximum capacity in S-band, which we refer to as S-band without limitations. Both network designs are compared with the fully transparent reference approach, denoted in the figures as transparent CLS.

A transparent design is always assumed for the C- and L-bands. however, for the first scenario, the capacity of the LPs in each frequency was calculated and then compared with the same frequency order on the C-band. As an example of the implementation of the proposed approaches, let's assume that 8QAM and QPSK
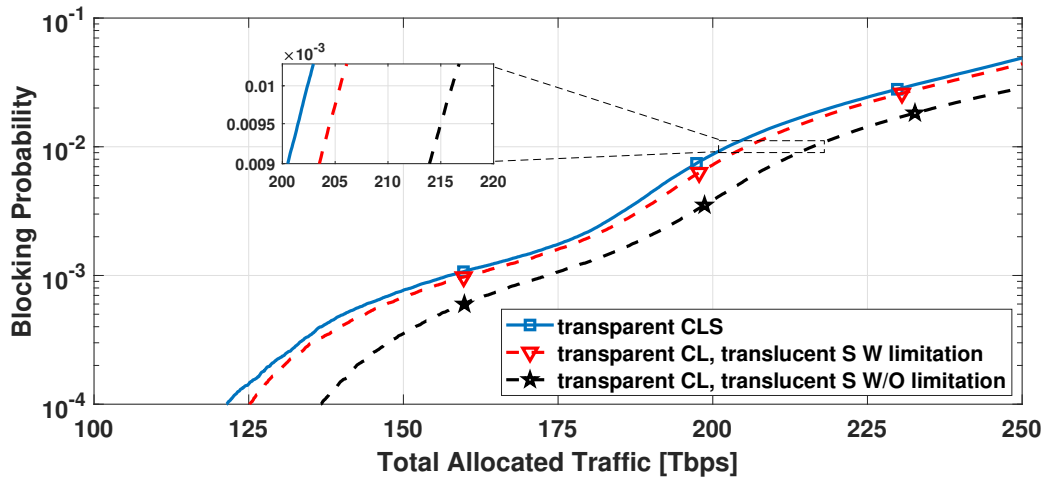
Fig. 5.1 Blocking probability versus total allocated traffic for the US-NET topology.

modulation formats are supported by a LP in the C- and S-bands, respectively. In this case, regenerators are assigned in the S-band to improve the overall QoT. In the S-band with limitations scenario, the minimum number of optical regenerators required to enable 8QAM transmission are deployed in the intermediate nodes. Conversely, in the S-band without limitations scenario, the minimum number of regenerators required to enable 16QAM transmission (the most efficient modulation format used by the TRX) are deployed. Concerning the regenerator assignment, if the maximum LPcapacity is different in the C- and S-bands, the algorithm evaluates all possible regenerator placement options with respect to the threshold GSNR (see Table 2.4) of each LP. Then, based on the scenario, the best option is selected. This regenerator assignment algorithm considers the least possible number of regenerators thus preventing unnecessary increase of cost and power consumption. Developed SNAP, already explained in chapter 2, is used to analyze the blocking probability vs. allocated traffic for the US-NET network topology by progressively loading the network with 100 Gbps connection requests. Moreover, traffic grooming is considered by the SNAP. In other words, when a request arrives, the SNAP checks the capacity of already deployed LPs between the source and destination of the request and if it finds any vacant capacity, it allocates the traffic in that LP till to reach the maximum capacity of it.

Fig. 5.1 shows the total allocated traffic for different blocking probabilities (BP) for the three investigated scenarios: the transparent CLS reference scenario, S-band with limitations, and S-band without limitations. Firstly, it is clear that the fully

transparent network design (solid blue) leads to the highest blocking probability. As an example, a BP of 1% is reached at a network capacity of approximately 200 Tbps. In the S-band with limitations scenario (red dashed line), there is a small capacity increase of almost 5 Tbps for the same BP. Finally, for the S-band without limitations scenario (dashed black curve) the total capacity is increased by about 15 Tbps for the same BP.

Figure 5.2 provides more details on the potential of the proposed approach. Fig. 5.2a shows the number of regenerators used in both S-band scenarios for different LP route distances. Considering first the S-band with limitations scenario, the total average number of regenerators used in the network is approximately 54, with about 38 LP routes in the range of 2000-2500 km. However, in the S-band without limitations scenario, the number of regenerators is approximately 111, with a maximum of approximately 50 corresponding to distances in the 2000-2500 km range. In this scenario, additional regenerators are used for LP longer than 2500 km to enable 16QAM modulation format.

The ratio between the number of LPs with and without regenerators is also shown for both network designs in Fig.5.2b. This figure shows that, when designing a translucent S-band with limitations, as the LP length increases, so does the number of required regenerators until only QPSK is supported in C-band. In this case, and assuming this modulation format is also supported in S-band, no optical regenerators are required. LPs being assigned regenerators for route lengths in 1000-1500, 1500-2000, and 2000-2500 km ranges, which are 0.9%, 9%, and 20% of total LPs, are a clear example of this. On the other hand, for the S-band without limitations case, we expect that the ratio of LP using regenerators increases proportionally to the LP route length; we find that this is the case, except for LPs in the 2500-3000km range, where the ratio of assigned regenerators drops to approximately 10 %. The reason for this drop is that, in this topological configuration and for several node pairs, the first option for traffic assignment is a route within this range, meaning that the majority of LPs are still assigned frequencies within the C- and L-bands. This condition greatly reduces the number of S-band samples within this range, correspondingly reducing the number of LP which may be assigned regenerators.

In Table. 5.1 we provide the total capacity, energy consumption, and TRX number (normalized with respect to the transparent reference scenario), along with the average number of LPs requiring regenerators. These results show that, for
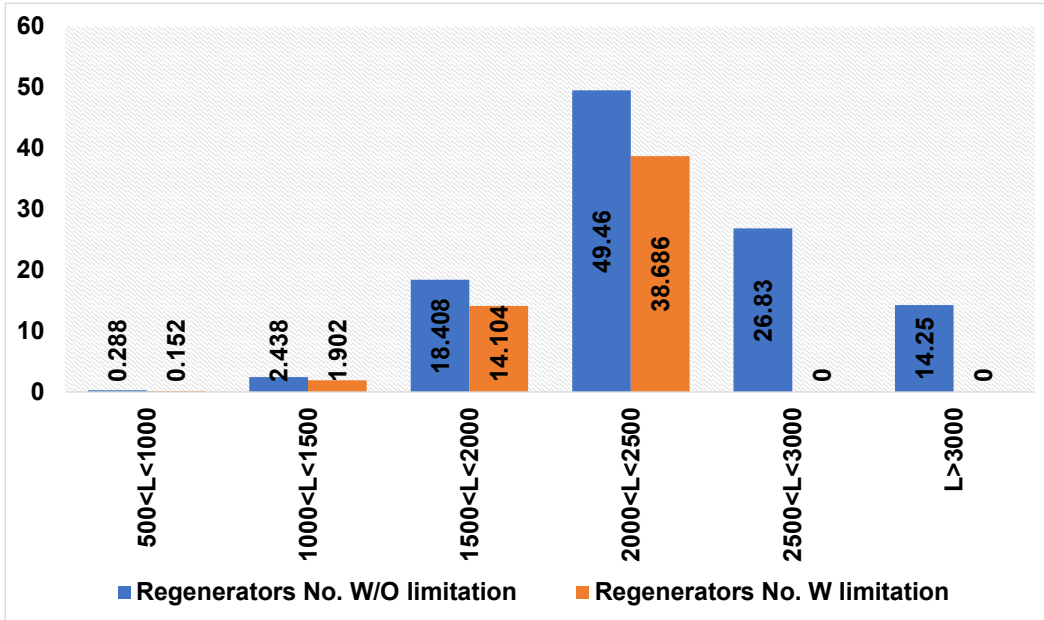
(a)
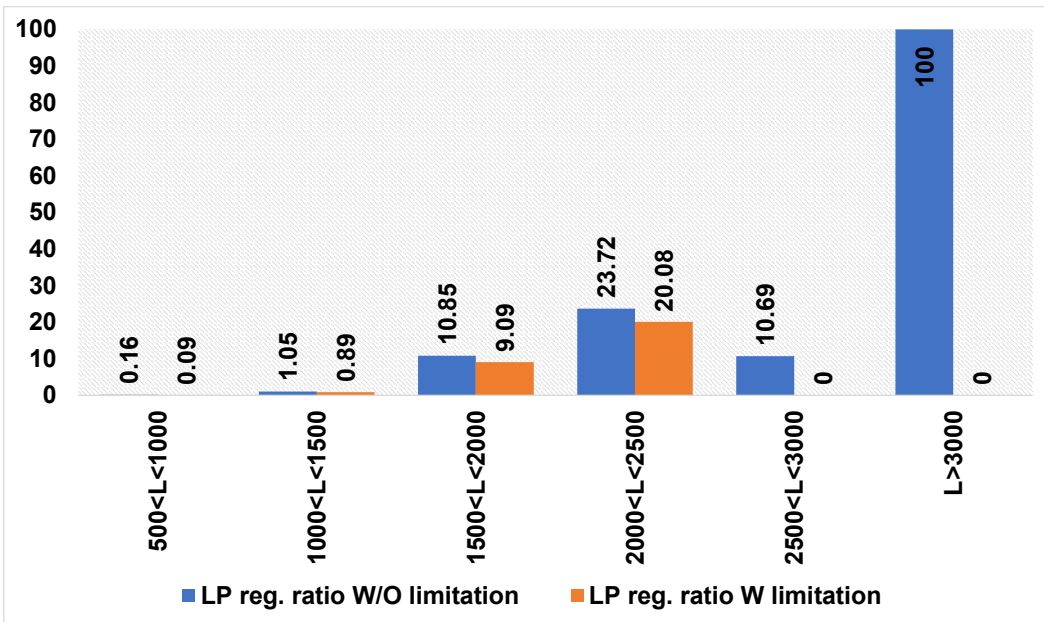
(b)

Fig. 5.2 The (a) regenerators quantity, and (b) LP regenerator assignment ratio, for a range of different route lengths within the US-NET topology.

both scenarios, the average energy consumption only marginally increases, along with a progressive but small increase in the number of required TRXs. Overall, we remark that, if there are strict power consumption limitations within the network, placing regenerators within the S-band with limitations can provide some capacity enhancement, which can be increased beyond the C+L reference level, if these limitations are not imposed.

Table 5.1 Multiplicative factor of capacity, energy consumption, TRX point-to-point number, and number of LPs assigned regenerators for the three scenarios under investigation.

	Capacity	Energy Consumption	TRX	Avg. # LPs with regenerators
Transparent CLS	1	1	1	0
Transparent CL, S band W limitation	1.01	1.00	1.04	54.84
Transparent CL, S band W/O limitation	1.06	1.01	1.10	111.67

5.2   Optimal Spectral Usage: U-band Versus Full S-band

In the previous section the optimal usage of the S-band has been investigated in terms of capacity, the number of required interfaces, energy consumption, etc. We showed that deploying 3R regenerator in the S-band due to having poor QoT compared to the other bands such as the C- and L-band leads to an increase in the network capacity along with increasing the energy consumption. In this section, we will compare the networking benefits of deploying full S-band or using half of the S-band and exploiting the U-band instead of the second half of the S-band which has a poor QoT compared to the first half due to the SRS effect.

In the remaining of this work, the physical layer abstraction is carried out assuming a fully-loaded spectrum, a WDM grid with 75 GHz frequency slots, optical channels operated with a symbol-rate of 64 GBaud, and fiber spans of 75 km. In Fig. 5.6a the GSNR profiles are presented for the two wideband configurations used in this work: (i) ULCS1, with 64 channels in each band (U-, L-, C- and S-) using only half of the S-band capacity; (ii) LCS2, without the U-band but exploring the full S-band capacity, dividing it into two sub-bands and using one amplifier for each. In both configurations, the number of wavelengths for each band is considered

equal to 64 (the only exception being S-band with 128 channels in LCS2) for a total of 256. The launch power profile strategy is performed following the same approach as [97]. The average GSNR per band for the ULCS1 configuration is 28.83, 30.67, 28.84, and 26.32 dB for the U-, L-, C- and S1-bands, respectively. For the LCS2 configuration, the average GSNR is 31.18, 30.06, 25.37, and 24.64 for L-, C-, S1- and S2-bands, respectively. After the detailed characterization of the physical layer, the network analysis is performed via the statistical network assessment process (SNAP) [61] in the US-NET topology. The k-shortest path algorithm is used to compute up to $k_{max} = 5$ candidate routing paths for each node pair and wavelength assignment enforces the first-fit algorithm. A progressive traffic load analysis is performed, where each new request consists of a 100 Gbps traffic demand. Additionally, before the establishment of a new LP, traffic grooming is first attempted, by checking the availability of idle capacity in existing LPs. When establishing a new LP is necessary that the optical controller selects the proper modulation format based on the estimated QoT and the TRX required GSNR (RGSNR) [82]. Three different channel provisioning scenarios are considered: transparent, translucent, and power-optimized translucent. In the transparent network scenario, a new LP is always established end-to-end, resorting to the highest order modulation format that is feasible without intermediate regeneration and guaranteeing the wavelength continuity constraint among all links in the path. In the translucent scenarios, this constraint is removed in the nodes where the regeneration is performed (realized as a pair of back-to-back TRXs). In the first translucent strategy, designated as General Translucent, the controller activates an extra pair of TRXs on intermediate nodes when this is strictly required to maintain the maximum bit rate for that LP, which is 400 Gbps (16QAM) in this work. Finally, in the second translucent strategy, designated as Pow. Opt. (Power Optimization), the controller finds all possible combinations between source and destination nodes of modulation format and the minimum number of regenerators needed. It then selects the most efficient modulation format and regenerator placement such that the total power consumption of the required TRXs is minimized. This results in a solution that, on average, can be more power-efficient than the general translucent, while being at the same time more spectrally efficient than the one obtained with the transparent strategy. Importantly, in both translucent strategies, the controller avoids deploying unnecessary regenerators to attain the target data rate, consequently preventing further increases in cost.

(a)

(b)
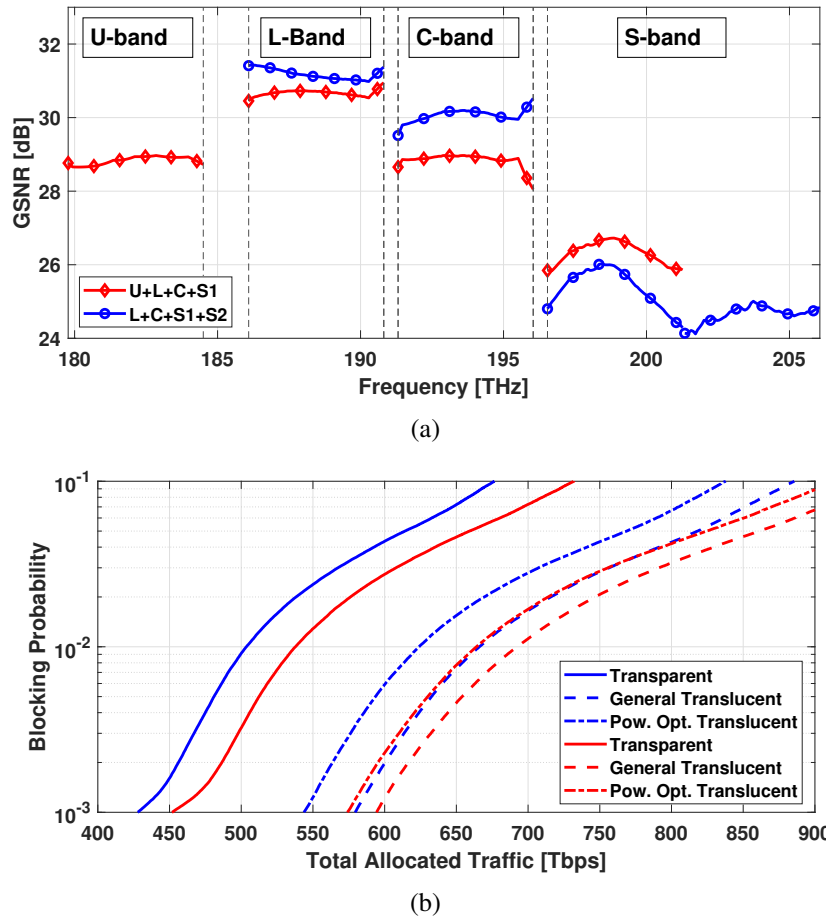
Fig. 5.3 (a) Frequency versus GSNR for the LCS2 and ULCS1 scenarios, and (b) total allocated traffic versus blocking probability for the US-NET topology (LCS2: Blue and ULCS1: Red).

5.2.1   Network simulation results and discussion

Network analysis has been executed considering the LCS2 and ULCS1 band configurations, keeping the same total number of channels and amplifiers. In Fig. 5.6b the total allocated traffic for different BPs has been shown. It is observable that due to its lower overall QoT, LCS2 (blue color) results in higher BP when compared to ULCS1 (red color) in both the transparent and general translucent scenarios. For instance, in the transparent network design, the utilization of the ULCS1 band configuration enables it to support approximately 6% more capacity, when compared to LCS2. Moreover, moving from the transparent to the translucent network design leads to an increase of capacity of between 24% to 37% in the Pow. Opt. and general
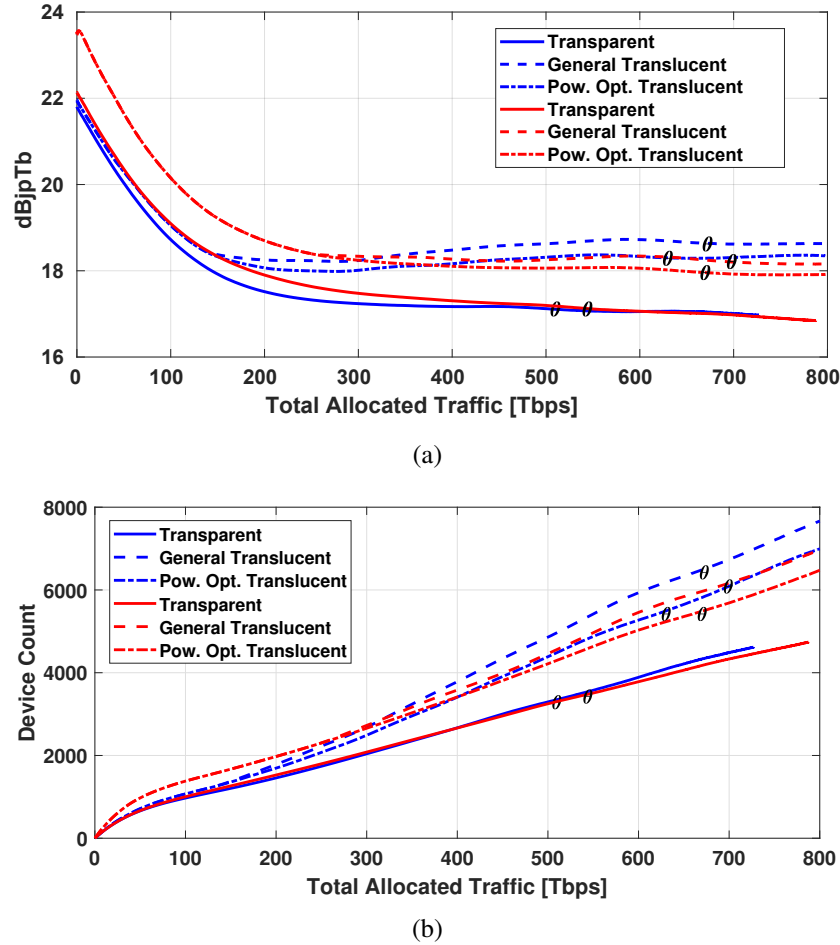
Fig. 5.4 (a) Energy consumption and (b) Device count versus total allocated traffic. Indicator θ determines the BP of 1% (LCS2: Blue and ULCS1: Red).

translucent network designs, respectively. From the energy consumption viewpoint, which is investigated as the energy consumed to transfer a bit in Fig. 5.4a. As can be seen, when starting to load a network the energy consumption is high, which is a consequence of having new LPs that are not fully loaded. However, as load increases, LPs will tend to be full and energy consumption decreases. According to Fig. 5.4a, the transparent network scenario with ULCS1 supports more traffic load than the same scenario with LCS2, while energy consumption is comparable, i.e., 17.1 dBjpb at a BP of 1% (marked with θ). In the ULCS1 band configuration with both translucent strategies, the energy consumption is high, flattening at around 300 Tbps. From this load value onward, energy consumption drops about 1 dBjpb below that of the LCS2 band configuration and reaches around 18 dBjpb. The
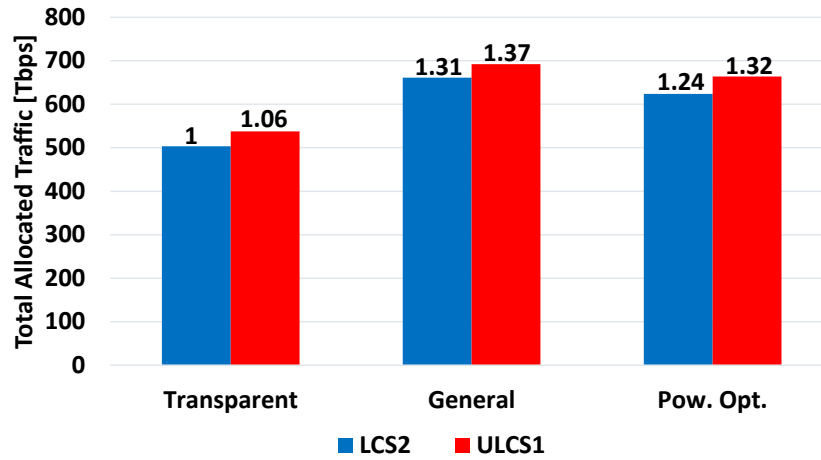
Fig. 5.5 Multiplicative factor at the BP=1% (with respect to the transparent LCS2).

Table 5.2 Multiplicative factor for 600 Tbps traffic load (with respect to the transparent LCS2).

Traffic = 600 Tbps		Transparent	General	Pow. Opt.
LCS2	Total Energy	1	1.09	1.07
	Device Count	1	1.52	1.35
ULCS1	Total Energy	1	1.07	1.05
	Device Count	0.99	1.40	1.29

number of used point-to-point TRXs for each scenario is depicted in Fig. 5.4b. Each regenerator is assumed to be realized as two TRXs. This figure shows that the transparent cases for both ULCS1 and LCS2 require almost the same amount of TRXs for a target capacity. As an example, for 500 Tbps, 3270 TRXs are required in the transparent network design. However, for a fairer comparison, one needs to consider the same BP value. For instance, for a BP of 1%, the number of used TRXs at Pow. Opt. scenarios are close to 5500 but the capacity supported is 667 and 625 Tbps, for the ULCS1 and LCS2, respectively. In other words, for the same number of TRXs an extra 40 Tbps of capacity is supported when using ULCS1 instead of LCS2 band configuration.

The multiplicative factor of the capacity results at a BP=1% is presented in Fig. 5.5, in which the transparent network design for the LCS2 configuration is considered as a reference. It can be observed that the capacity of the network in the transparent design increased ×1.06 times when using the U band instead of the full S-band. Additionally, this value increased ×1.37 and ×1.32 times in the translucent

design with different approaches namely general and Pow. Opt., respectively. Furthermore, Table 5.2 shows the multiplicative factor for both the energy consumption and TRX count considering a traffic load of 600 Tbps and assuming the transparent LCS2 case as a reference. Based on this, the energy consumption and the number of used TRXs are almost the same for the transparent network design in both ULCS1 and LCS2. Noteworthy, the energy consumption is slightly lower with the Pow. Opt. translucent strategy. The higher energy consumption observed with the LCS2 case is a result of this configuration making use of more TRXs than those required with ULCS1. For instance, the number of TRXs required by the General translucent network design is $1.52\times$ more than with the transparent design in the LCS2 case. However, this value drops to $1.40\times$ in the ULCS1 band configuration. Additionally, the minimum number of TRXs used in the Pow. Opt. translucent network design in the ULCS1 case is $1.29\times$ that with transparent network design.

At the conclusion of this section, we investigated the networking benefits of exploiting the U-band instead of the second half of the S-band (S2-band) in the transparent and translucent network configurations. In the next section of this thesis, the networking benefits of utilizing the U-band with the already used C+L-band will be presented and compared to the S1-band (C+L+S1-band) in terms of capacity and energy consumption in the transparent and translucent network designs.

5.3 U-band versus Half of S-band in the MBT Scenarios

According to the chapter 2 the GSNR value for different MBT scenarios namely C+L, C+L+S, and C+L+U-band have been evaluated in this section. it is worth mentioning that the S-band here denotes the first half of the full S-band (S1-band). The GSNR profile for three different configurations (C+L-, C+L+S-, and C+L+U-band) is depicted in Fig. 5.6a. The average GSNR value after a single span for the C- and L-band, in the C+L-band configuration, is equal to 29.4 dB and 30.4 dB, respectively. The latter value changes to 31 dB in the C+L+S-band configuration, in which case the GSNR value in the S-band is 26.5 dB. In the C+L+U-band configuration, the average GSNR value is 28.6 dB, 29.6 dB, and 28.6 dB for the C-, L-, and U-band, respectively. For the network analysis, the US-NET topology
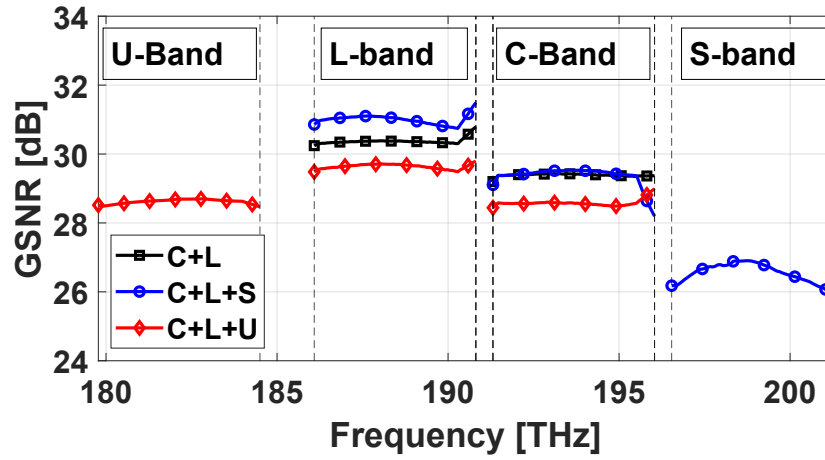
(a)
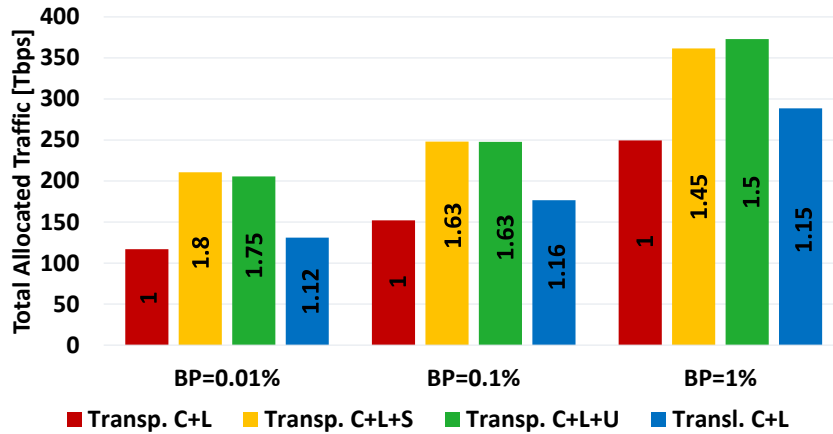
(b)

Fig. 5.6 (a) Frequency versus GSNR for the C+L-, C+L+S- and C+L+U-band scenarios, and (b) total allocated traffic versus three different targets BPs for the US-NET topology.

is progressively loaded with connection requests of 100 Gb/s. As per OpenZR+ MSA, each TRX supports three different modulation formats (16QAM, 8QAM, and QPSK), resulting in three different bit-rate (400, 300, and 200 Gb/s), power consumption figures (20, 18, 16 Watt) and Required GSNR (RGSNR) [29, 82]. Note that the utilization of the translucent network design approach consists of selectively deploying additional transceiver pairs to guarantee that end-to-end connections always support the highest data rate (i.e., 400 Gb/s).

In Fig. 5.6b, the total allocated traffic and multiplicative factor of network capacity (with respect to the baseline C+L-band case) are shown for a target BP of 0.01, 0.1, and 1%. According to this figure, signal regeneration in the C+L-

band translucent network leads to an average increase in network capacity of 14%. Conversely, network capacity is increased by around 62% for both C+L+S- and C+L+U-band transparent networks. The average energy consumption of each network with and without consideration of optical amplifiers' power consumption is depicted in Fig. 5.7a. The average length of the network links connecting a pair of ROADMs is 308 km and a total of 173 optical amplifiers was considered for each band with a power consumption of 20, 20, 30, and 30 Watts for the C-, L-, S-, and U-band, respectively. According to Fig. 5.7a, when considering only the transceivers contribution, the power consumption of the network in the transparent C+L, C+L+S, C+L+U, and translucent C+L is equal to 13.67, 13.67, 15, and 15.39 kW at the delivered traffic of 250 Tb/s, respectively. However, the average power consumption of the network grows about 9.5 kW by factoring in the amplifiers' power consumption. Precisely, the power consumption in the transparent C+L, C+L+S, C+L+U, and translucent C+L is equal to 20.6, 25.84, 27, and 22.36 kW at the delivered traffic of 250 Tb/s, respectively. To provide more insight into the energy consumption, Fig. 5.7b is presented at the same delivered traffic of 250 Tb/s for all four configurations. This figure shows that the average nodes' energy consumption in the C+L-band transparent network is less than the other scenarios (red circles). Moreover, the average nodes' energy consumption in the C+L+S- and C+L+U-band transparent networks are almost the same with only a small difference (Yellow and Green markers). On the contrary, the utilization of 3R regenerators in intermediate nodes to improve spectral efficiency (translucent design) results in an increase in the nodes' energy consumption, particularly visible in nodes that due to their location are natural candidates to host regenerators. This trend is visible, for instance, in *El Paso, Lincoln, Chicago, and Dallas*.
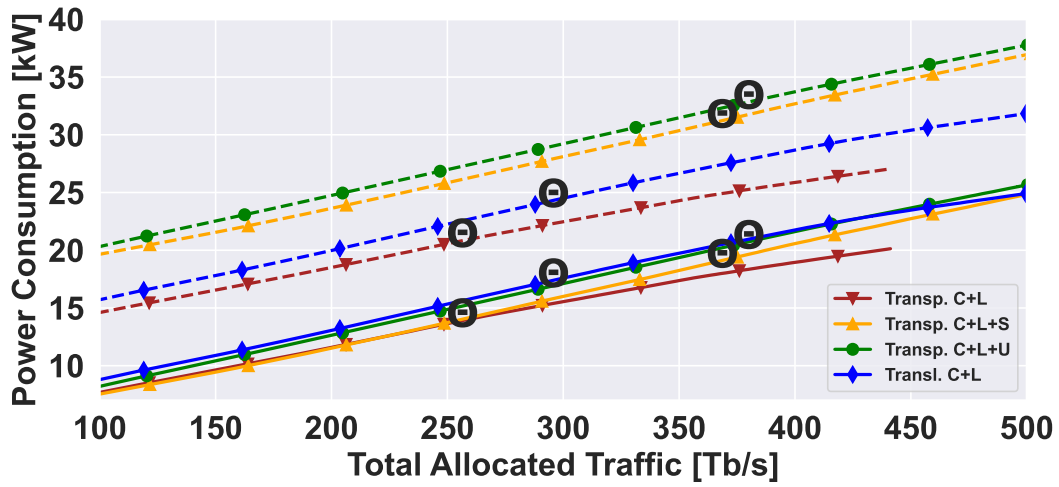
(a)
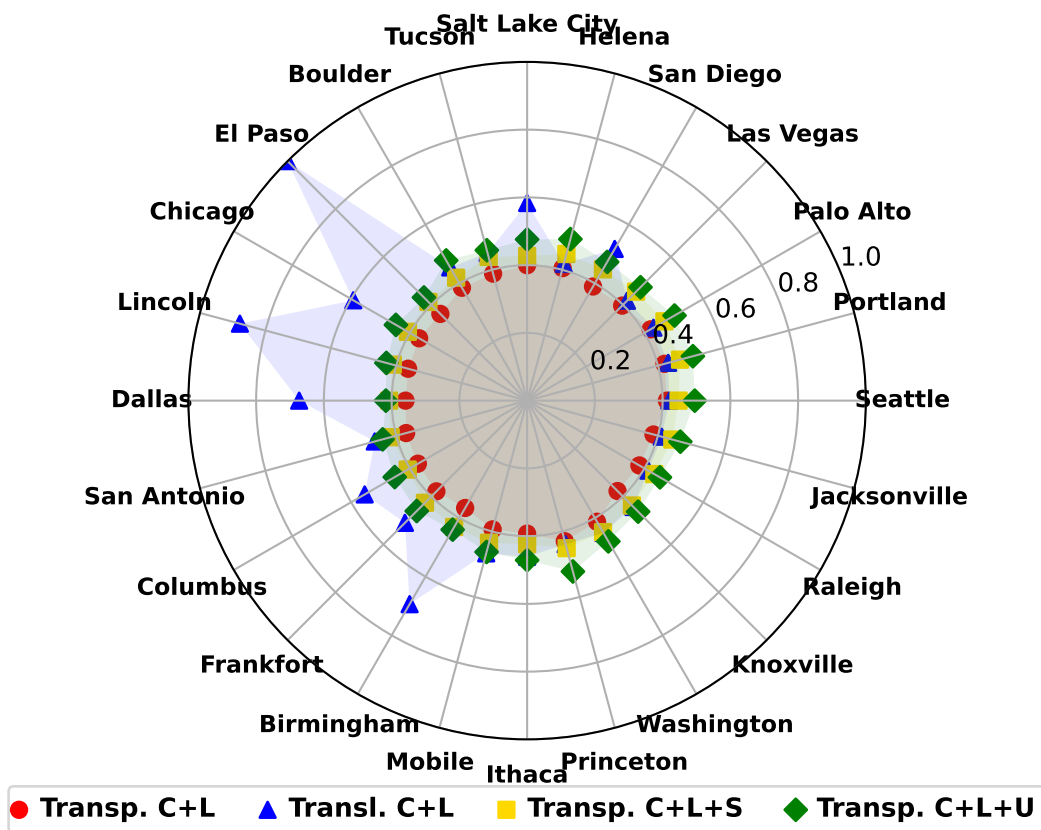
(b)

Fig. 5.7 (a) Energy consumption versus total allocated traffic without (solid curves) and with (dashed curves) amplifiers power consumption (BP of 1% marked with θ) and (b) consumed energy for each node in different scenarios at the same allocated traffic, 250 Tb/s.

Chapter 6

Conclusions

The continued rise in optical fiber demand is mostly driven by 5G and cloud-based applications. To satisfy the demands of networks that are continually expanding, the optical sector has responded by providing innovative solutions. Researchers offered a number of methods, primarily based on space division multiplexing (SDM) (e.g., including SDM based on multi-mode fibers) in order to meet this increasing demand for capacity. In this contribution, we describe an alternative strategy that intends to transmit throughout the whole SSMF low-loss optical spectrum, namely from $\approx$180 to $\approx$205 THz. This is known as MBT. The major goal of this work is to examine the benefits and drawbacks of MBT systems in the transparent ad translucent network designs in terms of network achievable capacity, energy consumption and the number of demanded interfaces in each scenario.

The thesis begins with a broad overview of optical networks and the motivation of this thesis. The first, open and disaggregated optical network was proposed and this type of network's benefits has been compared to the closed and aggregated optical networks. Moreover, SDN and its different layers have been proposed in the optical networks along with the outline of the thesis.

In chapter 2, methodology and metrics used to analyze an optical network topology have been discussed. In this chapter first physical layer of an optical network has been analyzed and the physical layer configuration for a single and MBT scenario has been described. Then, the GSNR value analyzed as a QoT metric has been evaluated for various MBT scenarios in the regular and super bands

namely the C, C+L, C+L+S, C+L+S+U, super C, and super C+L-band. To get the QoT values in the MBT configurations power optimization techniques have been implemented to get an almost flat and higher GSNR value which is vital to get a higher network capacity in the optical networks. After having an accurate physical layer model, a physical layer aware network tool (SNAP) has been proposed and explained with more details. In the network layer, two different network designs such as transparent and translucent have been analyzed. For a translucent network design, three algorithms were considered: the General, Pow. Opt., and Hybrid. Each algorithm enforces a different strategy to assign 3R regenerators to increase capacity.

After evaluation of the QoT by an accurate physical layer model in chapter 2 considering different combinations of spectral occupation within an MBT network scenario, analyzing the C-, C+L-, C+L+S-, and C+L+S+U-band scenarios. In chapter 3, we comprehensively analyzed the MBT transparent and translucent network designs in terms of capacity, energy consumption per Terabit, interface count, allocated LPs, and link congestion. For a translucent network design, three algorithms that have been proposed in chapter 2 were considered. Each algorithm enforces a different strategy to assign 3R regenerators to increase capacity. Results showed that focusing signal regeneration in poor-QoT bands leads to a comparable network capacity increase than using signal regeneration in all bands. Network-wide analyses indicated that exploiting an additional band in a transparent network scenario leads to the same or more capacity compared to the translucent network with the already-in-use band(s) and results in no additional energy consumption at the same BP. Moreover, we showed that depending on the number of bands exploited, MBT translucent network design can utilize more than two times the number of interfaces compared to an MBT transparent network. It also observed that signal regeneration leads to changes in the link congestion distribution in a network. According to this chapter, MBT transparent optical transmission is a cost-effective solution to augment the network capacity without significant increases in both cost and energy consumption.

Then, in chapter 4, we extended the previous chapter by comparing the regular bands with extended bandwidth bands. We have comprehensively analyzed the network performance for regular and extended bandwidth bands in terms of capacity and cost. The QoT has been evaluated (according to chapter 2) for different regular and super bands in an MBT network scenario, with different spectral occupations; we have investigated super C-, C+L-, super C+L-, and C+L+S1-band spectral con-

figurations with use of an accurate physical layer model. The benefits of extended bandwidth bands versus regular bands have been compared, for both transparent and translucent network designs, with uniform and nonuniform traffic distributions. We have shown that the use of selective 3R regeneration results in an increase in capacity when using a translucent network design and a uniform traffic distribution. Still, the number of extra interfaces to achieve this can be substantial. For MBT systems, the use of super bands offered higher capacity and only slightly higher interface count compared to regular band configurations, when considering the same number of exploited bands (i.e., C+L-band versus super C+L-band). However, the use of more regular bands, such as the inclusion of the S1 band – half of the S-band -, provides a significant capacity increase with respect to the use of just super bands (i.e., C+L+S1 versus super C+L-band), but requires a significantly larger amount of amplifiers. In summary, super C+L-band and regular C+L+S1-band configurations provide the expected increase in network throughput, and comparing the two solutions the super C+L-band is more cost-effective in terms of the required additional hardware.

In the last chapter, chapter 5, the network performance results have been presented for the C+L+S1-band configuration where signal regeneration has been done only in the S1-band which has a poor QoT compared to the other exploited bands such as C and L-band to reach the performance of this band in a same/higher than other already in used bands. After evaluation of the optimized S-band performance, its performance has been compared with the U-band which benefits from power transferring from higher frequencies to this band. In this first step, instead of exploiting the full S-band U band deployed and showed a better performance in terms of capacity, energy consumption, and demanded number of interfaces because of having a better QoT compared to the second half of S-band (S2-band). In the continue, network performance with U-band compared with S1-band in a MBT configuration (C+L+U-band compared with C+L+S1-band). Overall, the U-band due to having a higher GSNR value compared to the S-band (S1 and S2-band) performs better in the MBT combination scenarios.

Appendix

Regenerator Placement Algorithms

In this appendix, 3R regenerator placement algorithms namely "*General*" and "*Pow. Opt.*" have been presented with more details.

Algorithm 1 General Translucent Algorithm

Require: Channel (ch), source / destination route path ($path_{tot}$), list of RGSNR for all modulation formats (RGSNR$_{list}$)

Ensure: LP regeneration paths ($path_{reg}$)

1: RGSNR$_{aux} \leftarrow 0$
2: $path_{temp}$, $path_{pre}$, $path_{reg} \leftarrow \emptyset$
3: **while** RGSNR$_{list} \neq \emptyset$ AND LP not allocated **do**
4:     RGSNR$_{aux} \leftarrow$ Highest RGSNR of RGSNR$_{list}$
5:     RGSNR$_{list} \leftarrow$ RGSNR$_{list} \setminus$ RGSNR$_{aux}$
6:     **for all** links (l) in $path_{tot}$ **do**
7:         $path_{temp} \leftarrow path_{temp} \cup l$
8:         **if** GSNR($path_{temp}, ch$) $\geq$ RGSNR$_{aux}$ **then**
9:             $path_{pre} \leftarrow path_{temp}$
10:         **else**
11:             **if** GSNR($path_{pre}, ch$) $\geq$ RGSNR$_{aux}$ **then**
12:                 $path_{reg} \leftarrow path_{reg} + path_{pre}$ {New added transparent segment}
13:                 $path_{temp}, path_{pre} \leftarrow l$
14:             **else**
15:                 **break** {Not enough QoT for single link}
16:             **end if**
17:         **end if**
18:         **if** l is the last link **then**
19:             $path_{reg} \leftarrow path_{reg} + path_{temp}$ {New added transparent segment}
20:         **end if**
21:     **end for**
22: **end while**

Algorithm 2 Power-Optimized (Pow. Opt.) Translucent Algorithm
---
Require: Channel (ch), source / destination route path ($path_{tot}$)

Ensure: LP regeneration paths ($path_{reg}$)

  1: $P_{best} \leftarrow \infty$ {Powers}

  2: $C \leftarrow$ Combinations($path_{tot}$) {All regeneration possibilities of a path}

  3: $R_b, path_{reg} \leftarrow \emptyset$

  4: **for all** c in C **do**

  5:     $P_{temp} \leftarrow 0$

  6:     **for all** s in c **do**

  7:        $R_b \leftarrow R_b \cup$ Capacity(s, ch) {Bit-rate for the specific channel}

  8:        $P_{temp} \leftarrow P_{temp} +$ Power(s, ch) {Power for the specific channel}

  9:     **end for**

10:     **if** $P_{temp} \leq P_{best}$ AND All r_b in R_b are equal **then**

11:        $P_{best} \leftarrow P_{temp}$

12:        $path_{reg} \leftarrow c$

13:     **end if**

14: **end for**

Appendix2

Optical Network Topologies

The backbone network topologies investigated in this thesis are German DT network, European COST and the north American US-NET network which are depicted in the following. The average link length, other parameters and the references of these networks are reported in table 1.

Table 1 The summary of optical network topologies parameters.

	German DT	European COST	US-NET
Number of nodes	17	28	24
Number of links	26	41	43
Average node degree	3.06	3.93	3.58
Average link length	207 km	637 km	660 km
Reference figure	Fig. 1	Fig. 2	Fig. 3
Source	[98]	[98]	[99]
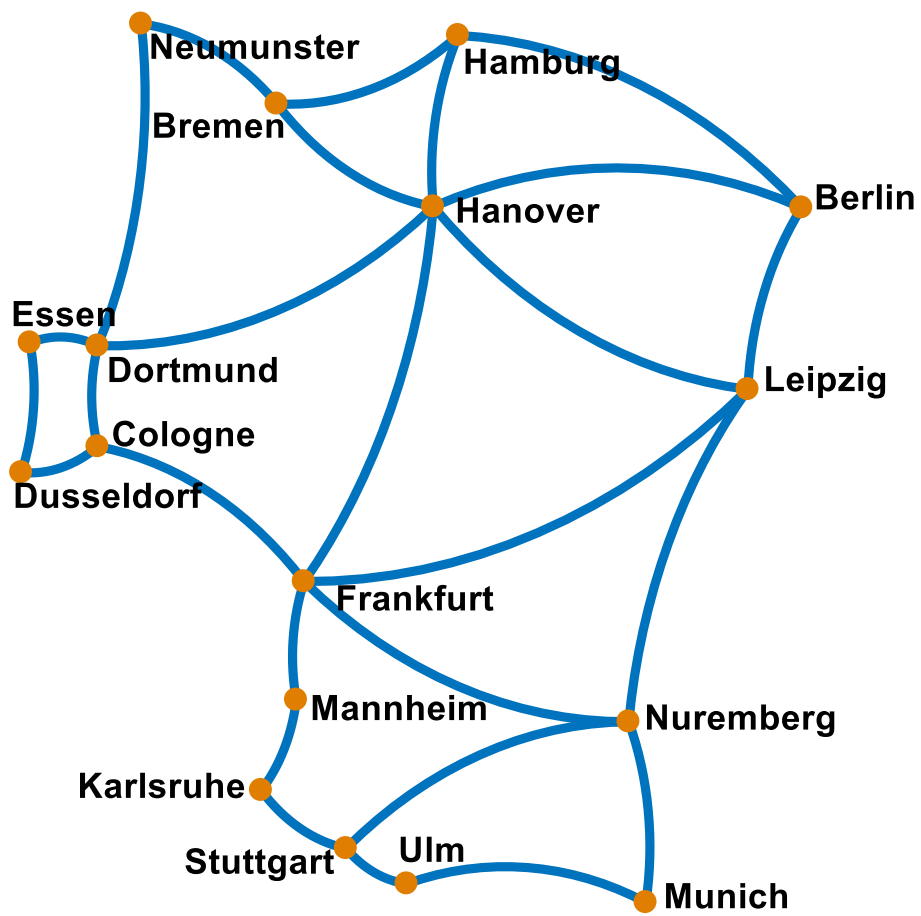
Fig. 1 German DT optical network topology.
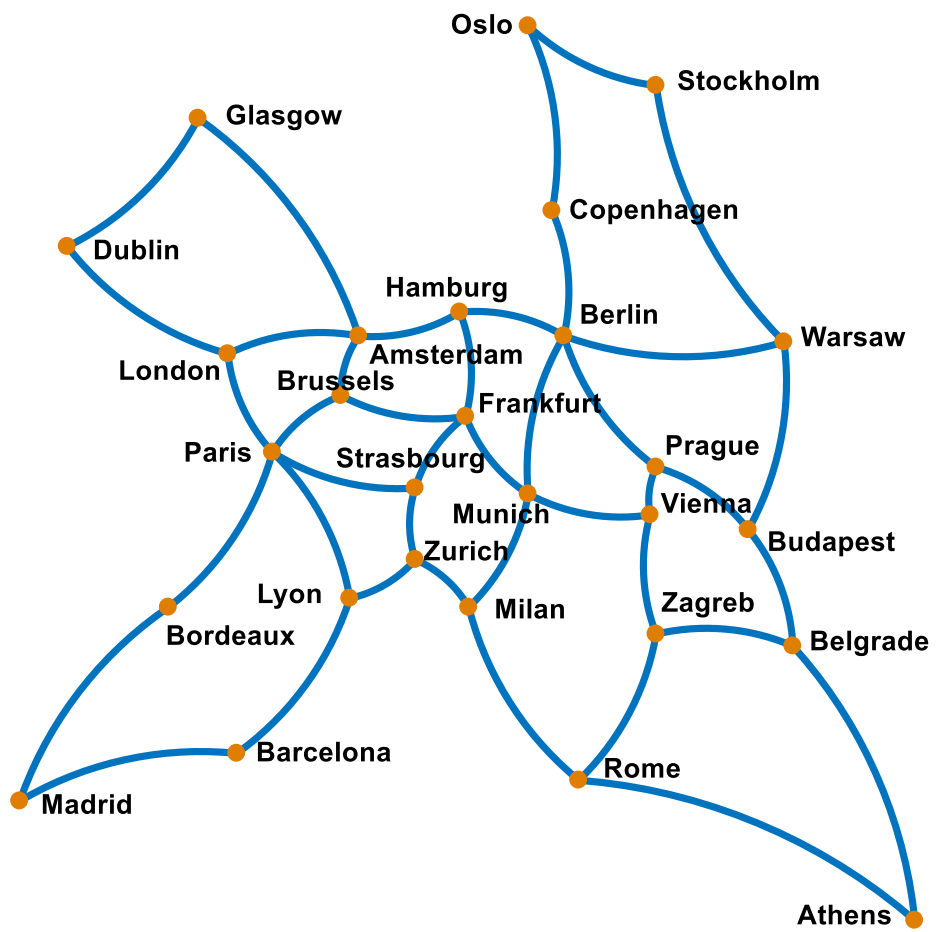
Fig. 2 European COST optical network topology.
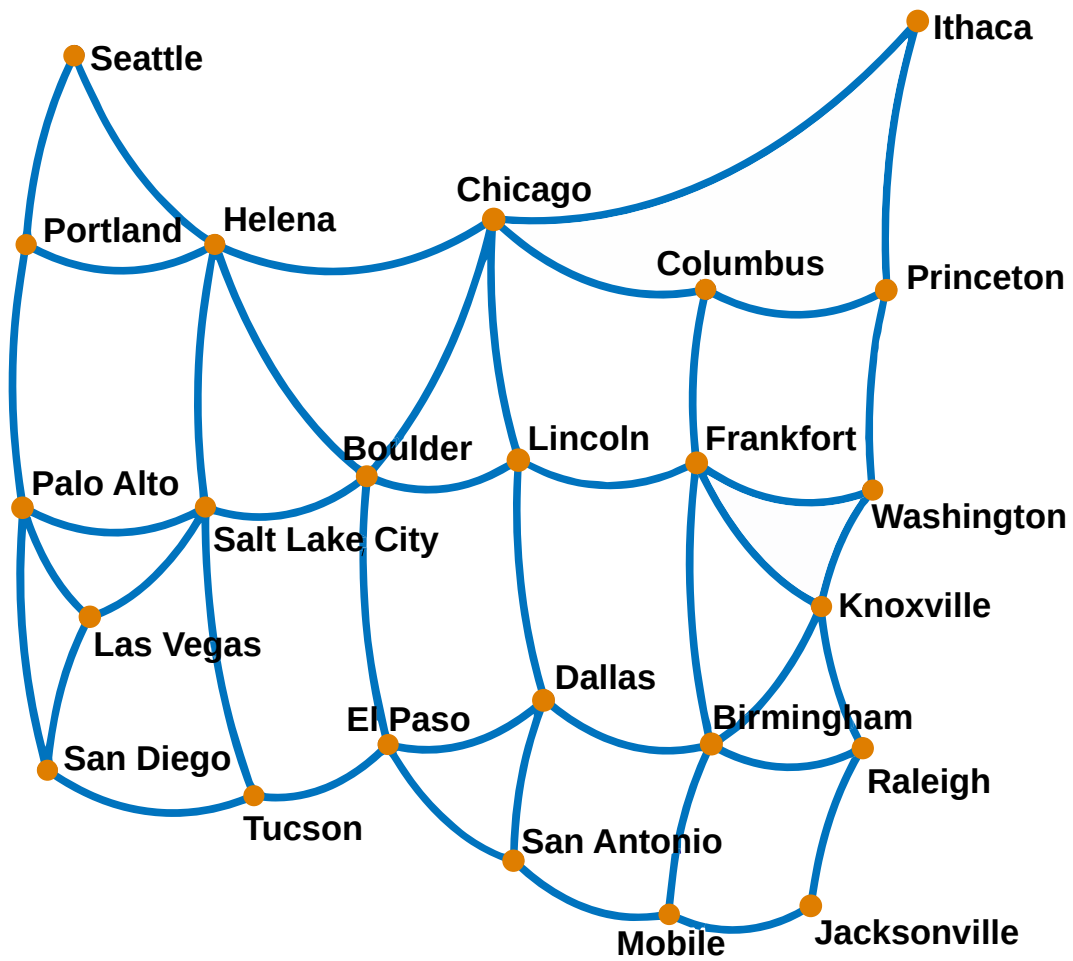
Fig. 3 US-NET optical network topology.

Acronyms

3R Re-amplification, Reshaping, and Re-timing. viii, xi, xiv, 37–41, 43, 46–50, 52, 55, 80, 90–92

API Application program interface. 5

ASE Amplified spontaneous emission. 11–14, 19, 21

AWGN Additive white Gaussian noise. 13

BP Blocking Probability. xi–xiv, 30, 44–54, 56, 57, 61–67, 69–74, 77, 78, 82–84, 86, 88, 90

CAPEX Capital Expenditure. 3, 38

DCI Data Center Interconnects. xi, 36

DSP Digital signal processing. 25

EDFA Erbium Doped Fiber Amplifier. 11, 13, 20, 23

EON Elastic optical networks. 38

FEC Forward error correction. 36

FF First-Fit. 37, 38, 60

FWM Four Waves Mixing. 16, 18

GGN Generalized Gaussian noise. 19

GSNR Generalized Signal-to-Noise Ratio. vii, x, xiii, xiv, 5, 6, 8, 12, 18–25, 27, 37, 40, 41, 58, 59, 61, 65, 67, 68, 77, 80–82, 85, 86, 89–91

IGSNR Inverted Generalized Signal to Noise Ratio. x, 26

JPDF Joint Probability Density Function. x, 27, 30–32, 60

LOGO Local-Optimization Global-Optimization. 21, 24

LP Lightpath. x, xii–xv, 8, 9, 11, 19, 20, 22, 25, 27, 30, 32, 35, 37, 39–41, 44–50, 52, 54, 55, 60, 61, 66, 67, 70, 77–81, 83, 90

MBT Multi-Band Transmission. vi–viii, x–xii, xiv, 1–3, 5–11, 15, 18, 20–23, 25, 42–50, 52, 54, 56, 58, 62, 65–67, 71–74, 85, 87, 89–91

MC Monte Carlo. 27, 30, 59, 60

MF Multiplicative Factor. xi, xii, 44, 45, 51–55, 63–66

MSA Multi-Source Agreement. 36, 40, 86

NF Noise figure. viii, x, xii, 9, 11, 13, 14, 20, 23, 24, 60–62, 68

NLI Nonlinear interference. 9, 12, 19

nm Nano Meter. 11, 12

NOS Networking Operating System. 5

OEO Optical-electro-optical. 38

OLS Optical line system. 10, 27

OPEX Operational expenditures. 38

OSI Open System Interconnection. 8

P2P Point to Point. 10

PLP packet loss probability. 34

PSD Power Spectral Density. 13

QAM Quadrature amplitude modulation. 35–37, 40, 59, 76–78, 81, 86

QoT Quality of transmission. vi–viii, xii, xiv, 5–9, 11, 12, 15, 18–24, 27, 30, 35, 37–41, 44, 45, 49, 52, 60, 61, 66–68, 71–77, 80–82, 89–91

QPSK Quadrature phase shift keying. 36, 37, 40, 60, 76, 78, 86

RGSNR Required Generalized Signal to Noise Ratio. 36, 37, 39, 40, 59, 81, 86

ROADM Reconfigurable optical add/drop multiplexers. 25, 32, 38, 87

RWA Routing and Wavelength Assignment. vii, x, 25, 30, 32–35

SDM Space Division Multiplexing. 89

SDN Software-Defined Networking. x, 1, 3–5, 22, 29, 30, 35, 40, 89

SE Spectral Efficiency. 39

SNAP Statistical Network Assessment Process. vii, x, 5, 6, 25, 27–30, 32, 35, 37, 43, 59, 60, 77, 81, 90

SPM Self-Phase Modulation. 16, 17

SRS Stimulated Raman Scattering. 12, 14, 15, 18, 19, 21, 24, 80

SSMF Standard Single-mode Fiber. x, 9, 12, 13, 15, 18, 89

TDFA Thulium-doped Fiber Amplifier. 11, 13, 20, 23

TRX Transceiver. xi, xiv, xv, 6, 21, 27, 36, 37, 39, 59, 66–68, 77, 78, 80, 81, 84–86

WA Wavelength Assignment. 37, 38

WDM Wavelength division multiplexing. x, 2, 9, 10, 13–18, 20, 26, 32, 58, 80

XPM Cross-Phase Modulation. 16, 17

References

[1] Xiang Liu and Ning Deng. Emerging optical communication technologies for 5g. In *Optical fiber telecommunications VII*, pages 751–783. Elsevier, 2020.

[2] Shirley Lim. How Fiber Optics Supports Cloud Technology. https://blog.viavisolutions.com/2020/12/15/how-fiber-optics-supports-cloud-technology/.

[3] Fukutaro Hamaoka, Masanori Nakamura, Seiji Okamoto, Kyo Minoguchi, Takeo Sasai, Asuka Matsushita, Etsushi Yamazaki, and Yoshiaki Kisaka. Ultra-wideband wdm transmission in s-, c-, and l-bands using signal power optimization scheme. *Journal of Lightwave Technology*, 37(8):1764–1771, 2019.

[4] Masahiro Nakagawa, Hiroki Kawahara, Kana Masumoto, Toshiya Matsuda, and Kazuyuki Matsumura. Performance evaluation of multi-band optical networks employing distance-adaptive resource allocation. In *2020 Opto-Electronics and Communications Conference (OECC)*, pages 1–3. IEEE, 2020.

[5] Cisco annual internet report (2018–2023).

[6] Francesco Musumeci, Massimo Tornatore, and Achille Pattavina. A power consumption analysis for IP-over-WDM core network architectures. *J. Opt. Commun. Netw.*, 4(2):108–117, Feb 2012.

[7] Yoshihisa Yamamoto and Tatsuya Kimura. Coherent optical fiber transmission systems. *IEEE Journal of Quantum Electronics*, 17(6):919–935, 1981.

[8] G Ramesh, S Sundara Vadivelu, and Jose Anand. A survey on wavelength division multiplexing (wdm) networks. *ICTACT Journal on Communication Technology*, 1, 2010.

[9] Alessio Ferrari, Antonio Napoli, Johannes K Fischer, Nelson Costa, Andrea D'Amico, João Pedro, Wladek Forysiak, Erwan Pincemin, Andrew Lord, Alexandros Stavdas, et al. Assessment on the achievable throughput of multi-band itu-t g. 652. d fiber transmission systems. *Journal of Lightwave Technology*, 38(16):4279–4291, 2020.

[10] Rasoul Sadeghi, Bruno Correia, Emanuele Virgillito, Nelson Costa, João Pedro, Antonio Napoli, and Vittorio Curri. Multi bands network performance assessment for different system upgrades. In *2020 IEEE Photonics Conference (IPC)*, pages 1–2. IEEE, 2020.

[11] Antonio Napoli, Nelson Costa, Johannes K Fischer, Joao Pedro, Silvio Abrate, Nicola Calabretta, Wladek Forysiak, Erwan Pincemin, Juan PF-P Gimenez, Chris Matrakidis, et al. Towards multiband optical systems. In *Photonic Networks and Devices*, pages NeTu3E–1. Optical Society of America, 2018.

[12] Seiji Okamoto, Kengo Horikoshi, Fukutaro Hamaoka, Kyo Minoguchi, and Akira Hirano. 5-band (o, e, s, c, and l) wdm transmission with wavelength adaptive modulation format allocation. In *ECOC 2016; 42nd European Conference on Optical Communication*, pages 1–3. VDE, 2016.

[13] Alessio Ferrari, Emanuele Virgillito, and Vittorio Curri. Band-division vs. space-division multiplexing: A network performance statistical assessment. *Journal of Lightwave Technology*, 38(5):1041–1049, 2020.

[14] Daniel Semrau, Eric Sillekens, Robert I Killey, and Polina Bayvel. The benefits of using the s-band in optical fiber communications and how to get there. In *2020 IEEE Photonics Conference (IPC)*, pages 1–2. IEEE, 2020.

[15] Maria Ionescu, Domaniç Lavery, Adrian Edwards, Eric Sillekens, Daniel Semrau, Lidia Galdino, Robert I Killey, Wayne Pelouch, Stuart Barnes, and Polina Bayvel. 74.38 tb/s transmission over 6300 km single mode fibre enabled by c+l amplification and geometrically shaped pdm-64qam. *Journal of Lightwave Technology*, 38(2):531–537, 2019.

[16] Mattia Cantono, Rene Schmogrow, Matt Newland, Vijay Vusirikala, and Tad Hofmeister. Opportunities and challenges of c+l transmission systems. *Journal of Lightwave Technology*, 38(5):1050–1060, 2020.

[17] Aymeric Arnould, Amirhossein Ghazisaeidi, Haik Mardoyan, Patrick Brindel, Maria Ionescu, and Jeremie Renaudier. High-speed and ultra-wideband devices for coherent transmission: challenges and opportunities. In *2020 22nd International Conference on Transparent Optical Networks (ICTON)*, pages 1–4. IEEE, 2020.

[18] Alessio Ferrari, Dario Pilori, Emanuele Virgillito, and Vittorio Curri. Power control strategies in c+l optical line systems. In *Optical Fiber Communication Conference*, pages W2A–48. Optica Publishing Group, 2019.

[19] Ian Roberts, Joseph M Kahn, James Harley, and David W Boertjes. Channel power optimization of wdm systems following gaussian noise nonlinearity model in presence of stimulated raman scattering. *Journal of Lightwave Technology*, 35(23):5237–5249, 2017.

[20] Daniela Moniz, Victor Lopez, and João Pedro. Design strategies exploiting c+l-band in networks with geographically-dependent fiber upgrade expenditures. In *Optical Fiber Communication Conference*, pages M2G–3. Optical Society of America, 2020.

[21] Victor Lopez, Benyuan Zhu, Daniela Moniz, Nelson Costa, Joao Pedro, Xian Xu, Ales Kumpera, Lee Dardis, Jeff Rahn, and Steve Sanders. Optimized design and challenges for c&l band optical line systems. *Journal of Lightwave Technology*, 38(5):1080–1091, 2020.

[22] Filippo Cugini, Francesco Paolucci, Francesco Fresi, Gianluca Meloni, Nicola Sambo, Luca Potí, Antonio D'Errico, and Piero Castoldi. Toward plug-and-play software-defined elastic optical networks. *Journal of Lightwave Technology*, 34(6):1494–1500, 2016.

[23] Kathleen Tse. Progress toward an open, sdn-controlled photonic network. In *2018 Optical Fiber Communications Conference and Exposition (OFC)*, pages 1–3. IEEE, 2018.

[24] Miquel Garrich, Francisco-Javier Moreno-Muro, María-Victoria Bueno Delgado, and Pablo Pavon Marino. Open-source network optimization software in the open sdn/nfv transport ecosystem. *Journal of Lightwave Technology*, 37(1):75–88, 2018.

[25] Sudhir K Routray, Mahesh K Jha, Abhishek Javali, Laxmi Sharma, Sutapa Sarkar, and T Ninikrishna. Software defined networking for optical networks. In *2016 IEEE Distributed Computing, VLSI, Electrical Circuits and Robotics (DISCOVER)*, pages 133–137. IEEE, 2016.

[26] Nick McKeown, Tom Anderson, Hari Balakrishnan, Guru Parulkar, Larry Peterson, Jennifer Rexford, Scott Shenker, and Jonathan Turner. Openflow: enabling innovation in campus networks. *ACM SIGCOMM computer communication review*, 38(2):69–74, 2008.

[27] Bruno Astuto A Nunes, Marc Mendonca, Xuan-Nam Nguyen, Katia Obraczka, and Thierry Turletti. A survey of software-defined networking: Past, present, and future of programmable networks. *IEEE Communications surveys & tutorials*, 16(3):1617–1634, 2014.

[28] Vittorio Curri. Gnpy model of the physical layer for open and disaggregated optical networking. *J. Opt. Commun. Netw.*, 14(6):C92–C104, Jun 2022.

[29] Open ZR+ MSA Technical Specification. https://openzrplus.org/site/assets/files/1075/openzrplus_1p0.pdf.

[30] C-band optical amplifier (EDFA). https://www.fiberlabs.com/1u_amp/1500nm-1u-amp/.

[31] L-band optical amplifier (EDFA). https://www.fiberlabs.com/1u_amp/1600nm-1u-amp/.

[32] S-band optical amplifier (TDFA). https://www.fiberlabs.com/bt_amp_index/s-band-bt-amp/.

[33] Maurice Gagnaire and Sawsan Al Zahr. Impairment-aware routing and wavelength assignment in translucent networks: State of the art. *IEEE Communications Magazine*, 47(5):55–61, 2009.

[34] Chava Vijaya Saradhi and Suresh Subramaniam. Physical layer impairment aware routing (pliar) in wdm optical networks: Issues and challenges. *IEEE Communications Surveys & Tutorials*, 11(4):109–130, 2009.

[35] Takeshi Hoshida, Vittorio Curri, Lidia Galdino, David T. Neilson, Wladek Forysiak, Johannes K. Fischer, Tomoyuki Kato, and Pierluigi Poggiolini. Ultra-wideband systems and networks: Beyond c + l-band. *Proceedings of the IEEE*, 110(11):1725–1741, 2022.

[36] Leonid G Kazovsky, Sergio Benedetto, and Alan E Willner. *Optical fiber communication systems*. Artech House Optoelectronics L, 1996.

[37] Joseph C Palais. Technology-enhanced fiber-optic education. In *Education and Training in Optics and Photonics*, page NTE252. Optica Publishing Group, 1999.

[38] C. T. Politi, C. Matrakidis, and A. Stavdas. *A Tutorial on Physical-Layer Impairments in Optical Networks*, pages 5–29. Springer US, Boston, MA, 2013.

[39] Rasoul Sadeghi, Bruno Correia, André Souza, Nelson Costa, João Pedro, Antonio Napoli, and Vittorio Curri. Transparent vs translucent multi-band optical networking: Capacity and energy analyses. *Journal of Lightwave Technology*, 40(11):3486–3498, 2022.

[40] G.P. Agrawal. *Nonlinear Fiber Optics*. Optics and Photonics. Elsevier Science, 2012.

[41] Vittorio Curri and Andrea Carena. Merit of raman pumping in uniform and uncompensated links supporting nywdm transmission. *Journal of Lightwave Technology*, 34(2):554–565, 2015.

[42] Mohammed N Islam. Raman amplifiers for telecommunications. *IEEE Journal of selected topics in Quantum Electronics*, 8(3):548–559, 2002.

[43] Chandrasekhara Venkata Raman. A new radiation. *Indian Journal of physics*, 2:387–398, 1928.

[44] Biswanath Mukherjee. *Optical WDM networks*. Springer Science & Business Media, 2006.

[45] AR Chraplyvy. Optical power limits in multi-channel wavelength-division-multiplexed systems due to stimulated raman scattering. *Electronics letters*, 2(20):58–59, 1984.

[46] John Kerr. Xl. a new relation between electricity and light: Dielectrified media birefringent. *The London, Edinburgh, and Dublin Philosophical Magazine and Journal of Science*, 50(332):337–348, 1875.

[47] Vittorio Curri. Gnpy model for design of open and disaggregated optical networks. In *2021 European Conference on Optical Communication (ECOC)*, pages 1–86, 2021.

[48] Emanuele Virgillito, Rasoul Sadeghi, Alessio Ferrari, Giacomo Borraccini, Antonio Napoli, and Vittorio Curri. Network Performance Assessment of C+L Upgrades vs. Fiber Doubling SDM Solutions. In *Optical Fiber Communication Conference (OFC) 2020*, page M2G.4. OSA, 2020.

[49] Mattia Cantono, Dario Pilori, Alessio Ferrari, Clara Catanese, Jordane Thouras, Jean-Luc Augé, and Vittorio Curri. On the Interplay of Nonlinear Interference Generation with Stimulated Raman Scattering for QoT Estimation. *JLT*, PP(99):1–1, 2018.

[50] V Kamalov, M Cantono, V Vusirikala, L Jovanovski, M Salsi, A Pilipetskii, D Kovsh Maxim Bolshtyansky, G Mohs, E Rivera Hartling, and S Grubb. The subsea fiber as a Shannon channel. In *In Proceedings of the SubOptic*, 2019.

[51] Vittorio Curri. Software-defined wdm optical transport in disaggregated open optical networks. In *ICTON 2020*, page We.C2.1, 2020.

[52] Alessio Ferrari, Mark Filer, Karthikeyan Balasubramanian, Yawei Yin, Esther Le Rouzic, Jan Kundrát, Gert Grammel, Gabriele Galimberti, and Vittorio Curri. Gnpy: an open source application for physical layer aware open optical networks. *JOCN*, 12(6):C31–C40, 2020.

[53] Bruno Correia, Rasoul Sadeghi, Emanuele Virgillito, Antonio Napoli, Nelson Costa, Jo ao Pedro, and Vittorio Curri. Power control strategies and network performance assessment for C+L+S multiband optical transport. *J. Opt. Commun. Netw.*, 13(7):147–157, Jul 2021.

[54] Mark Filer, Jamie Gaudette, Yawei Yin, Denizcan Billor, Zahra Bakhtiari, and Jeffrey L Cox. Low-margin optical networking at cloud scale. *Journal of Optical Communications and Networking*, 11(10):C94–C108, 2019.

[55] Yasuhuo Ando. Statistical analysis of insertion-loss improvement for optical connectors using the orientation method for fiber-core offset. *IEEE photonics technology letters*, 3(10):939–941, 1991.

[56] Vittorio Curri, Andrea Carena, Andrea Arduino, Gabriella Bosco, Pierluigi Poggiolini, Antonino Nespola, and Fabrizio Forghieri. Design strategies and merit of system parameters for uniform uncompensated links supporting nyquist-wdm transmission. *JLT*, 33(18):3921–3932, 2015.

[57] Bruno Correia, Rasoul Sadeghi, Emanuele Virgillito, Antonio Napoli, and Vittorio Curri. Optical Power Control Strategies for Optimized C + L + S-bands Network Performance. In *Optical Fiber Communication Conference (OFC) 2021*, page W1F.8, 2021.

[58] Bruno Correia, Rasoul Sadeghi, Emanuele Virgillito, Antonio Napoli, and Vittorio Curri. Optical Power Control Strategies for Optimized C + L + S-bands Network Performance. In *Optical Fiber Communication Conference (OFC) 2021*, page W1F.8, 2021.

[59] Alessio Ferrari, Mark Filer, Karthikeyan Balasubramanian, Yawei Yin, Esther Le Rouzic, Jan Kundrát, Gert Grammel, Gabriele Galimberti, and Vittorio Curri. Gnpy: an open source application for physical layer aware open optical networks. *J. Opt. Commun. Netw.*, 12(6):C31–C40, Jun 2020.

[60] Adel A. M. Saleh and Jane M. Simmons. All-optical networking—evolution, benefits, challenges, and future vision. *Proceedings of the IEEE*, 100(5):1105–1117, 2012.

[61] Vittorio Curri, Mattia Cantono, and Roberto Gaudino. Elastic all-optical networks: a new paradigm enabled by the physical layer. how to optimize network performances? *Journal of Lightwave Technology*, 35(6):1211–1221, 2017.

[62] Raül Muñoz, Ricard Vilalta, Ramon Casellas, Ricardo Martínez, Frederic Francois, Mayur Channegowda, Ali Hammad, Shuping Peng, Reza Nejabati, Dimitra Simeonidou, et al. Transport network orchestration for end-to-end multilayer provisioning across heterogeneous sdn/openflow and gmpls/pce control domains. *Journal of Lightwave Technology*, 33(8):1540–1548, 2015.

[63] Fernando P Guiomar, Rixin Li, Chris RS Fludger, Andrea Carena, and Vittorio Curri. Hybrid modulation formats enabling elastic fixed-grid optical networks. *Journal of Optical Communications and Networking*, 8(7):A92–A100, 2016.

[64] Emanuele Virgillito, Rasoul Sadeghi, Alessio Ferrari, Antonio Napoli, Bruno Correia, and Vittorio Curri. Network performance assessment with uniform and non-uniform nodes distribution in c+l upgrades vs. fiber doubling sdm solutions. In *2020 International Conference on Optical Network Design and Modeling (ONDM)*, pages 1–6, 2020.

[65] Rudra Dutta, Ahmed E Kamal, and George N Rouskas. *Traffic grooming for optical networks: foundations, techniques and frontiers.* Springer Science & Business Media, 2008.

[66] Tarek S El-Bawab. *Optical switching.* Springer Science & Business Media, 2008.

[67] Anshul Agrawal, Lev B Sofman, and Tarek S El-Bawab. Enhancement of bandwidth efficiency by traffic grooming in optical-cross-connect based networks. In *Optical Transmission Systems and Equipment for WDM Networking II*, volume 5247, pages 196–202. SPIE, 2003.

[68] Felix Frey, Robert Elschner, and Johannes K. Fischer. Estimation of trends for coherent DSP ASIC power dissipation for different bitrates and transmission reaches. In *Photonic Networks; 18. ITG-Symposium*, pages 1–8, 2017.

[69] W. M. Holt. 1.1 moore's law: A path going forward. In *2016 IEEE International Solid-State Circuits Conference (ISSCC)*, pages 8–13, 2016.

[70] Charles Laperle. Advances in high-speed ADCs, DACs, and DSP for optical transceivers. In *Optical Fiber Communication Conference/National Fiber Optic Engineers Conference 2013*, page OTh1F.5. Optical Society of America, 2013.

[71] Damián A. Morero, Mario A. Castrillón, Alejandro Aguirre, Mario R. Hueda, and Oscar E. Agazzi. Design tradeoffs and challenges in practical coherent optical transceiver implementations. *J. Lightwave Technol.*, 34(1):121–136, Jan 2016.

[72] O. Ishida, K. Takei, and E. Yamazaki. Power efficient DSP implementation for 100G-and-beyond multi-haul coherent fiber-optic communications. In *2016 Optical Fiber Communications Conference and Exhibition (OFC)*, pages 1–3, 2016.

[73] Maxim Kuschnerov, Thomas Bex, and Peter Kainzmaier. Energy efficient digital signal processing. *Optical Fiber Communication Conference*, page Th3E.7, 2014.

[74] Nina Skorin-Kapov, Francisco Javier Moreno Muro, María-Victoria Bueno Delgado, and Pablo Pavon Marino. Point-to-multipoint coherent optics for re-thinking the optical transport: case study in 5g optical metro networks. In *2021 International Conference on Optical Network Design and Modeling (ONDM)*, pages 1–4. IEEE, 2021.

[75] Xiaoxia Wu, Dirk van den Borne, Jeffery J Maki, Steven Alleston, and Domenico Di Mola. Interoperable coherent pluggables beyond 400zr. In *Asia Communications and Photonics Conference*, pages T2C–4. Optica Publishing Group, 2019.

[76] E Pincemin, Y Loussouarn, A Sotomayor, G Losio, M McCarthy, L Nelson, A Malik, I Riggs, T Nielsen, T Williams, et al. End-to-end interoperable 400-gbe optical communications through 2-km 400gbase-fr4, 8x100-km 400g-openroadm and 125-km 400-zr fiber lines. *Journal of Lightwave Technology*, 2022.

[77] Pablo Pavon-Marino, Nina Skorin-Kapov, and Antonio Napoli. A network dimensioning algorithm for exploiting the capabilities of subcarrier-based point-to-multipoint coherent optics. In *2022 European Conference on Optical Communication (ECOC)*, pages 1–4. IEEE, 2022.

[78] Zhensheng Jia and L Alberto Campos. Coherent optics ready for prime time in short-haul networks. *IEEE Network*, 35(2):8–14, 2021.

[79] Mohammad Mohammad Hosseini, João Pedro, Antonio Napoli, Nelson Costa, Jaroslaw E Prilepsky, and Sergei K Turitsyn. Multi-period planning in metro-aggregation networks exploiting point-to-multipoint coherent transceivers. *Journal of Optical Communications and Networking*, 15(3):155–162, 2023.

[80] OIF 400ZR IA. https://www.oiforum.com/wp-content/uploads/OIF-400ZR-01.0_reduced2.pdf.

[81] Jo{ ao Pedro, Nelson Costa, and Steve Sanders. Scaling regional optical transport networks with pluggable and integrated high-capacity line interfaces. In *Optical Fiber Communication Conference and Exhibition (OFC) 2021*, pages 1–3. OSA, 2021.

[82] J. Pedro and S. Pato. Capacity increase and hardware savings in DWDM networks exploiting next-generation optical line interfaces. In *2018 20th International Conference on Transparent Optical Networks (ICTON)*, pages 1–6, 2018.

[83] Jane M Simmons. Network design in realistic" all-optical" backbone networks. *IEEE Communications Magazine*, 44(11):88–94, 2006.

[84] João Pedro. Predeployment of regenerators for fast service provisioning in dwdm transport networks. *Journal of Optical Communications and Networking*, 7(2):A190–A199, 2015.

[85] Chava Vijaya Saradhi, Shmuel Zaks, Riccardo Fedrizzi, Andrea Zanardi, and Elio Salvadori. Practical and deployment issues to be considered in regenerator placement and operation of translucent optical networks. In *2010 12th International Conference on Transparent Optical Networks*, pages 1–4. IEEE, 2010.

[86] Jaisingh Thangaraj. Review and analysis of elastic optical network and sliceable bandwidth variable transponder architecture. *Optical Engineering*, 57(11):110802–110802, 2018.

[87] Mark D Feuer, Sheryl L Woodward, Inwoong Kim, Paparao Palacharla, Xi Wang, Daniel Bihon, Balagangadhar G Bathula, Weiyi Zhang, Rakesh Sinha, Guangzhi Li, et al. Simulations of a service velocity network employing regenerator site concentration. In *National Fiber Optic Engineers Conference*, pages NTu2J–5. Optica Publishing Group, 2012.

[88] Li Yan, Yuxin Xu, Maïté Brandt-Pearce, Nishan Dharmaweera, and Erik Agrell. Robust regenerator allocation in nonlinear flexible-grid optical networks with time-varying data rates. *Journal of Optical Communications and Networking*, 10(11):823–831, 2018.

[89] Xiangyong Li and Yash P Aneja. A new branch-and-cut approach for the generalized regenerator location problem. *Annals of Operations Research*, 295(1):229–255, 2020.

[90] Si Chen, Ivana Ljubić, and Subramanian Raghavan. The generalized regenerator location problem. *INFORMS Journal on Computing*, 27(2):204–220, 2015.

[91] Chava Vijaya Saradhi, Riccardo Fedrizzi, Andrea Zanardi, Elio Salvadori, Gabriele Maria Galimberti, Alberto Tanzi, Giovanni Martinelli, and Ori Gerstel. Traffic independent heuristics for regenerator site selection for providing any-to-any optical connectivity. In *2010 Conference on Optical Fiber Communication (OFC/NFOEC), collocated National Fiber Optic Engineers Conference*, pages 1–3. IEEE, 2010.

[92] Xi Yang and Byrav Ramamurthy. Sparse regeneration in translucent wavelength-routed optical networks: Architecture, network design and wavelength routing. *Photonic network communications*, 10(1):39–53, 2005.

[93] Neil Barakat and Alberto Leon-Garcia. An analytical model for predicting the locations and frequencies of 3r regenerations in all-optical wavelength-routed wdm networks. In *2002 IEEE International Conference on Communications. Conference Proceedings. ICC 2002 (Cat. No. 02CH37333)*, volume 5, pages 2812–2816. IEEE, 2002.

[94] Rasoul Sadeghi, Bruno Correia, Emanuele Virgilito, Elliot London, Nelson Costa, Jox00E3;o Pedro, Antonio Napoli, and Vittorio Curri. Optimized translucent s-band transmission in multi-band optical networks. In *2021 European Conference on Optical Communication (ECOC)*, pages 1–4, 2021.

[95] João Pedro, Nelson Costa, and Steve Sanders. Scaling regional optical transport networks with pluggable and integrated high-capacity line interfaces. In *Optical Fiber Communication Conference (OFC) 2021*, page M3E.1. OSA, 2021.

[96] Rasoul Sadeghi, Bruno Correia, André Souza, Nelson Costa, Joao Pedro, Antonio Napoli, and Vittorio Curri. Transparent vs translucent multi-band optical networking: Capacity and energy analyses. *J. Lightwave Technol.*, 40(11):3486–3498, Jun 2022.

[97] Bruno Correia, Rasoul Sadeghi, Emanuele Virgillito, Antonio Napoli, Nelson Costa, João Pedro, and Vittorio Curri. Optical power control strategies for optimized c+ l+ s-bands network performance. In *Optical Fiber Communication Conference*, pages W1F–8. Optica Publishing Group, 2021.

[98] Andreas Betker, Christoph Gerlach, Ralf Hülsermann, Monika Jäger, Marc Barry, Stefan Bodamer, Jan Späth, Christoph Gauger, and Martin Köhn. Reference transport network scenarios. *MultiTeraNet Report*, pages 1–15, 2003.

[99] Gangxiang Shen and Rodney S Tucker. Energy-minimized design for ip over wdm networks. *Journal of Optical Communications and Networking*, 1(1):176–186, 2009.